

# UC Irvine

## UC Irvine Electronic Theses and Dissertations

### Title

Defining the role of plaque-associated microglia in Alzheimer's disease pathogenesis and disease outcomes

### Permalink

<https://escholarship.org/uc/item/8rr872xt>

### Author

Henningfield, Caden Michael

### Publication Date

2024

Peer reviewed|Thesis/dissertation

UNIVERSITY OF CALIFORNIA,  
IRVINE

Defining the role of plaque-associated microglia in Alzheimer's disease pathogenesis  
and disease outcomes

DISSERTATION

Submitted in partial satisfaction of the requirements  
for the degree of

DOCTOR OF PHILOSOPHY

In Biological Sciences

by

Caden Michael Henningfield, B.S.

Dissertation Committee:  
Professor Kim Green, Chair  
Professor Grant MacGregor  
Professor Vivek Swarup

2024

Chapter 1 © 2021 John Wiley & Sons, Inc

Chapter 3 © 2024 Caden Michael Henningfield

All other materials © 2024 Caden Michael Henningfield

## Dedication

Dedicated to my loved ones. I could not have done this without all your support.

Special dedication to my love, Lauren, who has supported me and believed in me  
through this entire journey.

“All's well that ends better.”

— J.R.R. Tolkien, The Lord of the Rings

## Table of Contents

List of Figures	iii
List of Abbreviations	v
Acknowledgments	vi
Vita	vii
Abstract of the Dissertation	x
Introduction	1
Chapter One: Microglia-specific ApoE knock-out does not alter Alzheimer's disease plaque pathogenesis or gene expression	9
Chapter Two: Generation of a novel, inducible destabilized Cre mouse line to specifically target disease associated microglia	40
Chapter Three: Selective targeting and modulation of plaque associated microglia via systemic dendrimer administration in an Alzheimer's disease mouse model	68
Dissertation Concluding Remarks	97
References	101

## List of Figures

		Page
Figure 1.1	Csf1r-cre ApoE <sup>fl/fl</sup> mouse model specifically knocks-out microglial-expressed ApoE with few changes in hippocampal gene expression	19
Figure 1.2	Microglial-specific ApoE knock-out increases average plaque size while plaque number and A $\beta$ levels are unchanged in a 5xFAD mouse model	21
Supp. Figure 1.1	Microglial-specific ApoE knock-out results in no changes in cerebral amyloid angiopathy (CAA)	23
Figure 1.3	No microglial or astrocytic change associated with microglial-specific ApoE knock-out	25
Supp. Figure 1.2	P2ry12 intensity is reduced with microglial-specific ApoE knock-out	27
Figure 1.4	Microglial-specific ApoE knock-out induces pre- and post-synaptic reduction	30
Figure 1.5	Few RNA changes associated with microglial-specific ApoE knock-out	33
Supp. Figure 1.3	Few changes in gene expression associated with microglial-specific ApoE knock-out in 5xFAD mice at 4 months of age	34
Table 2.1	Conflicting reports of TREM2/microglial impact on AD	44-45
Figure 2.1	Novel Cst7 <sup>DD-Cre</sup> mouse line specifically targets plaque associated microglia (PAMs)	53
Figure 2.2	tdTomato <sup>+</sup> cells colocalize more specifically to DAM markers	56
Figure 2.3	WT/Cst7 <sup>DD-Cre</sup> /Ai14 <sup>tdtomato(+/-)</sup> mice fed a demyelinating cuprizone diet and treated with TMP show tdTomato expression in white matter-associated microglia	58
Figure 2.4	Spatial transcriptomics analyses reveal increased DAM expression in tdTomato <sup>+</sup> PAMs vs tdTomato <sup>-</sup> PAMs	61
Supp. Figure 2.1	Microglia subcluster 4 is comprised of A $\beta$ plaques	64

Figure 3.1	G4 PAMAM hydroxyl dendrimers are phagocytosed by plaque associated microglia (PAM)	77
Figure 3.2	Intraperitoneal administration of PAMAM hydroxyl dendrimers conjugated to Dasatinib rescues elevated plus maze performance in 5xFAD mice	79
Figure 3.3	D-45113 treatment reduces A $\beta$ plaque levels in the brains of 5xFAD mice	82
Figure 3.4	D-45113 treatment reduces the number of microglia in aged 5xFAD mice	84
Figure 3.5	Bulk RNA-seq inflammatory gene expression is downregulated in 5xFAD mice treated with D45113	88
Supp. Fig 3.1	WGCNA analysis reveals microglia-specific inflammatory module associated with 5xFAD genotype	90
Figure 3.6	Axonal damage in 5xFAD mice is not rescued with D45113 treatment	92

## List of Abbreviations

A $\beta$	Amyloid-Beta
AD	Alzheimer's disease
ApoE	Apolipoprotein E
BCL2	B-cell lymphoma 2
BBB	Blood-brain barrier
CAA	Cerebral amyloid angiopathy
CD11c	Cluster of differentiation 11c; aka ITGAX
CD74	Cluster of differentiation 74
CSF1R	Colony stimulating factor 1 receptor
CST7	Cystatin F
ddCre	Destabilized Cre-recombinase
DAM	Disease associated microglia
DEG	Differential expressed genes
GFAP	Glial fibrillary acidic protein
GWAS	Genome wide association studies
HSCs	Hematopoietic stem cells
HC	Hippocampus
IBA1	Ionized calcium binding adaptor molecule
LRP1	Low density lipoprotein receptor-related protein 1
NFT	Neurofibrillary tangle
NPAM	Non-plaque-associated microglia
PAM	Plaque-associated microglia
PAMAM	Polyamidoamine
PSD95	Postsynaptic density protein 95
SNPs	Single nucleotide polymorphisms
S100 $\beta$	S100 Calcium Binding Protein B
ssCtx	Somatosensory cortex
TREM2	Triggering receptor expressed on myeloid cells 2
Vis Ctx	Visual cortex
WGCNA	Weighted gene co-expression network analysis
WT	Wild-type



# Acknowledgments

I am extremely grateful for the support from my mentor, Dr. Kim Green. His enthusiasm for science has inspired me throughout my PhD, and it has been a joy to work in the lab. Kim is a great leader and that is reflected in the environment and atmosphere of the lab.

I would also like to thank my committee members Dr. Grant MacGregor, Dr. Vivek Swarup, and Dr. Craig Walsh for all their helpful and thoughtful suggestions throughout my time at UCI.

Special thanks to everyone in the Green Lab. Thank you especially to Dr. Lindsay Hohsfield, and Dr. Giedre Milinkeviciute for their mentorship in lab, and Dr. Miguel Arreola and Rocio Barahona for showing me how to be a selfless and kind lab mate. Thank you also to Neelakshi Soni, Kristine Tran, Kate Tsourmas, Nellie Kwang, Claire Butler, Minseong Ki, Sung Jin Kim (Steve), Angela Gomez Arboledas, Celia Da Cunha, Philip Lu, Christiana Prekopa, and Ryan Lee for making lab a place I looked forward to going each day.

I would like to thank my family for their unconditional support not just for the past 6 years, but for my whole life. I could not have done this without all of you.

Finally, I would like to thank my wonderful partner, Lauren. You inspire me every day with how you approach life, and I am the luckiest person in the world to have you by my side for over 10 years now. Thank you for always giving me your full support, helping me relax after long days, and pushing me to always be my best.

This work was supported by the NIH under the following awards: R01NS083801 (NINDS), R01AG056768 (NIA), and U54 AG054349 [NIA Model Organism Development and Evaluation for Late-onset Alzheimer's Disease (MODEL-AD)] to K.N.G.; F31AG072852-01 (NIA) to C.M.H.

Chapter 1 of this dissertation is a reprint of the material as it appears in "Microglia-specific ApoE knock-out does not alter Alzheimer's disease plaque pathogenesis or gene expression" in *Glia*, used with permission from Wiley Periodicals LLC. The coauthors in this publication are Miguel A. Arreola, Neelakshi Soni, Elizabeth E. Spangenberg, and Kim N. Green. Kim N. Green directed and supervised research which forms the basis for this dissertation.

Chapter 3 of this dissertation is an adaptation of the material as it appears in "Selective targeting and modulation of plaque associated microglia via systemic hydroxyl dendrimer administration in an Alzheimer's disease mouse model" in *Alzheimer's Research & Therapy*, used with permission from BMC ([CC BY 4.0](#)). The coauthors in this publication are Neelakshi Soni, Ryan W. Lee, Rishi Sharma, Jeffrey L. Cleland, and Kim N. Green. Kim N. Green directed and supervised research which forms the basis for this dissertation.

# VITA

## **CADEN M. HENNINGFIELD**

7419 Palo Verde Rd. Irvine, CA 92617  
(661) 714-5916 | [chenning@uci.edu](mailto:chenning@uci.edu)  
[www.linkedin.com/in/cadenhenningfield](http://www.linkedin.com/in/cadenhenningfield)

### **PUBLICATIONS, POSTERS AND PRESENTATIONS**

#### **Peer-Reviewed Articles:**

- 1) **Henningfield CM**, Arreola MA, Soni N, Spangenberg EE, Green KN. Microglia-specific ApoE knock-out does not alter Alzheimer's Disease plaque pathogenesis or gene expression. *Glia* 2021;70:2. Published 2021 October 13. DOI: [doi.org/10.1002/glia.24105](https://doi.org/10.1002/glia.24105)
- 2) **Henningfield CM**, Soni N, Lee RW, Sharma R, Cleland JL, Green KN. Selective targeting and modulation of plaque associated microglia via systemic dendrimer administration in an Alzheimer's disease mouse model. *Alzheimer's Research and Therapy* 2024;16:101. Published 2024 May 06. DOI: [doi.org/10.1186/s13195-024-01470-3](https://doi.org/10.1186/s13195-024-01470-3)
- 3) Butler CA, Mendoza AA, Milinkeviciute G,... **Henningfield CM**,... Green KN. The Abca7V1613M variant reduces A $\beta$  generation, plaque load, and neuronal damage. *Alzheimer's & Dementia*. Published 2024 March 20. DOI: [doi.org/10.1002/alz.13783](https://doi.org/10.1002/alz.13783)
- 4) Miyoshi E, Morabito S, **Henningfield CM**, Rahimzadeh N,... Green KN, Swarup VS. Spatial and single-nucleus transcriptomic analysis of genetic and sporadic forms of Alzheimer's Disease. Accepted. *Nature Genetics*.
- 5) Syage AR, **Henningfield CM**, Pachow C,... Green KN, Lane TE. Cystatin F influences neuroinflammation and demyelination following murine coronavirus infection of the central nervous system. In Revision. *J. Neuroinflammation*.
- 6) Hohsfield LA, Najafi AR, Ghorbanian Y, Soni N, Crapser JD, Figueroa Velez DX, Jiang S, Royer, SE, Kim SJ, **Henningfield CM**, Anderson A, Gandhi SP, Mortizavi A, Inlay MA, and Green KN. Subventricular zone/white matter microglia reconstitute the empty adult microglial niche in a dynamic wave. *eLife* 2021;10:e66738. Published 2021 Aug 23 DOI: [10.7554/eLife.66738](https://doi.org/10.7554/eLife.66738)
- 7) Milinkeviciute G, **Henningfield CM**, Muniak MA, Chokr SM, Green KN, Cramer KS. Microglia Regulate Pruning of Specialized Synapses in the Auditory Brainstem. *Front Neural Circuits*. 2019;13:55. Published 2019 Aug 28. doi:[10.3389/fncir.2019.00055](https://doi.org/10.3389/fncir.2019.00055)
- 8) Clemenson GD, **Henningfield CM**, Stark CEL. Improving Hippocampal Memory Through the Experience of a Rich Minecraft Environment. *Front Behav Neurosci*. 2019;13:57. Published 2019 Mar 21. doi:[10.3389/fnbeh.2019.00057](https://doi.org/10.3389/fnbeh.2019.00057)

#### **In Preparation:**

- 1) **Henningfield CM**, Kawauchi S, MacGregor GR, Neumann JN, Green KN. A novel genetic approach to specifically target and manipulate disease-associated microglia in 5xFAD mice. *In preparation*.

#### **Poster Presentations:**

- 1) **Henningfield CM**, Kawauchi S, MacGregor GR, Nuemann JN, Green KN. A novel genetic approach to specifically target and manipulate disease-associated microglia in mice. Alzheimers International Conference (AAIC), San Diego 2022.

- 2) DiProspero ND, Noche JA, Chappel-FarleyMG, **Henningfield CM**, Yassa MO. Building a sustainable model of neuroscience education and community outreach. Society for Neuroscience Conference (SfN), San Diego 2022.
- 3) **Henningfield CM**, Cleland JL, Sharma R, Green KN. Selective targeting of Plaque Associated Microglia through peripheral dendrimer administration in an Alzheimer's disease model. Alzheimer's Association International Conference (AAIC), Amsterdam 2020.
- 4) Milinkeveciute G, **Henningfield CM**, Muniak MA, Green KN, Cramer KS. Microglia Regulate Synaptic Pruning in the Mammalian Auditory Brainstem. Association for Research in Otolaryngology Annual Conference, Baltimore, Maryland 2019.
- 5) **Henningfield CM**, Nekanti, U, Badner, A, Reinhardt, EK, Petersen, CA, Cribbs, DH, Anderson, AJ Cummings, BJ. Inflammatory Characterization of Immune Cell Populations in a Model of Repeated Mild Traumatic Brain Injury. UC Irvine Immunology Fair, Irvine, CA. 2018.
- 6) Milinkeveciute G, **Henningfield CM**, Muniak MA, Green KN, Cramer KS. Microglia regulate development of neural circuits in the auditory brainstem in the mouse. Southern California Hearing Conference, Los Angeles, CA 2018.
- 7) **Henningfield CM**, Clemenson GD, Stark CEL. Spatial exploration through the world of Minecraft leads to improvements in hippocampus-associated behaviors. Society for Neuroscience Annual Conference, San Diego, CA 2018.

### **TECHNICAL SKILLS**

- Manuscript writing
- Immunohistochemistry and RNA in situ hybridization
- Fluorescent confocal and whole-slide scanner microscopy
- Super resolution imaging
- Image analysis via Bitplane Imaris and Image J
- Protein and RNA isolation, western blotting, and MSD assays
- Spatial transcriptomics
- Basic bulk-tissue RNA sequencing analysis
- Cryostat, microtome, and vibratome slicing
- Mouse handling and AAV injection

### **EDUCATION**

#### **University of California, Irvine**

*Graduation expected May 2024*

PhD in Neurobiology and Behavior, in progress

Courses taken: Molecular Neuroscience, Systems Neuroscience, Cellular Neuroscience, Behavioral Neuroscience, Statistics, Introduction to Programming, Bioinformatics, Grant writing

GPA: 3.94

#### **University of California, Irvine**

*Fall 2014- Spring 2018*

BS in Biological Sciences, completed

### **AWARDS AND HONORS**

- F31 National Research Service Award (NRSA) fellowship (NIA) *Spring 2021*
- UCI Biological Sciences, William D. Redfield Graduate Award *Spring 2022*
- Center for the Neurobiology of Learning and Memory Director's Excellence Award *Spring 2022*
- Neurobiology and Behavior Retreat Outstanding Poster Award *Fall 2023*
- Friends of the UCI CNLM Award *Spring 2018*

### **PROFESSIONAL AFFILIATIONS:**

- UCI Graduate Professional Success in STEM (UCI-GPS-STEM)
- University of California Institute for Memory Impairments and Neurological Disorders (UCI MIND)
- Research and Education in Memory Impairments and Neurological Disorders (ReMIND)

### **TEACHING EXPERIENCE**

- **Teaching Assistant**, UCI. Bio 93: From DNA to Organisms (Fall 2019). Prepare and present lecture and course material; prepare and grade assignments and exams.
- **Teaching Assistant**, UCI. Neurobiology Lab (Spring 2020). Prepared and presented lecture and course material; prepared and graded assignments and exams; conducted laboratory section.

### **OUTREACH IN STEM**

- **Co-chair** – CNLM Ambassadors program *2021-Present*
- **Co-chair** – Irvine Brain Bee *2019-2021*
- **Mentor** – Brain Explorer Academy *2018-2019*
- **Ambassador** – Center for the Neurobiology of Learning and Memory (CNLM) *2018-Present*

## **Abstract of the Dissertation**

Defining the role of plaque-associated microglia in Alzheimer's disease pathogenesis  
and disease outcomes

By

Caden Michael Henningfield

Doctor of Philosophy in Biological Sciences

University of California, Irvine 2024

Professor Kim Green, Chair

Genetic data implicate microglia, the immune cells of the brain, in the development of Alzheimer's disease (AD). Within the AD brain, microglia surround extracellular plaques and mount a chronic inflammatory response. These plaque-associated microglia (PAMs) are characterized by specific disease-associated gene expression signatures, including *ApoE*, *Cst7*, *Trem2*, *Clec7a*, *Itgax*, and *Csf1*. Data from animal models of AD have identified that microglia play critical roles in plaque formation and plaque compaction as well as contributing to synaptic and neuronal dysfunction and loss. However, examination of TREM2 knock-out mice, in which microglia fail to react to plaques, have produced data suggesting that the reaction of microglia to plaques is protective, counter to conventional views that microglia are a major factor in seeding plaques and contributing to neuronal cell death and synaptic loss via neuroinflammation, indicating that microglia may have both beneficial and detrimental effects depending on model used or disease stage studied. A significant caveat with these experiments is that TREM2 is knocked out of all myeloid cells. Moreover, loss of TREM2 function in humans causes a neurodegenerative disease called Nasu-Hakola disease suggesting that the global knockout of TREM2 as utilized in the above studies induces neurodegeneration that may confound proper

interpretations of its effects in AD. Thus, interpretations about the roles of microglia need to be reassessed with strategies that specifically delineate the contributions of PAMs from the non-plaque-associated microglia (NPAM). We have developed novel strategies to target PAMs that can be used specifically during disease pathogenesis. Further, we include a genetic approach as well as a pharmacological approach to deliver specific therapeutic payloads to this cell population. My thesis further develops these tools and utilizes them to understand the roles of PAMs in AD pathogenesis.

### **Chapter 1: Microglia-specific ApoE knock-out does not alter Alzheimer's disease plaque pathogenesis or gene expression**

Previous studies suggest that microglial-expressed Apolipoprotein E (ApoE) is necessary to shift microglia into a neurodegenerative transcriptional state in Alzheimer's disease (AD) mouse models. On the other hand, elimination of microglia shifts amyloid beta ( $A\beta$ ) accumulation from parenchymal plaques to cerebral amyloid angiopathy (CAA), mimicking the effects of global APOE\*4 knock-in. ApoE is very lowly expressed by microglia in the healthy brain, but upon the introduction of  $A\beta$ , PAMs in the brain highly upregulate expression. Here, we specifically knock-out microglial-expressed ApoE, which should be the ApoE produced primarily by PAMs, while keeping astrocytic-expressed ApoE intact. When microglial-specific ApoE is knocked-out of a 5xFAD mouse model of AD, we found a ~35% increase in average  $A\beta$  plaque size, but no changes in plaque load, microglial number, microglial clustering around  $A\beta$  plaques, nor the formation of CAA. Immunostaining revealed ApoE protein present in PAMs in 5xFAD mice with microglial-specific ApoE knockout, suggesting that microglia can take up ApoE from other cellular sources. Mice with *ApoE* knocked-out of microglia had lower synaptic protein levels than

control mice, indicating that microglial-expressed ApoE may have a role in synapse maintenance. Surprisingly, microglial-specific ApoE knock-out resulted in few differentially expressed genes in both 5xFAD and control mice; however, some rescue of 5xFAD associated neuronal networks may occur with microglial-specific ApoE knock-out as shown by weighted gene co-expression analysis. Altogether, our data indicates that microglial-expressed ApoE may not be necessary for plaque formation or for the microglial transcriptional shift into a disease associated microglia (DAM) state that is associated with reactivity to plaques but may be necessary for plaque homeostasis in disease and synaptic maintenance under normal conditions.

## **Chapter 2: Generation of a novel, inducible destabilized Cre mouse line to specifically target disease associated microglia**

To explore the roles of DAMs in the pathogenesis and progression of AD, we need to develop models which specifically target diverse microglia subpopulations. Using gene expression datasets from microglia-depleted mice, we determined that *Cst7* was not expressed in the non-diseased brain but was highly upregulated in microglia upon the formation of plaques. Here, we develop a destabilized Cre recombinase (DD-Cre) mouse line knocked-in to the *Cst7* locus (*Cst7<sup>DD-Cre</sup>*) and crossed this line to the 5xFAD mouse model of AD and a tdTomato reporter line. We found that at early and aged disease timepoints, we can specifically label disease associated microglia (DAMs) that are around amyloid-beta (A $\beta$ ) plaques. Interestingly, the DAMs appear to be a subset of plaque-associated microglia (PAMs), and DAM expression appears to increase with age. These results were replicated using an inducible, demyelinating cuprizone model which is known to induce a DAM phenotype. Utilizing spatial transcriptomics approaches to identify

tdTomato<sup>+</sup> cells, we found that DAMs specifically labelled by our model have increased disease and inflammatory gene expression compared to other microglial populations, including when compared to other PAMs that are not labelled. This model can specifically target and manipulate DAMs and underlines the importance of targeted approaches when studying microglia in AD.

### **Chapter 3: Selective targeting and modulation of plaque associated microglia via systemic dendrimer administration in an Alzheimer's disease mouse model**

Identifying approaches to specifically target PAMs without interfering in the homeostatic functions of non-plaque associated microglia would afford a powerful tool and potential therapeutic avenue. While Chapter 2 developed a model to understand the relative contributions of DAMs/PAMs in AD, we need to develop ways to potentially target this population therapeutically. Here, we identified that peripherally administered drug delivering nanomolecules called polyamidoamine (PAMAM) hydroxyl dendrimers can cross the blood brain barrier and are preferentially taken up by PAMs in a mouse model of AD. As proof of principle for biologically active payload delivery, we conjugated the tyrosine kinase inhibitor, Dasatinib, to these dendrimers (D-45113) and treated the 5xFAD mouse model of amyloidosis for 4 weeks via peripheral administration. Treatment resulted in significant reductions in amyloid-beta (A $\beta$ ) and a stark reduction in the number of microglia in the subiculum and somatosensory cortex, as well as a downregulation in microglial, inflammatory, and synaptic gene expression compared to vehicle treated 5xFAD mice. This Chapter demonstrates that systemic administration of hydroxyl dendrimers may be utilized as a payload delivery tool to target and modulate PAMs and provides proof of principle that these dendrimers have therapeutic capability in the brain.



## Introduction

### Alzheimer's disease pathology

Alzheimer's disease (AD) is the most prevalent age-related neurodegenerative disease, impacting more than 10% of the population aged 65, and 50% aged 85 and older [62]. Additionally, AD cases are expected to triple by 2050 [63]. Thus, it is essential to understand the mechanisms underlying the disease so we can develop effective therapies against it. AD is classically characterized by the presence of extracellular plaques comprised of amyloid-beta ( $A\beta$ ) and intracellular neurofibrillary tangles comprised of tau. A central theory in the field revolves around  $A\beta$  and is known as the amyloid cascade hypothesis. Here, it is hypothesized that the presence of aggregated  $A\beta$  initiates common effects associated with AD, such as, neuroinflammation, tau hyperphosphorylation, and synaptic and neuronal loss [60]. In line with this theory, amyloid deposits have been shown to present decades before the cognitive deficits associated with AD [132]. Recently, several landmark immunotherapy clinical trials have shown that clearance of  $A\beta$  from the human brain leads to very little to modest, yet impactful, rescue in the cognitive decline of AD patients, indicating that while  $A\beta$  is an important hallmark in AD, it may not be the only key factor in disease outcomes [21, 181, 195]. Of note, tau pathology is observed following  $A\beta$  deposition and is more closely correlated with neurodegeneration than amyloid pathology [140]. In preclinical models, tau immunotherapy has shown promise in clearing tau and preventing tau seeding in the murine brain while rescuing cognitive impairment in multiple tauopathy mouse models [2, 19, 89, 175] and several clinical trials are underway targeting tau in human AD patients.

Along with A $\beta$  plaques and tau tangles, another critical component of AD, which has recently garnered more attention, is the chronic neuroinflammatory response by microglia and astrocytes [1]. All these key pathological hallmarks collectively lead to brain degeneration which manifests as memory impairments and behavioral changes in affected patients. The importance of treating this disease at its earliest stages cannot be understated, as patients with mild cognitive impairment (MCI) present substantial A $\beta$  and tau accumulation, inflammation, and neuronal loss [136].

### **Microglial homeostasis**

Microglia, the brain's resident immune cells, comprise approximately 5-12% of all brain cells. In the healthy adult brain, microglia are highly dynamic and constantly survey the entirety of the brain [142]. As surveyors, microglia exhibit a ramified morphology, supporting neuronal function by secreting factors which promote tissue homeostasis. However, once microglia detect insult or injury in the brain parenchyma, they transform from a ramified morphology into an amoeboid morphology. These "activated" microglia secrete proinflammatory cytokines, including, tumor necrosis factor- $\alpha$  (TNF $\alpha$ ), interleukin (IL)-6, and nitric oxide (NO) [1]. In acute neuroinflammatory events, the proinflammatory microglial response resolves, microglial morphology is reverted back to a ramified state, and neuroimmune regulatory proteins (NiReg) such as insulin-like growth factor 1 (IGF-1), brain-derived neurotrophic factor (BDNF), transforming-growth factor- $\beta$  (TGF- $\beta$ ), and nerve growth factor (NGF) resolve the inflammatory process [157]. However, neurodegenerative diseases such as AD induce chronic changes in microglia, creating an inflammatory feed-forward mechanism which promotes tissue atrophy.

### **Microglia in Alzheimer's disease**

Over one-hundred years ago, Alois Alzheimer identified plaque-associated microglia (PAMs) in post-mortem brains [3]. Studies have shown microglial number increases proportionally to plaque size [203] and microglia proliferate at amyloid deposits [18, 42]. Additionally, PAMs encircle plaques and regulate plaque dynamics in AD mice [17, 27, 184]. Importantly, evidence from positron emission tomography (PET) imaging suggests microglial activation occurs well before clinical symptoms of cognitive decline in patients [56, 207]. Altogether, these data implicate microglia as key participants in AD, particularly in pathology focused around A $\beta$  plaques. This idea is bolstered by genome wide association studies which show that single nucleotide polymorphisms of genes highly enriched or exclusively expressed in myeloid cells confer heightened risk of developing AD, including *TREM2*, *CD33*, *CR1*, *CLU*, *EPHA1*, *CST7*, and *ABCA7* [58, 81, 101, 103, 188].

The role of microglial inflammation in AD progression is well documented. When microglia are exposed to A $\beta$ , proinflammatory cytokines including IL-1 $\beta$ , IL-6, TNF $\alpha$ , TGF- $\beta$ , and chemokines such as macrophage inflammatory proteins (MIP)-1a, 1b, -2, and chemokine (C-C Motif) ligand 2 (CCL2) are released in an attempt to facilitate A $\beta$  clearance [1]. However, attempts by microglia to degrade and clear amyloid plaques from the AD brain is futile, as plaques endure in the brain even with microglia constantly surrounding them. As a consequence of this inability to clear amyloid plaques, surrounding cells endure chronic neuroinflammation for the duration of the disease. This neuroinflammatory environment is, in part, built upon microglia-derived neurotoxic factors including TNF- $\alpha$ , NO, IL-1 $\beta$ , and ROS [118]. Knockout of NLRP3 – a major contributor to neuroinflammatory insult in the CNS produced by microglia [53]– mitigates inflammatory

signaling, decreases deposition of A $\beta$ , restores synaptic plasticity, and improves cognitive function in APP/PS1 mice [66]. Moreover, the secretion of IL-1, TNF- $\alpha$ , and C1q by microglia induces astrocyte reactivity, which further promotes neuronal and oligodendrocytic cell death [113]. Altogether, these data indicate that the chronic microglial inflammatory response drives neurodegeneration in AD while doing relatively little to clear A $\beta$  plaques from the brain.

### *Microglial regulation of A $\beta$ plaques*

Traditionally, microglia were believed to clear A $\beta$  deposits from the brain via phagocytosis of A $\beta$ -fibrils [149], however elimination of microglia from plaque bearing mice does not result in increased A $\beta$  or plaque levels [185], and switching off APP expression in mice after the formation of plaques does not result in their degradation by surrounding microglia [80]. *In vitro* and *in vivo* studies have shown that microglia do, in fact, maintain the capacity to internalize A $\beta$  [65, 96, 97, 112, 151, 152, 184, 202]. However, microglia may retain fibrillar A $\beta$  for weeks without degrading the A $\beta$  peptides [151] and primary mouse microglia have been shown to release fibrillar A $\beta$  after they have internalized it [26]. Interestingly, microglia stimulated with macrophage colony-stimulating factor (M-CSF), gamma oscillations, ultrasound, and IL-33, enable them to efficiently degrade fibrillar A $\beta$  [44, 76, 107, 121]. Taken together, these studies suggest that A $\beta$  plaque formation may be a consequence of microglia's inability to efficiently degrade A $\beta$ .

Recently, the relationship between A $\beta$  and microglia has been further explored. Our lab has shown that the sustained elimination of microglia through Colony stimulating factor 1 receptor (CSF1R) inhibition prior to plaque onset leads to a significant reduction in total plaque development. Instead A $\beta$  is found to accumulate within the blood vessels as CAA

at early stages of disease in 5xFAD mice, an aggressive model of AD [184]. Additionally, we only observe plaques in regions where surviving microglia persist. At more advanced stages of AD pathology and plaque deposition, the elimination of microglia still prevents both synaptic and neuronal loss despite there being no change in plaque number or volume, suggesting that these cells are key mediators of the detrimental effects of plaque pathology in disease once they form [185]. Furthermore, our lab and others have shown that low-dose CSF1R inhibition in AD (at doses that do not kill microglia) can inhibit microglial association with plaques. In doing so, mice exhibit improved cognition, synaptic integrity, and the resolution of inflammation in several mouse AD models [31, 146] suggesting that microglia have a role in driving plaque pathogenesis and worsening synaptic function in AD mouse models.

### **Plaque-associated microglia in Alzheimer's Disease**

Following our observation that microglia are necessary for plaque formation, we hypothesized that microglia would phagocytose A $\beta$  produced by neurons, and then shuttle it into their lysosomes where it could concentrate and aggregate, given the inability for microglia to effectively degrade A $\beta$ . We postulated that this material could be the initial seed for extracellular plaques, after being released from the microglia. In support of our hypothesis, knock-out of microglial phagocytic mediators AXL and MERTK, which are upregulated by PAMs in the AD brain [94], reduces parenchymal plaque deposition and increases CAA, further suggesting that microglial phagocytosis of A $\beta$  may serve as a potential mechanism for plaque deposition in the brain [73]. If PAMs are the main phagocytic cell in the brain interacting with A $\beta$ , then targeting these specific cells is crucial

to determine the mechanism of plaque deposition and homeostasis. Thus, it is necessary to target microglial genes associated with microglial-plaque interaction.

One such gene which is responsible for the PAM response is Apolipoprotein E (ApoE), which encodes a glycoprotein normally involved in lipid transport. In humans, APOE is expressed as three different isoforms, *APOE\* $\epsilon$ 2*, *APOE\* $\epsilon$ 3*, and *APOE\* $\epsilon$ 4*, with *APOE\* $\epsilon$ 3/APOE\* $\epsilon$ 3* being the most common variant. Importantly *APOE* is one of the earliest and most impactful genetic risk determinants in late-onset AD [29, 48, 103] with *APOE\* $\epsilon$ 4* associated with an increase in AD risk [29, 171], with individuals carrying two copies of the *APOE\* $\epsilon$ 4* allele being even higher at risk, and *APOE\* $\epsilon$ 2* associated with a decreased risk in AD [28, 37, 161], but an increased risk in CAA, kidney disease, hypercholesterolemia, and cancer [93, 141, 147, 167, 211]. In mice, there are no separate isoforms of ApoE, but similar to in humans, ApoE can directly interact with A $\beta$  peptides and form an A $\beta$ /ApoE complex [102]. These complexes are subsequently phagocytosed by microglia through interactions with Low density lipoprotein receptor-related protein 1 (LRP1) or Triggering receptor expressed on myeloid cells 2 (TREM2) [8, 10, 91, 208]. When ApoE is knocked out of the mouse brain, plaque deposition is lessened, implicating ApoE, and the receptors it binds to, in plaque formation, possibly due to lessened uptake of A $\beta$  through LRP1 and TREM2 in microglia [11, 70, 194]. While these studies have helped uncover the importance of ApoE in AD, the importance of microglial-expressed ApoE in AD has yet to be determined. Under normal conditions in the mouse brain, ApoE is primarily produced by astrocytes [20, 156]. However, in AD, microglial *ApoE* mRNA and snRNA are highly enriched [94, 126, 155, 160] while snRNA levels of astrocytic *ApoE* are downregulated [126]. In this proposal, we examine the

effects of constitutive microglial-specific ApoE knock-out on AD pathogenesis and homeostasis in 5xFAD mice. Our results will lend insight to the mechanisms behind microglia's involvement in plaque pathogenesis and homeostasis.

Another gene which is crucial to the microglial response to A $\beta$  is *Trem2* and its direct downstream effector, *Tyrobp*. Single cell RNA sequencing studies have found heterogenous subsets of microglia in AD, demarcated by the expression of genes such as *Trem2* and *Tyrobp* that conventionally differentiate between disease- vs non-disease-associated microglia (DAM), which in AD roughly correspond to plaque- and non-plaque-associated microglia (PAM and NPAM) respectively [94]. When the TREM2 receptor at the microglial cell membrane is contacted by ApoE or A $\beta$ , subsequent phosphorylation of TYROBP occurs, leading to modulation of downstream inflammatory signaling and phagocytic pathways [52]. However, it is unknown whether induction of this pathway in microglia in response to A $\beta$  is overall beneficial or harmful to disease outcome, with many studies yielding contradicting results, indicating there may be both harmful and beneficial roles [51, 52, 85, 86, 105, 106, 153, 200]. For example, when *Trem2* is knocked out in a mouse model of AD, microglia fail to mount an inflammatory response to A $\beta$  plaques, and yet there is an increase in amyloid seeding in the brain, worsened neuritic damage, and greater cognitive impairments [153, 201]. Additionally, TREM2 overexpression rescues spatial cognitive impairments and lowers neuronal and synaptic loss in a mouse model of tauopathy [87]. On the other hand, a TREM2 knockout in a different tauopathy model instead ameliorates disease-related neurodegeneration and pro-inflammatory cytokine induction [110] and deletion of the downstream *Tyrobp* gene, which prevents microglia from mounting a response to plaques, leads to decreased brain A $\beta$  levels and improved

spatial memory in the APP/PSEN1 mouse model of AD [61]. Outside of AD, TREM2 is necessary under homeostatic conditions to phagocytose apoptotic neurons, cellular debris, and bacterial products [47, 71, 137, 189]. Additionally, inhibitory variants in the *Trem2* gene in humans have been linked with Nasu-Hakola disease, presenting with early dementia and bone cysts with fractures [206], thereby suggesting that the global knockout of TREM2 as utilized in the above studies induces neurodegeneration that may confound proper interpretations of its effects in AD.

The studies mentioned above have contributed to our understanding of PAMs in AD. However, the question is still outstanding: Are PAMs beneficial or harmful in AD, and is it disease stage dependent? One reason this question has eluded us is due to our inability to specifically target these cells in AD. To tease apart these effects, we propose to create and use selective genetic and pharmacological models to specifically target, identify, and manipulate subsets of disease microglia and determine the direct link between microglia (or microglial subsets) and A $\beta$  plaques as it relates to disease progression.



## Chapter One:

### Determine the role of microglial-specific ApoE in AD pathogenesis and homeostasis

#### Introduction

Alzheimer's disease (AD) is the most prevalent neurodegenerative disease and clinically manifests as memory and cognitive deficits in affected patients. A key hallmark of the disease is the progressive accumulation of amyloid- $\beta$  ( $A\beta$ ) plaques throughout the brain, culminating in synaptic and neuronal loss [59, 79]. Although the mechanisms behind the emergence of AD are currently unknown, microglia have consistently been shown to play a key role in the disease as suggested by Genome Wide Association Studies which show that single nucleotide polymorphisms of genes highly enriched or exclusively associated with myeloid cells confer heightened risk of developing AD [58, 81, 101, 103, 188].

Normally involved in immune surveillance and debris clearance, microglia actively regulate plaque morphology (e.g. compaction) by clustering around  $A\beta$  plaques in multiple mouse models of AD [17, 27]. A possible avenue by which microglia interact with  $A\beta$  plaques involves Apolipoprotein E (ApoE) - a glycoprotein normally involved in lipid transport. *APOE* is considered a major genetic risk determinant in late-onset AD [29, 48, 103] with three isoforms of *APOE* (*APOE\** $\epsilon$ 2, *APOE\** $\epsilon$ 3, and *APOE\** $\epsilon$ 4) being expressed in the human brain. *APOE\** $\epsilon$ 4 carriers have an increased risk to develop AD [29, 171] while *APOE\** $\epsilon$ 2 carriers have a decreased risk [28, 37, 161]. Studies looking into *APOE\** $\epsilon$ 4 effects on AD pathology revealed exacerbated plaque deposition [22, 115, 158, 173, 191] and synaptic degeneration and synaptic protein loss in postmortem AD patients [5, 117] and mice [114, 210], along with increased microglial reactivity to  $A\beta$  plaques [164],

and increased proinflammatory RNA signature [180]. APOE\* $\epsilon$ 2 on the other hand is associated with reduced numbers of neuritic plaques [176].

With regards to the proposed mode of action by which ApoE may be affecting A $\beta$  deposition, ApoE can directly interact with A $\beta$  peptides and form an A $\beta$ /ApoE complex [102]. These complexes are subsequently phagocytosed by microglia through interactions with Low density lipoprotein receptor-related protein 1 (LRP1) or Triggering receptor expressed on myeloid cells 2 (TREM2) [8, 10, 91, 208]. Our lab and others have shown ApoE immunoreactivity in dense core plaques as well as in microglial processes around the plaque cores [184, 193], perhaps indicative of the interactions described in the studies above. Additionally, microglial depletion in the plaque-laden 5xFAD mouse model of AD reduces plaque load [184], suggesting that ApoE-microglia interaction may influence microglia-plaque interaction and plaque formation. This finding has been recently replicated with knock-out of the phagocytic mediators *Axl* and *Mertk*, resulting in reduced parenchymal plaque deposition and increased cerebral amyloid angiopathy (CAA), collectively suggesting that microglia play a critical role in plaque formation [73]. Similarly, previous ApoE knock-out studies demonstrated a reduction in A $\beta$  plaque load and synaptic proteins [11, 70, 114, 194, 210], as well as a rescue in the microglial homeostatic signature [99], suggesting a critical link between microglia and ApoE in disease pathogenesis.

Although ApoE has been extensively studied in AD, the importance of microglial-expressed ApoE in AD has yet to be determined. Under normal conditions in the mouse brain, ApoE is primarily produced by astrocytes, with very little expression seen in microglia [20, 156, 215, 216]. However, in AD, microglial *ApoE* mRNA and single nuclei

RNA are highly enriched [94, 126, 155, 160] while single nuclei RNA levels of astrocytic *ApoE* are downregulated [126]. Hence, the ApoE that is expressed by microglia should be coming from the disease/ plaque associated microglial (PAM) population. Here, we examine the effects of constitutive PAM specific ApoE knock-out, which we will call microglial expressed ApoE knock-out, on AD pathogenesis and homeostasis in 5xFAD mice. In 4-month-old mice, microglial-specific ApoE knock-out has no effect on plaque formation, A $\beta$  production, or microglial and astrocytic number. At 12 months of age, the average plaque size in the hippocampus is ~35% larger than in 5xFAD controls, but found no differences in microglial interaction with plaques, nor microglial and astrocytic numbers. However, there was a reduction in microglial homeostatic marker P2ry12 intensity in microglial-expressed ApoE knock-out, 5xFAD, and 5xFAD microglial-expressed ApoE knock-out groups when compared to controls. Interestingly, ApoE-intact mice have significantly higher levels of pre- and post-synaptic markers when compared to mice with microglial-expressed ApoE depleted, 5xFAD mice, and 5xFAD mice with microglial-expressed ApoE depleted. Although modest changes in plaque size and synaptic proteins are observed, few RNA expression changes are observed; however, weighted gene co-expression analysis (WGCNA) indicates that neuronal networks downregulated in 5xFAD mice may be preserved with microglial-specific ApoE knock-out. While we show microglial-expressed ApoE is absent from our mouse model, ApoE protein still colocalizes with microglia and the surrounding plaques. Our findings indicate that microglial-expressed ApoE may not be necessary for the microglial response to A $\beta$  plaques and that other sources of ApoE may be sufficient to induce microglial transcriptional changes in AD.

## **Methods**

### **Animals**

All animal experiments performed in this study were approved by the UC Irvine Institutional Animal Care and Use Committee (IACUC) and were compliant with ethical regulations for animal research and testing. The 5xFAD mouse expresses 5 familial AD genes (APP Swedish, Florida, and London; PSEN1 M146L +L286V) [144] and is characterized by aggressive amyloid pathology throughout the brain and synaptic and neuronal loss in the subiculum. The following primers were used to genotype these animals: PS1 Forward 5' - AAT AGA GAA CGG CAG GAG CA – 3' and PS1 Reverse 5' - GCC ATG AGG GCA CTA ATC AT – 3'. To generate *Apoe* knock-out specifically in myeloid cells, the following mice were obtained from Jackson Laboratory: *Csf1r-cre* (C57BL/6Tg(Csf1r-cre)1Mnz/J; Stock No: 029206) and *Apoe<sup>fl/fl</sup>* (B6.129S6-*Apoe<sup>tm1.1Mae</sup>/MazzJ*; Stock No: 028530). Progeny from *Apoe<sup>fl/fl</sup>*, *Csf1r-cre*, and 5xFAD mice were used to produce four groups of interest. Each group of interest consisted of nearly equal numbers of male and female mice. For genotyping *Csf1r-cre*, the following primers were used: Forward 5' - AGA TGC CAG GAC ATC AGG AAC CTG – 3' and Reverse 5' - ATC AGC CAC ACC AGA CAC AGA GAT – 3'. For genotyping *Apoe<sup>fl/fl</sup>*, the following primers were used: Forward 5' - GGC TTA GTG GGT AAA GGT GCT – 3' and Reverse 5' - GAC TAG GCA GGT GTG GAA TTA GA – 3'. All mice were sacrificed and perfused at either 4 or 12 months of age for this study. Half-brains were subsequently flash frozen for biochemical analyses or drop-fixed in 4% paraformaldehyde for immunohistochemical analyses. 4-month-old drop-fixed brains were sliced on a microtome and stored in a 1xPBS and .01% NaAzide solution at 4°C. 12 month drop-fixed

brains were sliced using a microtome; however, they were then stored in a 1xPBS, 30% glycerol, and 30% ethylene glycol solution at -20°C. This allowed for the preservation of RNA in our 12-month tissue which we used for RNA *in situ* hybridization.

### **Immunohistochemistry**

Primary antibodies and dilutions are used as follows: anti-ionized calcium-binding adapter molecule 1 (IBA1; 1:1000; 019–19741; Wako, Osaka, Japan), anti-A $\beta$ 1–16 (6E10; 1:1000; 803001; BioLegend), PU.1 (1:500; 2266S, Cell Signaling), CD68 (1:200; MCA1957T; BioRad), anti-lysosomal associated membrane protein 1 (LAMP1; 1:200; sc-20011), anti-S100 $\beta$  (1:200; ab52642; Abcam), anti-gial fibrillary protein (GFAP; 1:1000; ab4674; Abcam), anti-P2ry12 (1:200; HPA014518; Sigma), anti-Apolipoprotein E (ApoE; 1:200; ab19606; Abcam) Synaptophysin (1:1000; S5768; Millipore), PSD95 (1:500; ab18258; Abcam). Amylo-Glo (TR-300-AG; Biosensis, Thebarton, South Australia, AU) was used according to manufacturer's instructions to visualize fibrillar A $\beta$  plaques. For Amylo-Glo staining, tissue sections were washed in 70% ethanol 1X5 minutes, followed by a 1X2 minute wash in distilled water. Sections were then 1% Amylo-Glo solution for 1X10 minutes then washed with .9% saline for 1x5 minutes and distilled water for 1X15 seconds. Sections were then briefly rinsed in 1XPBS and immersed in normal serum blocking solution (5% normal serum with 0.2% Triton-X100 in 1XPBS) for 60 minutes. Tissue was then incubated overnight in primary antibody at the dilutions described above in normal serum blocking solution at 4 degrees Celsius. The next day tissue sections were washed in 1XPBS 3X10 minutes before being placed in appropriate secondary antibody in normal serum blocking solution (1:200 for all species and wavelengths; Invitrogen) for 60 minutes. Tissue sections were then washed for 3X10 minutes in 1XPBS before tissue

was mounted and coverslipped. High resolution fluorescent images were obtained using a Leica TCS SPE-II confocal microscope and LAS-X software. To capture whole brain stitches, automated slide scanning was performed using a Zeiss AxioScan.Z1 equipped with a Colibri camera and Zen AxioScan 2.3 software.

### ***In Situ Hybridization***

RNAscope *In Situ* Hybridization was performed following manufacturer's instructions. Mounted tissue sections were warmed on a 40°C hot plate for 15 minutes and then dehydrated with 50%, 70%, and 100% ethyl alcohol for 5 minutes at each gradient, followed by hydrogen peroxide (Cat No.322335 ACDBio) treatment for 10 minutes. After washing the tissue with Deionized (DI) water, tissue sections were placed in boiling Target Retrieval Reagent (Cat No.322380 ACDBio) for 15 minutes and then immediately transferred to DI water. Slides were then blocked in Protease III (Cat No.322337 ACDBio) for 30 minutes at 40 °C. *ApoE* probe (Cat No. 313271-C2) was then added for 2 hours at 40 °C within a humidity control chamber. Signal amplification and detection reagents (Cat No.322310 ACDBio) were applied sequentially and incubated in AMP 1, AMP 2, and AMP 3 for 30 minutes each. Before adding each AMP reagent, samples were washed twice with washing buffer (Cat NO.310091 ACDBio). Respective HRPs were placed on slides for 15 minutes at 40 °C followed by 30 minutes of respective Opal dye (FP1487001KT Akoya Biosciences) for 30 minutes at 40 °C and HRP blocker for 15 minutes at 40 °C.

### **A $\beta$ Elisa**

To isolate protein for the Elisa, flash-frozen brain hemispheres were microdissected into cortical, hippocampal, and thalamic regions and grounded to a powder. Tissue was then homogenized in Tissue Protein Extraction Reagent (TPER (Life Technologies, Grand

Island, NY)) with protease and phosphatase inhibitors present. Samples were then centrifuged at 100,000 g for 1 hour at 4 °C to generate TPER-soluble fractions. To generate formic acid fractions, protein pellets from the TPER-soluble fraction were then homogenized in 70% formic acid and centrifuged at 100,000 g for 1 hour at 4 °C, the formic acid fraction is then neutralized. Isolated protein samples were transferred to a blocked MSD Mouse (4G8) A $\beta$  triplex ELISA plate (A $\beta$ 1–38, A $\beta$ 1–40, A $\beta$ 1–42) and incubated for two hours at room temperature with an orbital shaker. The plate was then washed, and measurements were obtained using a SECTOR Imager 2400, per the manufacturer's instructions (Meso Scale Discovery, Gaithersburg, MD).

### **RNA Sequencing**

Whole transcriptome RNA sequencing (RNA-Seq) libraries were produced from hippocampal tissue of Control, *Csf1r-Apoe-KO*, 5xFAD, and 5xFAD/*Csf1r-Apoe-KO* mice sacrificed at 4 and 12 months of age. RNA was isolated with an RNA Plus Universal Mini Kit (Qiagen, Valencia, USA) according to the manufacturer's instructions. Library preparation, RNA-seq, and read mapping analysis were performed by Novogene Co. Gene expression was analyzed using Limma, edgeR, and org.Mm.eg.db packages [163] with expression values normalized into FPKM (fragments per kilobase of transcript per million mapped reads). Differentially-expressed genes were selected by using false discovery rate (FDR) <0.05. Heatmaps were created using Morpheus (Morpheus, <https://software.broadinstitute.org/morpheus>) and volcano plots were created using VolcanoR [49].

*Weighted correlation network analysis*: Network analysis was performed using weighted gene co-expression analysis (WGCNA) package in R [213]. First, bi-weighted mid-

correlations were calculated for all gene pairs, and then used to generate an eigengene network matrix, which reflects the similarity between genes according to their expression profiles. This matrix was then raised to power  $\beta$  ( $\beta=16$ ). Modules were defined using specific module cutting parameters (minimum module size = 100 genes, deepSplit = 4 and threshold of correlation = 0.2). Modules with a correlation greater than 0.8 were merged. We used first principal component of the module, called signed bicor network, to correlate AD genotype, sex, and *ApoE* genotype. Hub genes were defined using intra-modular connectivity (kME) parameter of the WGCNA package. Gene enrichment analysis: Gene-set enrichment analysis was done using enrichR [100].

### **Data Analysis and Statistics**

Both male and female mice were used in all statistical analyses. Plaque, microglial, S100 $\beta$  astrocyte, PSD95, and Synaptophysin counts were measured via the spots function and plaque volume, Lamp1 area, and 6E10 volume and P2ry12 intensity were measured via the surfaces function on Imaris version 9.6. GFAP and Cd68 % area were measured via Image J. 1 FOV was used per animal per brain region for each analysis listed above. Microglial and astrocytic colocalization to *ApoE* RNA, and microglial and plaque colocalization to ApoE protein was measured using the colocalization function followed by the surfaces function in Bitplane Imaris 9.6. The colocalization function created a new channel which showed colocalized signal and the subsequent surface function then measured the volume of the total signal in the channel. The total volume was then normalized to the total volume of IBA1, GFAP or Amylo-Glo for microglia, astrocytes, and plaques, accordingly. Statistical analysis was accomplished using Prism GraphPad (v9.0.0). To compare two groups, the unpaired Student's t-test was used. To compare all



four groups at a single timepoint or in a single brain region, one-way ANOVA with Tukey's multiple comparison correction was performed. To compare all four groups at either different timepoints or brain regions, two-way ANOVA with Tukey's multiple comparison correction was used. For all analyses, statistical significance was accepted at  $p < 0.05$ . and significance expressed as follows: \* $p < 0.05$ , \*\* $p < 0.01$ , \*\*\* $p < 0.001$ .

## **Results**

### **Microglial-specific ApoE knock-out does not significantly alter gene expression in mice**

To determine the role of microglial-expressed ApoE in AD pathogenesis we undertook a strategy to specifically knock-out *ApoE* from microglia in 5xFAD mice. To that end, we utilized a Cre mouse driver line targeting colony stimulating factor 1 receptor (*Csf1r*) expressing cells (*Csf1r-cre*); *Csf1r* is exclusively expressed by microglia in the adult brain, and produces >95% recombination when combined with reporter lines [185]. *Csf1r-cre* mice were bred with the 5xFAD mouse model of AD and *ApoE<sup>fl/fl</sup>* mice (Fig. 1.1a, a'). Four groups were created for all subsequent analyses: *ApoE<sup>fl/fl</sup>* (**Control**), *Csf1r-cre/ApoE<sup>fl/fl</sup>* (***Csf1r-ApoE-KO***), *5xFAD<sup>+/-</sup>/ApoE<sup>fl/fl</sup>* (**5xFAD**), and *5xFAD<sup>+/-</sup>/Csf1r-cre/ApoE<sup>fl/fl</sup>* (**5xFAD/*Csf1r-ApoE-KO***). Mice were sacrificed at 4 and 12 months of age to observe changes in early and late stage 5xFAD pathology. To confirm successful knock-out of microglial-expressed ApoE, we performed *in situ* hybridization via RNAscope for *ApoE* mRNA on 12-month-old mice (Fig. 1.1b). Notably, microglial-expressed ApoE was highly upregulated in 5xFAD mice but was nearly absent in 5xFAD/*Csf1r-ApoE-KO* mice (Fig. 1.1c). *ApoE* colocalized with GFAP<sup>+</sup> astrocytes in the hippocampus, however; Control

and *Csf1r-Apoe*-KO mice had significantly higher levels of GFAP-*Apoe* colocalization than 5xFAD and 5xFAD/*Csf1r-Apoe*-KO mice (Fig. 1.1d). These results confirm that microglia express ApoE in 5xFAD mice, and that ApoE expression in microglia is successfully knocked-out with the addition of the *Csf1r-cre* driver. We performed bulk-tissue RNA sequencing of microdissected hippocampi from Control and *Csf1r-Apoe*-KO mice to determine if deletion of *Apoe* from microglia would result in unexpected broad effects on hippocampal gene expression at 4 and 12 months of age (Fig. 1.1e, f). We found only 7 differentially expressed genes (Gm9825, Hmga1b, Atp6v0c-ps2, Rps2-ps10, Gm14292, Gm11361) between Control and *Csf1r-Apoe*-KO mice at 12 months of age, indicating the loss of microglial-expressed ApoE does not broadly alter gene expression in the brain. Of these genes, there are 5 pseudogenes, 1 predicted gene (Gm11361), and 1 gene, Hmga1b, that encodes a non-histone chromatin protein involved in gene transcription and can interact with p53 to inhibit apoptotic activity [154].

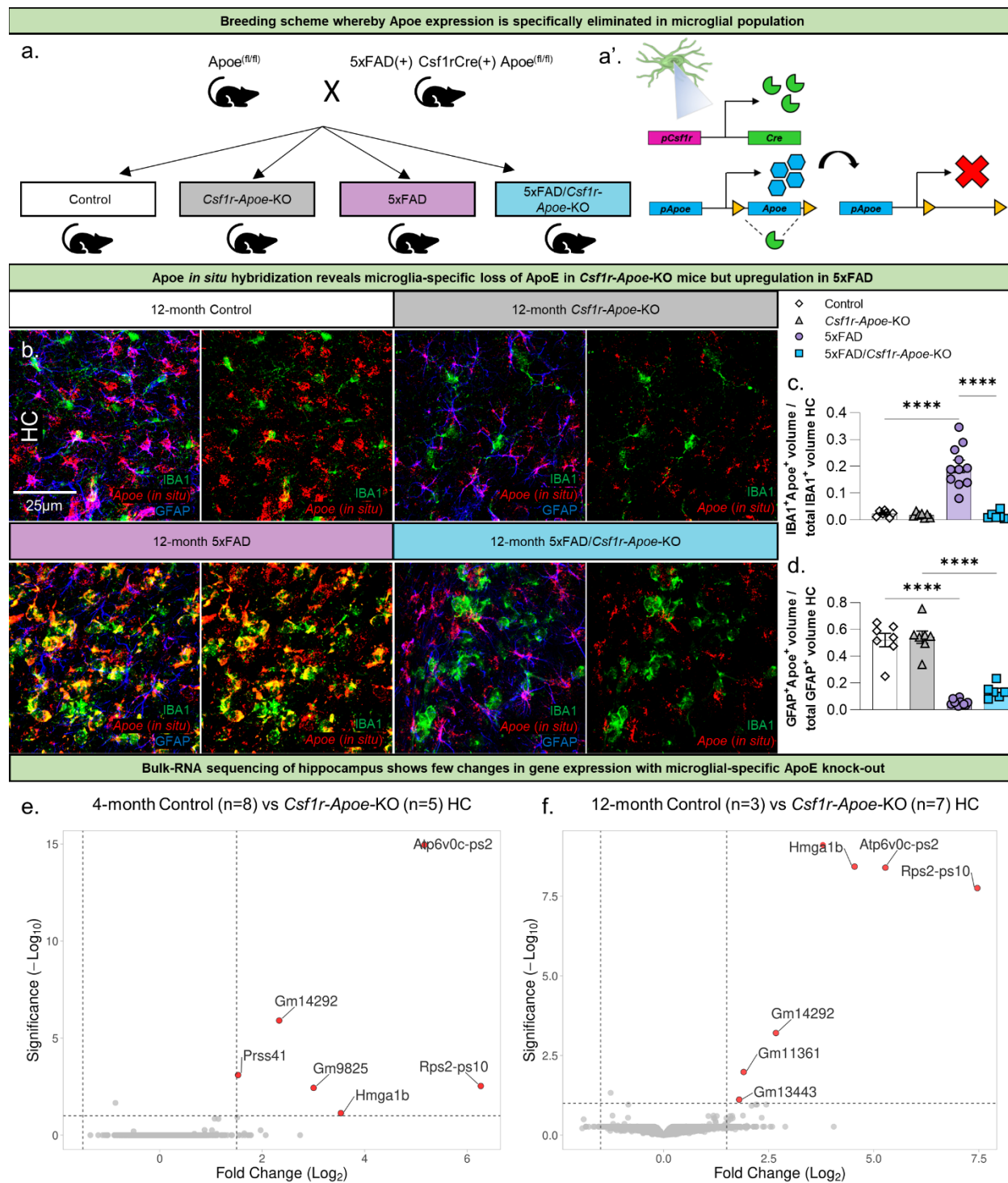


**Fig. 1**

**Figure 1.1:  $Csf1r$ -cre  $ApoE^{fl/fl}$  mouse model specifically knocks-out microglial-expressed ApoE with few changes in hippocampal gene expression.** Schematic of experimental design (a). Mice homozygous for  $ApoE^{fl/fl}$  are crossed with mice that are heterozygous for 5xFAD and  $Csf1r$ -cre, and homozygous for  $ApoE^{fl/fl}$  to create four groups of interest (all groups are  $ApoE^{fl/fl}$ ): Control,  $Csf1r$ -ApoE-KO, 5xFAD, and 5xFAD/ $Csf1r$ -ApoE-KO. Mice were sacrificed at 4 and 12 months of age for subsequent analysis.

Representative 63x images of IBA1 and GFAP immunofluorescence with ApoE in situ hybridization (b). Microglial ApoE is significantly upregulated in 12-month-old 5xFAD (n=11) mice but is depleted in 5xFAD/Csf1r-ApoE-KO (n=6) mice in the hippocampus (c). GFAP+ astrocytic ApoE is present at high levels in 12-month-old Control (n=7) and Csf1r-ApoE-KO (n=7) mice, but significantly reduced in 5xFAD (n=11) and 5xFAD/Csf1r-ApoE-KO (n=6) mice in the hippocampus (d). Volcano plot comparing differentially expressed genes in the hippocampus between Control (4 months n=8; 12 months n=3) and Csf1r-ApoE-KO (4 months n=5; 12 months n=7) groups shows few genes are differentially expressed with microglial-expressed ApoE knock-out in 4- and 12-month-old mice (e, f). Statistical analysis for c, d used a one-way ANOVA with Tukey's multiple comparisons correction. Significance indicated as \*  $p < 0.05$ ; \*\*  $p < 0.01$ ; \*\*\*  $p < 0.001$ ; \*\*\*\*  $p < 0.0001$ ; #  $0.05 < p < 0.1$ .

## **Microglial-specific ApoE knock-out significantly increases plaque volume in aged 5xFAD mice**

We next investigated the role of microglial-expressed ApoE in plaque formation and homeostasis by performing immunohistochemistry (IHC) using Amylo-Glo (amyloid-specific dye for dense core plaques), and 6E10 (APP/A $\beta$ ; Fig. 1.2a, b). At 4- and 12-months of age, we found no differences in dense core plaque counts between 5xFAD and 5xFAD/*Csf1r-ApoE-KO* mice in the hippocampus or somatosensory cortex (Fig. 1.2c, d). However, 12-month-old mice lacking microglial-expressed ApoE had larger dense core plaques in the hippocampus compared to 5xFAD mice with intact microglial-expressed ApoE ( $P < .01$ ) (Fig. 1.2e, f). No differences were seen in 6E10<sup>+</sup> diffuse plaques between 5xFAD and 5xFAD/*Csf1r-ApoE-KO* mice (Fig. 1.2g). Notably, no CAA was observed in 5xFAD mice, nor was CAA induced in 5xFAD/*Csf1r-ApoE-KO* mice (Supp. Fig. 1.1a). No differences in insoluble or soluble A $\beta$ 1-40 and A $\beta$ 1-42 were seen between 5xFAD and 5xFAD/*Csf1r-ApoE-KO* mice at both 4 and 12 months of age, indicating that microglial-expressed ApoE may not contribute to overall A $\beta$  levels in the mouse brain (Fig. 1.2h-k). Importantly, for all analyses above there were no significant sex differences. Altogether, microglial-specific ApoE knock-out modestly affects plaque size, but not number of A $\beta$  plaques or overall A $\beta$  load.

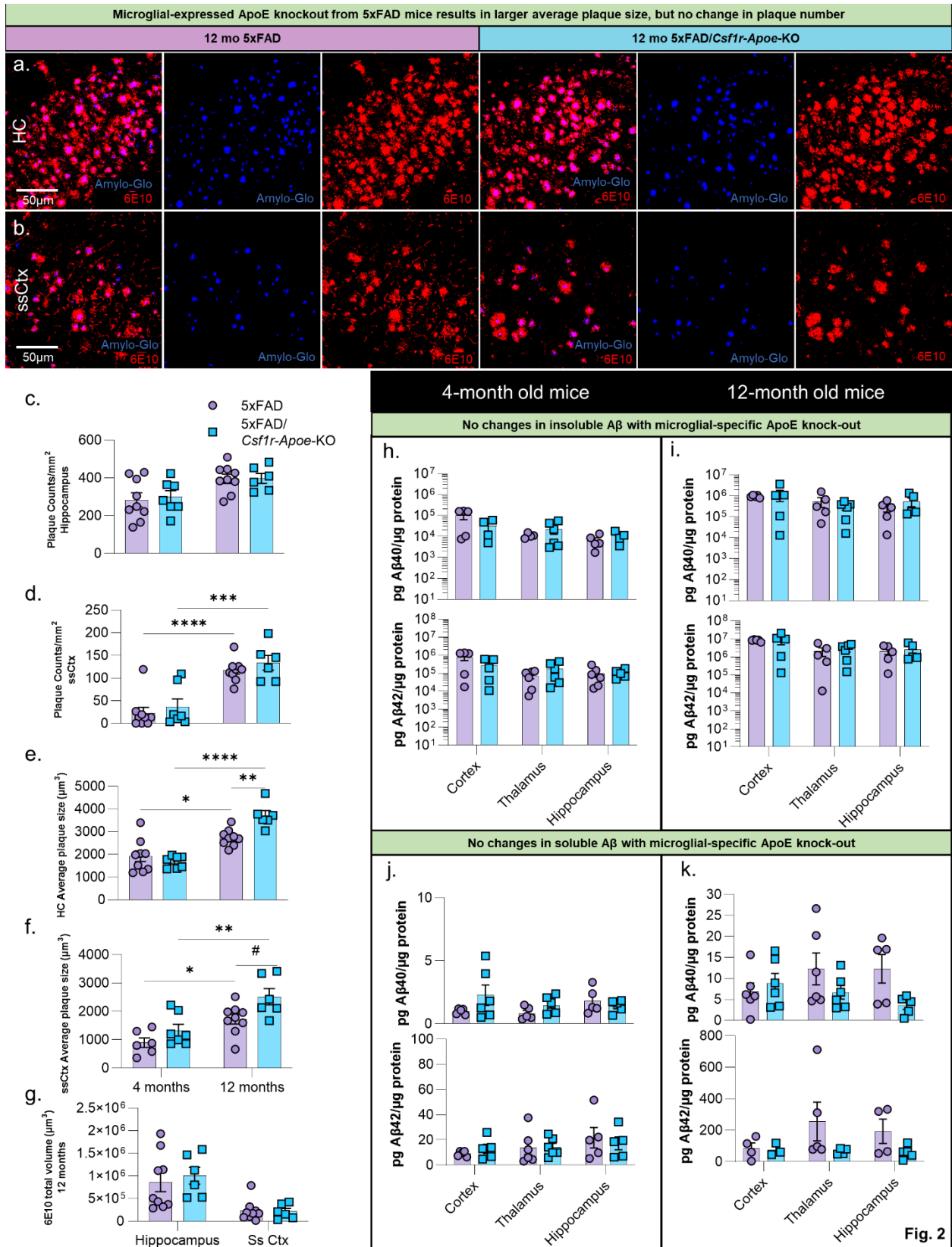
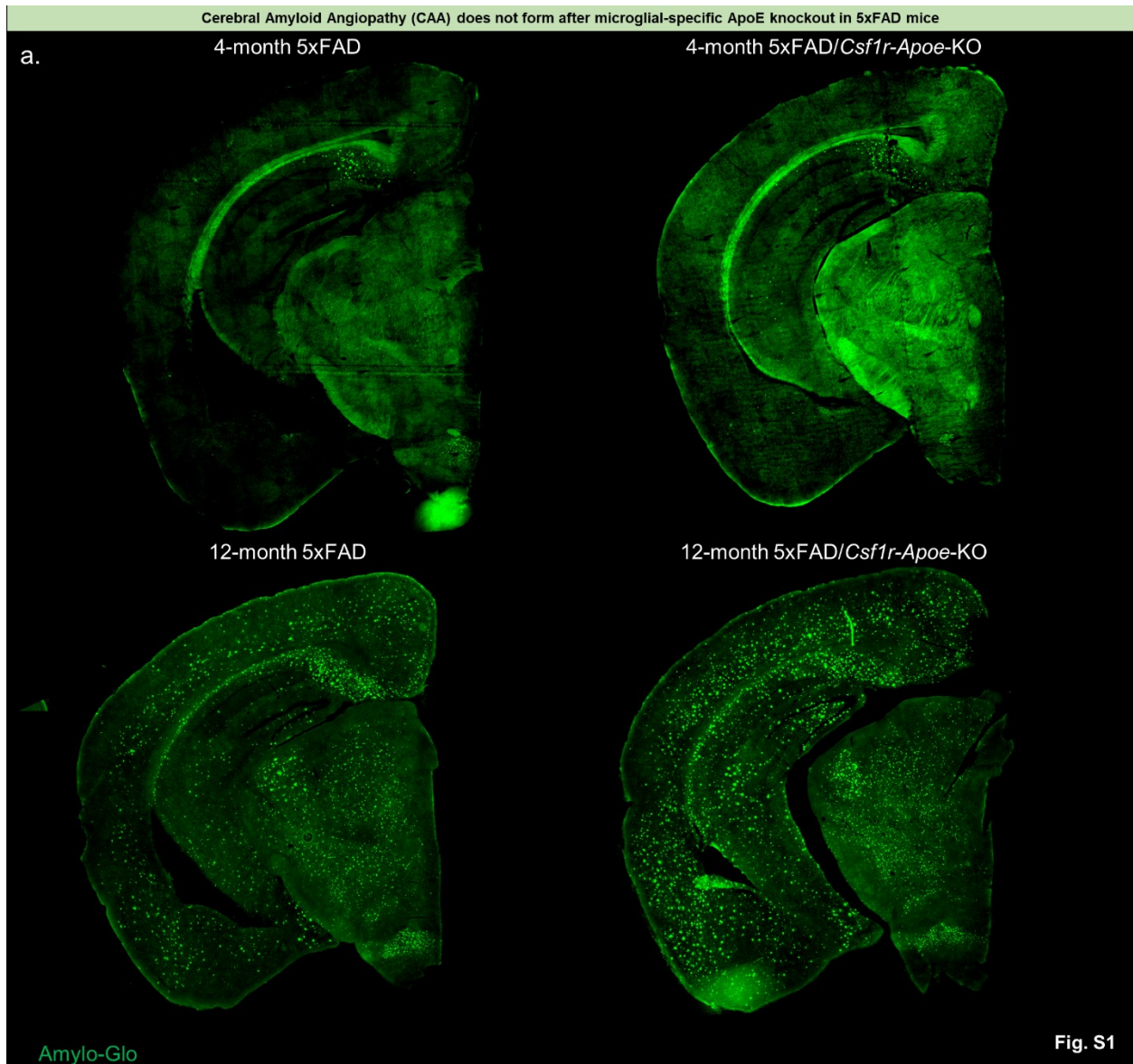


**Figure 1.2: Microglial-specific ApoE knock-out increases average plaque size while plaque number and A $\beta$  levels are unchanged in a 5xFAD mouse model.** Representative 20x images of Amylo-Glo (dense-plaque core) dye staining and 6E10 (diffuse amyloid plaques) immunofluorescence in 12-month-old 5xFAD and 5xFAD/*Csf1r-Apoe*-KO mice in the hippocampus **(a)** and somatosensory cortex **(b)**. No difference in plaque number was seen in the hippocampus between 5xFAD (4months n=9; 12 months n=9) and 5xFAD/*Csf1r-Apoe*-KO (4 months n=7; 12 months n=6) mice **(c)** or somatosensory cortex **(d)**. At 12 months of age, plaque volume was significantly increased in 5xFAD/*Csf1r-Apoe*-KO mice in the hippocampus **(e)** but not in the somatosensory cortex **(f)**. **(g)** No changes in diffuse A $\beta$  volume (6E10) associated with microglial-expressed ApoE knock-out were observed in the hippocampus or somatosensory cortex. No differences in insoluble A $\beta$ 40 or A $\beta$ 42 were present between 5xFAD (4 and 12 months: n= 5-6/brain region) and 5xFAD/*Csf1r-Apoe*-KO (4 and 12 months: n= 5-6/brain region) mice in the cortex, thalamus, or hippocampus at 4- **(h)** or 12-months **(i)** of age. Additionally, no difference in soluble A $\beta$ 40 or A $\beta$ 42 were observed between 5xFAD 5xFAD (4 and 12 months: n= 5-6/brain region) and 5xFAD/*Csf1r-Apoe*-KO 5xFAD (4 and 12 months: n= 3-6/brain region) in all regions at 4- **(j)** and 12-months **(k)** of age. Statistical analysis used a two-way ANOVA with Tukey's multiple comparisons correction. Significance indicated as \* p < 0.05; \*\* p < 0.01; \*\*\* p < 0.001; # 0.05 < p < 0.1.



**Supp. Figure 1.1: Microglial-specific ApoE knock-out results in no changes in cerebral amyloid angiopathy (CAA).** Slide-scanned images of sliced half-brains show no traces of CAA in 5xFAD and 5xFAD/*Csf1r*-*ApoE*-KO at both 4 and 12 months of age (**a**).

### **Microglial number and plaque association are unaltered with microglial-specific ApoE knock-out**

Having demonstrated that microglial-specific ApoE knock-out has modest effects on plaque size, but not plaque number, we sought to determine the effect of *ApoE* knock-out on microglial and astrocytic number, as well as microglial association with A $\beta$  plaques.

To assess microglial changes, we stained tissue from 4-month and 12-month-old mice with microglial markers IBA1 (Fig. 1.3a, b) and Pu.1 (Fig. 1.3a', b'). As expected, microglial numbers increased in 5xFAD and 5xFAD/*Csf1r-ApoE*-KO mice compared to Control and *Csf1r-ApoE*-KO mice at both 4- and 12-months of age in the hippocampus (Fig. 1.3e). In the somatosensory cortex, we also observed an increase in microglial number in the 5xFAD groups compared to the WT groups at 12 months of age, but not at 4 months of age (Fig. 1.3f). In both regions and at both timepoints, there were no differences in microglial number when comparing the 5xFAD with 5xFAD/*Csf1r-ApoE*-KO mice and Control with *Csf1r-ApoE*-KO mice, indicating that microglial-specific ApoE knock-out does not alter microglia number (Fig. 1.3e, f). Previously, microglia have been shown to actively regulate plaque compaction [17, 27, 184]. Having demonstrated that microglial-specific ApoE knock-out in 5xFAD mice resulted in significantly larger plaques, we sought to determine if *ApoE* deficient microglia were reacting differently to plaques. However, we found no difference in the number of plaque-associated microglia per  $\mu\text{m}$  of plaque diameter between our 5xFAD and 5xFAD/*Csf1r-ApoE*-KO mice in the hippocampus or somatosensory cortex, indicating microglial-expressed ApoE does not impact microglial presence around A $\beta$  plaques (Fig. 1.3c, d). Overall, while we do see changes in plaque size in microglial-expressed ApoE deficient mice, no changes in microglia number or plaque association were observed.



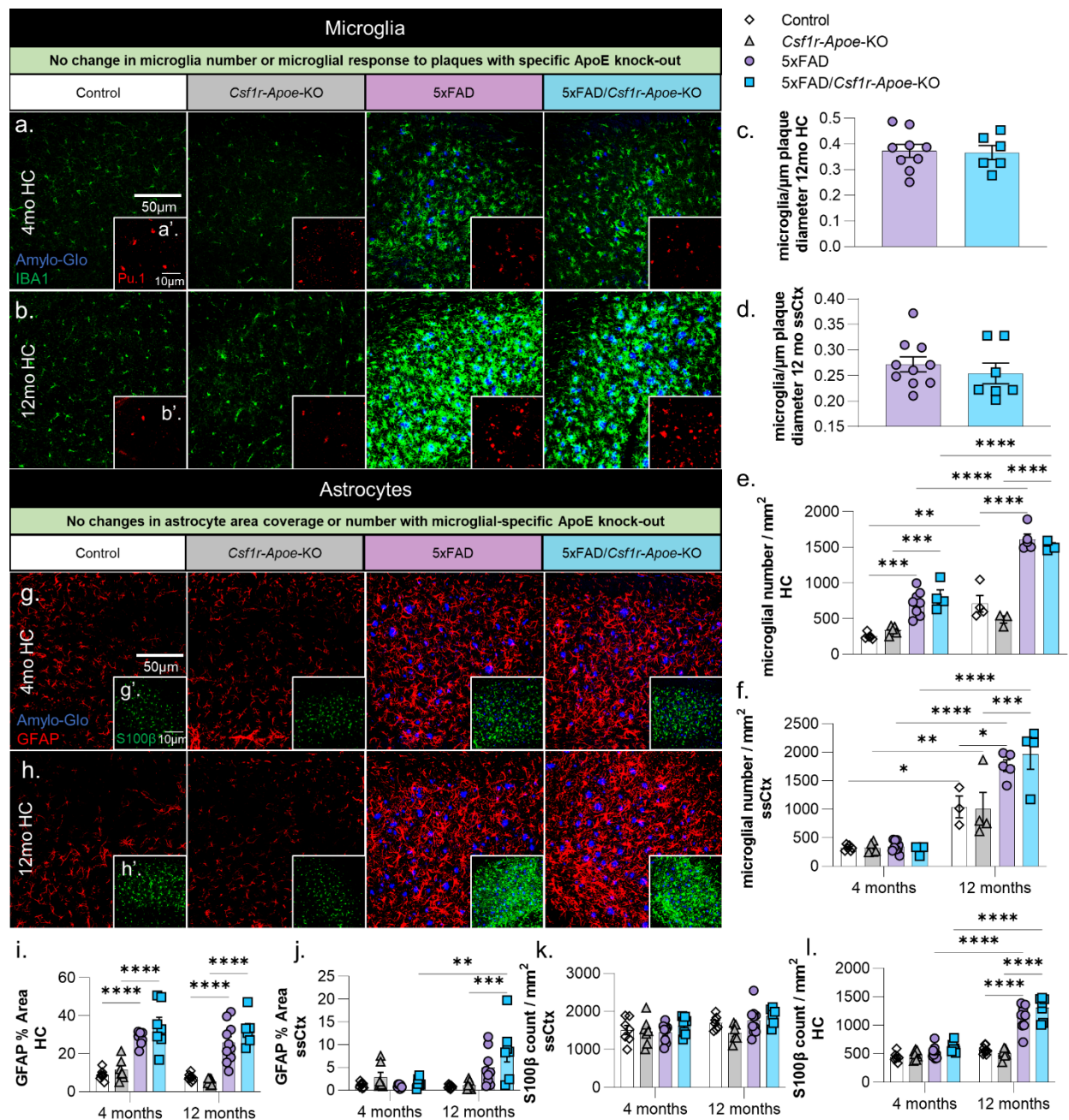


**Fig. 3**

**Figure 1.3: No microglial or astrocytic changes associated with microglial-specific ApoE knock-out.**

Representative 20x images of Amylo-Glo dye staining and IBA1 (microglia) immunofluorescence in Control, *Csf1r-Apoe-KO*, 5xFAD, and 5xFAD/*Csf1r-Apoe-KO* mice at 4- (a) and 12-months (b) of age in the hippocampus. Additional Amylo-Glo staining and Pu.1 (microglia) immunofluorescence images of all groups at 4- (a') and 12-months (b') of age in the hippocampus. No difference in the number of microglia/plaque diameter ( $\mu\text{m}$ ) was observed between 5xFAD (n=9) and 5xFAD/*Csf1r-Apoe-KO* (n=7) mice in the hippocampus (c) nor somatosensory cortex (d). Microglial number between Control and 5xFAD mice is increased at 12-months of age in but no differences in microglial number were seen between Control (4 months n=5; 12 months n=4) and *Csf1r-Apoe-KO* (4 months n=5; 12 months n=3) or 5xFAD (4 months n=8; 12 months n=5) and 5xFAD/*Csf1r-Apoe-KO* (4 months n=4; 12 months n=4) mice in the hippocampus (e)

nor somatosensory cortex (**f**). Representative 20x images of Amylo-Glo dye staining and GFAP (reactive astrocytes) immunofluorescence in all four groups at 4- (**g**) and 12-months (**h**) of age in the hippocampus. Additional Amylo-Glo staining and S100 $\beta$  (astrocyte cell bodies) immunofluorescence images of all groups at 4- (**g'**) and 12-months (**h'**) of age in the hippocampus. We observed significant increases in GFAP percent area quantifications in 5xFAD (4 months n=8; 12 months n=10) and 5xFAD/*Csf1r-Apoe*-KO (4 months n=7; 12 months n=6) groups compared to the Control (4 months n=7; 12 months n=8) and *Csf1r-Apoe*-KO (4 months n=7; 12 months n=7) in the hippocampus (**i**) at 4 and 12 months of age, and in the somatosensory cortex (**j**) at 12 months of age. In both the hippocampus and somatosensory cortex, no differences in astrocyte percent area were seen between Control and *Csf1r-Apoe*-KO groups or 5xFAD and 5xFAD/*Csf1r-Apoe*-KO groups. S100 $\beta$  astrocyte counts show no differences between Control and *Csf1r-Apoe*-KO groups or 5xFAD and 5xFAD/*Csf1r-Apoe*-KO groups in the hippocampus (**k**) or somatosensory cortex (**l**). Statistical analysis used a two-way ANOVA with Tukey's multiple comparisons correction and a two-tailed t-test for the microglia/plaque diameter ( $\mu$ m) quantification. Significance indicated as \*  $p < 0.05$ ; \*\*  $p < 0.01$ ; \*\*\*  $p < 0.001$ ; #  $0.05 < p < 0.1$ .

To gauge if there were changes in microglial activation associated with microglial-specific ApoE knock-out, we stained tissue from 4-month and 12-month-old mice with Cd68, a marker for microglial lysosomes (Supp. Fig. 1.2a, b). At 4- and 12-months of age in the hippocampus (Supp. Fig. 1.2a, c) and somatosensory cortex (Supp. Fig. 1.2b, d) we found no significant changes in Cd68 percent area between 5xFAD and 5xFAD/*Csf1r-Apoe*-KO mice. We next looked at homeostatic microglial marker P2ry12 and found a small but significant reduction in intensity when comparing the Control group with all other groups indicative of a loss of homeostatic function with disease, as expected, as well as with microglial-expressed ApoE knockout (Supp. Fig. 1.2e, f). Notably, this reduction was not further exacerbated with microglial-specific ApoE knock-out in tandem with AD pathology. Given the absence of *Apoe* mRNA from 5xFAD/*Csf1r-Apoe*-KO mice, we stained for ApoE protein to investigate if plaque associated microglia were taking up ApoE from other cellular sources. Colocalization of ApoE signal with either microglia or Amylo-Glo (representing dense core plaques) revealed that both contained ApoE protein in 5xFAD and 5xFAD/*Csf1r-Apoe*-KO mice (Supp. Fig. 1.2g-i).

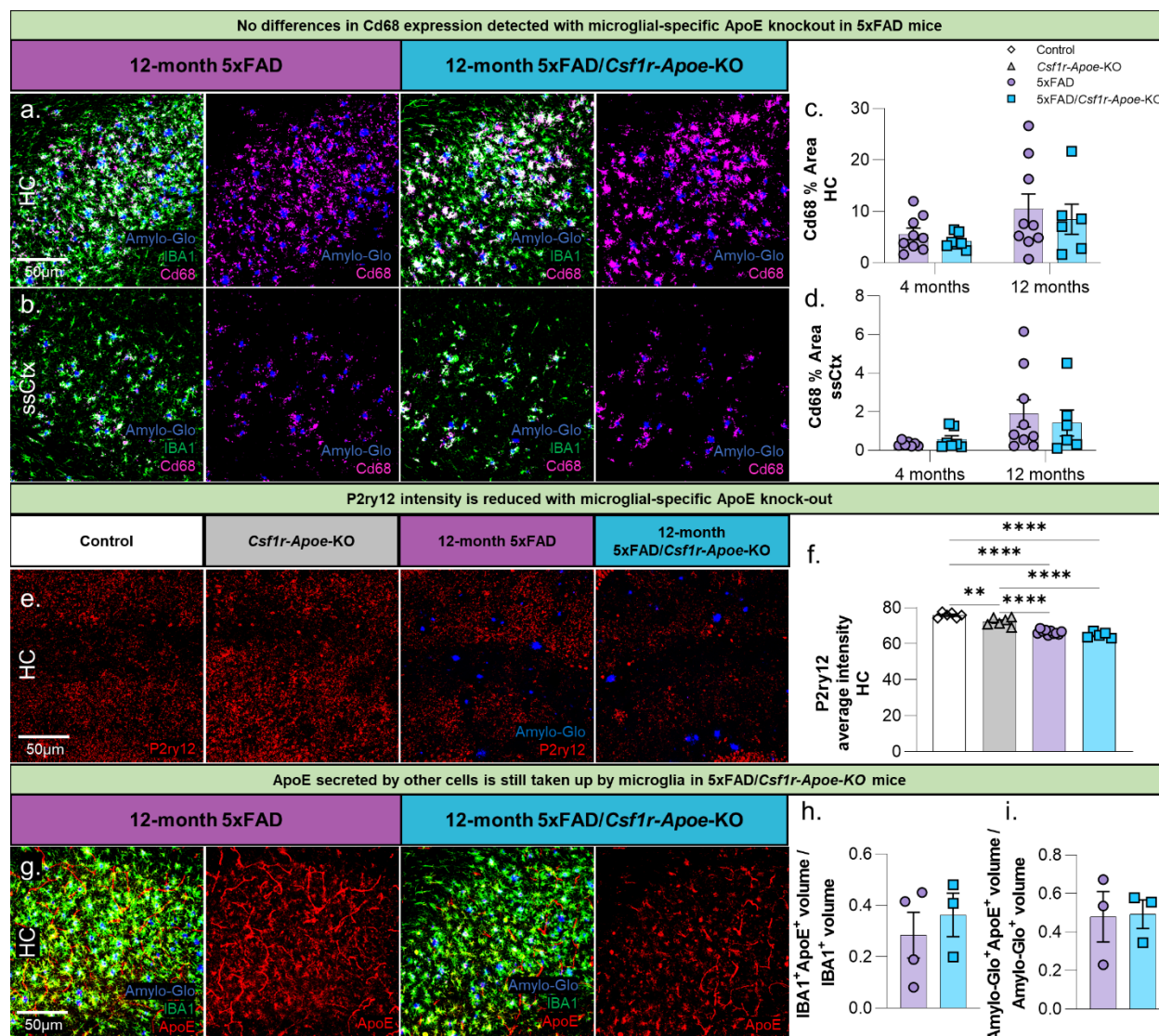


Fig. S2

**Supp. Figure 1.2: P2ry12 intensity is reduced with microglial-specific ApoE knock-out.**

Representative 20x images of Amylo-Glo dye staining and IBA1 and Cd68 immunofluorescence in 12-month-old 5xFAD and 5xFAD/*Csf1r*-ApoE-KO mice (a, b). No significant change in Cd68 percent coverage was observed between 5xFAD (4 months n=9; 12 months n=9) and 5xFAD/*Csf1r*-ApoE-KO (4 months n=7; 12 months n=6) mice in the hippocampus (c) nor the somatosensory cortex (d). Representative 20x images of Amylo-Glo dye staining and P2ry12 immunofluorescence in the hippocampus in Control, *Csf1r*-ApoE-KO, 5xFAD, and 5xFAD/*Csf1r*-ApoE-KO mice at 12 months of age (e). A significant reduction in P2ry12 staining was observed in *Csf1r*-ApoE-KO (n=6), 5xFAD (n=10), and 5xFAD/*Csf1r*-ApoE-KO (n=5) mice compared to Control (n=6) mice (f). Representative 20x images of Amylo-Glo dye staining and IBA1 and ApoE immunofluorescence in 5xFAD and 5xFAD/*Csf1r*-ApoE-KO mice. IBA1<sup>+</sup>ApoE<sup>+</sup> colocalized volume is unchanged between 5xFAD (n=4) and 5xFAD/*Csf1r*-ApoE-KO (n=3) mice (h) as is Amylo-Glo<sup>+</sup>ApoE<sup>+</sup> colocalized volume (i). Statistical analysis used a two-way ANOVA with Tukey's multiple comparisons correction for Cd68 % Area, a one-way ANOVA with Tukey's multiple comparisons correction for P2ry12 intensity, and a two-tailed t-test for the ApoE quantifications. Significance indicated as \* p < 0.05; \*\* p < 0.01; \*\*\* p < 0.001; # 0.05 < p < 0.1.

Under homeostatic conditions, astrocytes are the primary producer of ApoE in the mouse brain [20, 156, 215, 216]. We quantified astrocyte percent coverage and counts with GFAP and S100 $\beta$ , respectively (Fig. 1.3g, h). In the hippocampus, GFAP-positive astrocyte coverage was higher in 5xFAD and 5xFAD/*Csf1r-Apoe-KO* compared to Control and *Csf1r-Apoe-KO* mice at 4 and 12 months of age, as expected (Fig. 1.3i). The somatosensory cortex contained far less GFAP-positive astrocytes than in the hippocampus, however; GFAP-positive astrocyte coverage in 5xFAD/*Csf1r-Apoe-KO* mice was still significantly higher than in *Csf1r-Apoe-KO* mice at 12 months of age (Fig. 1.3j). In both regions and timepoints, there were no differences in GFAP positive astrocyte coverage when comparing the 5xFAD with 5xFAD/*Csf1r-Apoe-KO* mice and Control with *Csf1r-Apoe-KO* mice (Fig. 1.3i, j). S100 $\beta$  astrocyte counts in the hippocampus were elevated in 5xFAD and 5xFAD/*Csf1r-Apoe-KO* compared to Control and *Csf1r-Apoe-KO* in 12-month-old mice (Fig. 1.3k), but no differences in S100 $\beta$  counts were found in the somatosensory cortex (Fig. 1.3l). Additionally, no differences were seen between 5xFAD and 5xFAD/*Csf1r-Apoe-KO* mice, and Control and *Csf1r-Apoe-KO* mice in either brain region (Fig. 1.3k, l). Importantly, for all analyses above there were no significant sex differences. Altogether, no changes in astrocyte number or coverage were observed with microglial-specific ApoE knock-out.

### **Microglial-specific ApoE knock-out is associated with reductions in pre- and post-synaptic markers**

Recent studies indicate that Trem2-dependent microglial plaque compaction attenuates neuritic dystrophy and that knock-out of *Trem2* reduces the amount of plaque-associated ApoE [109, 153]. We sought to determine if the lack of microglial-expressed ApoE and

resultant increase in average plaque size in our 5xFAD/*Csf1r-Apoe*-KO would result in a change in dystrophic neurites. To that end, we observed a downward trend in Lamp1 dystrophic neurites in the hippocampus between 5xFAD and 5xFAD/*Csf1r-Apoe*-KO groups (Fig. 1.4a-c;  $p=.076$ ). To assess whether synaptic changes occurred with microglial-specific ApoE knock-out, we stained all groups with the post-synaptic marker, PSD95 (Fig. 1.4d, e), and presynaptic marker, Synaptophysin (Fig. 1.4h, i). Surprisingly, 12-month-old mice had significant reductions in both PSD95 and Synaptophysin in *Csf1r-Apoe*-KO, 5xFAD, and 5xFAD/*Csf1r-Apoe*-KO mice when compared to Control mice in both the hippocampus and visual cortex (Fig. 1.4f, g, j, k). No differences in synaptic markers were seen between 5xFAD and 5xFAD/*Csf1r-Apoe*-KO mice. These results suggest that microglial knock-out of ApoE drives reductions in synaptic puncta, however, synaptic puncta are not further reduced with microglial-specific ApoE knock-out in conjunction with AD pathology.

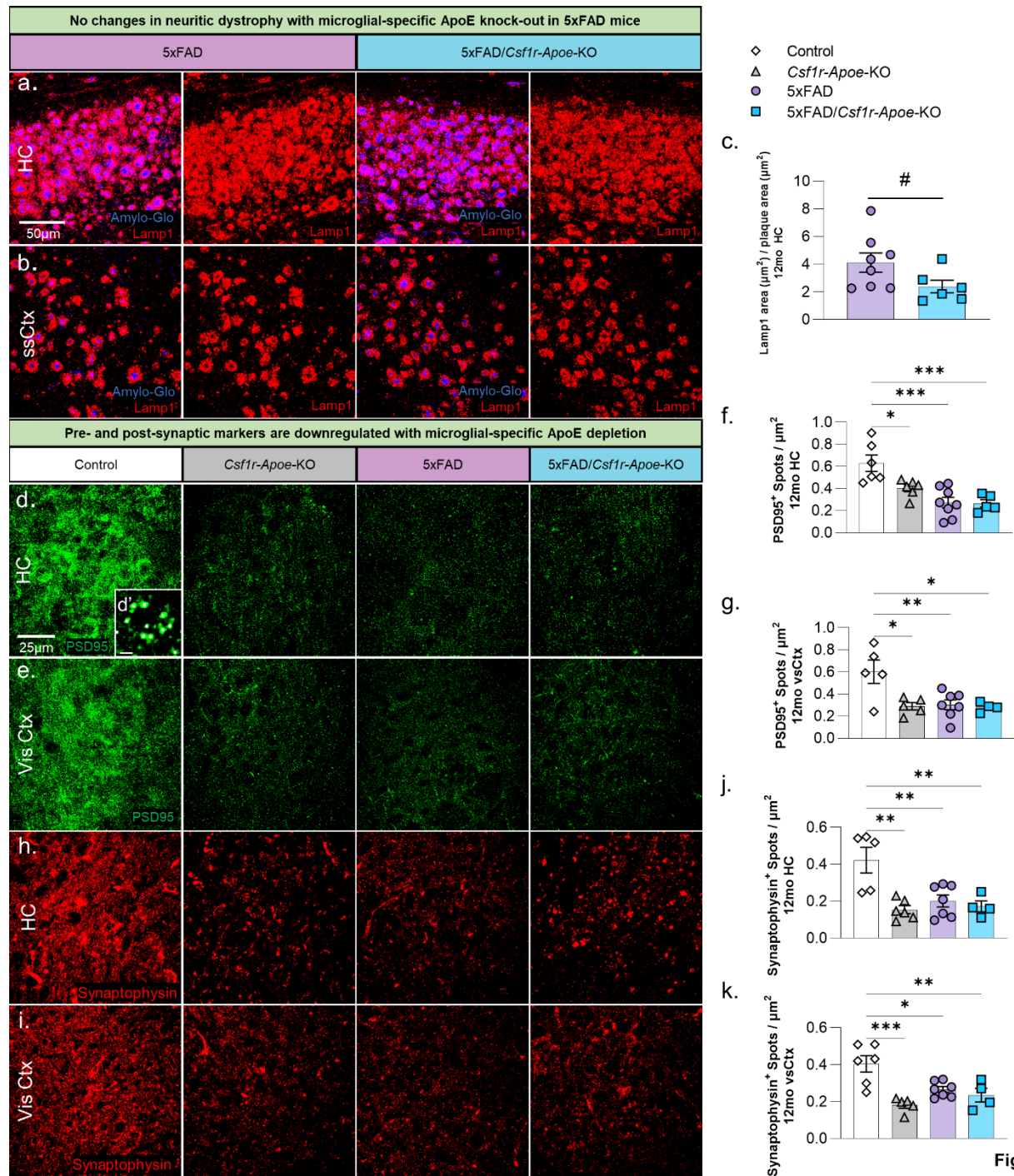


**Figure 1.4: Microglial-specific ApoE knock-out induces pre- and post-synaptic reduction.** Representative 20x images of Amylo-Glo dye staining and Lamp1 (dystrophic neurites) immunofluorescence in 12-month-old 5xFAD (n=8) and 5xFAD/*Csf1r*-*ApoE*-KO (n=6) mice in the hippocampus (a) and somatosensory cortex (b). No significant change in Lamp1 area/area of plaques ( $\mu\text{m}^2$ ) was observed in the hippocampus between both groups (c). Representative 63x images of post-synaptic marker, PSD95, immunofluorescence in Control, *Csf1r*-*ApoE*-KO, 5xFAD, and 5xFAD/*Csf1r*-*ApoE*-KO mice at 12 months of age in the hippocampus (d) and visual cortex (e). Inset image (d') shows individual post-synaptic puncta with each white dot representing one punctate. The number of PSD95 puncta was

significantly reduced in the *Csf1r-Apoe*-KO (HC n=6; vsCtx n=5), 5xFAD (HC n=8; vsCtx n=7), and 5xFAD/*Csf1r-Apoe*-KO (HC n=5; vsCtx n=4) groups compared to the Control (HC n=6; vsCtx n=5) group in the hippocampus (f) and the visual cortex (g). Representative 63x images of pre-synaptic marker, Synaptophysin, immunofluorescence in all four groups in the hippocampus (h) and visual cortex (i). Like PSD95, the number of Synaptophysin puncta was significantly reduced in the *Csf1r-Apoe*-KO (HC n=6; vsCtx n=5), 5xFAD (HC n=7; vsCtx n=7), and 5xFAD/*Csf1r-Apoe*-KO (HC n=4; vsCtx n=4) groups compared to the Control (HC n=5; vsCtx n=6) group in the hippocampus (j) and the visual cortex (k). Statistical analysis used a one-way ANOVA with Tukey's multiple comparisons correction and a two-tailed t-test for the Lamp1 quantification. Significance indicated as \* p < 0.05; \*\* p < 0.01; \*\*\* p < 0.001; # 0.05 < p < 0.1.

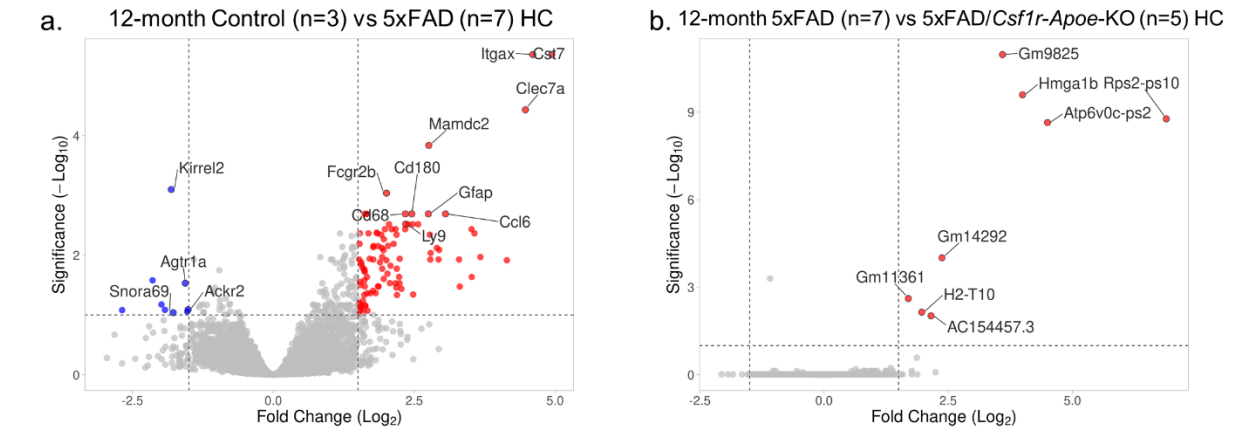
## **Few RNA changes associated with microglial-specific ApoE knock-out in an 5xFAD mice**

To determine whether microglial-specific ApoE knock-out affects overall gene expression in 5xFAD mice, bulk-tissue RNA sequencing of the mouse hippocampus was performed. As expected, expression of inflammatory genes was higher in 5xFAD mice compared to Control mice at both 4 and 12 months of age (Fig. 1.5a, Supp. Fig. 1.3a). This includes genes known as disease associated microglia (DAM) genes [94], such as *Cst7*, *Clec7a*, and *Itgax*, to name a few. When microglial-specific ApoE is knocked-out of 5xFAD mice, we found there is remarkably little change in gene expression at 4 and 12 months of age (Fig. 1.5b, Supp. Fig. 1.3b), indicating that microglial-specific ApoE knock-out in 5xFAD mice does not induce significant hippocampal gene expression changes at the bulk-tissue level. To explore changes in network gene expression, we utilized weighted gene co-expression network analysis (WGCNA) and identified 15 independent modules (Supp. Fig. 1.3c). Correlation of each module to either AD genotype (Fig. 1.5c) or *Apoe* KO genotype (Fig. 1.5d) revealed several modules of interest. Particularly, the *turquoise* module is highly correlated to AD genotype (5xFAD vs. non-5xFAD) and consists of 1398 genes, while the *green* module is highly correlated to both AD genotype and *Apoe* KO genotype (microglial-ApoE intact vs microglial-ApoE KO; correlation scores >.4) and

consists of 392 genes, with the *turquoise* module displaying gene network changes associated with microglia (Fig. 1.5e). For the *green* and *turquoise* modules, eigengenes were counted and plotted (Fig. 1.5f, g). While the *turquoise* module is strongly associated with AD genotype, it is not associated with *ApoE* KO genotype, and is upregulated in both 5xFAD and 5xFAD/*Csf1r*-*ApoE*-KO mice. It consists of microglial genes such as *Clec7a*, *Ctsl*, and *Ctsh* while pathway analyses identified GO terms such as *viral gene expression* and *viral transcription* (Fig 1.5h). Notably, the *green* module is associated with both AD and *ApoE* KO genotypes, and is only downregulated in 5xFAD mice, not 5xFAD/*Csf1r*-*ApoE*-KO mice, suggesting that microglial-specific knockout of ApoE prevents this network of genes from being downregulated. This *green* module is strongly enriched for genes associated with *axonogenesis*, *microtubule bundle formation*, and *chromatin remodeling*, with hub genes such as *Eif4g3*, *Ncoa1*, and *Huwe1* (Fig. 1.5i).



Few changes in gene expression associated with microglial-specific ApoE knock-out in 5xFAD mice at 12 months of age



Subtle rescue of 5xFAD associated neuronal networks may occur with microglial-specific ApoE knock-out

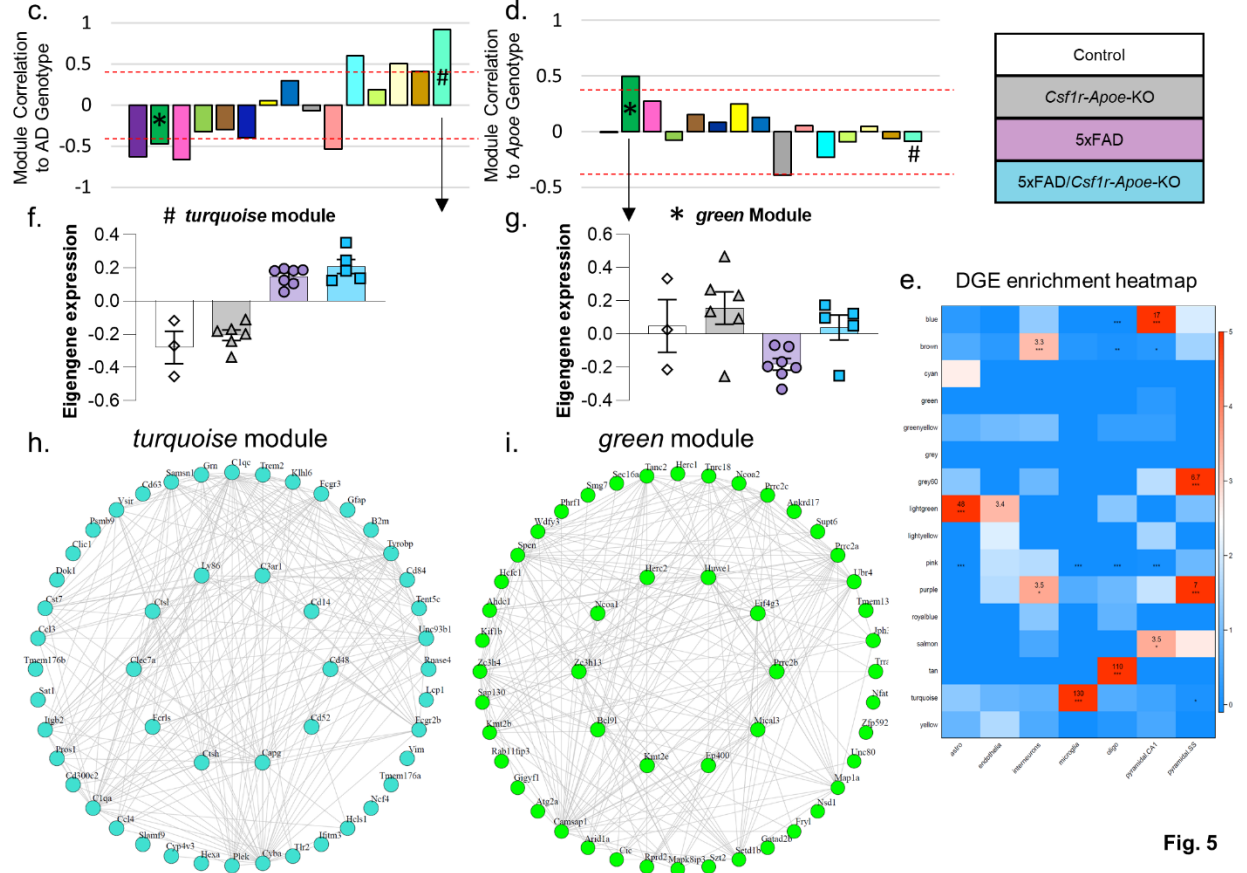
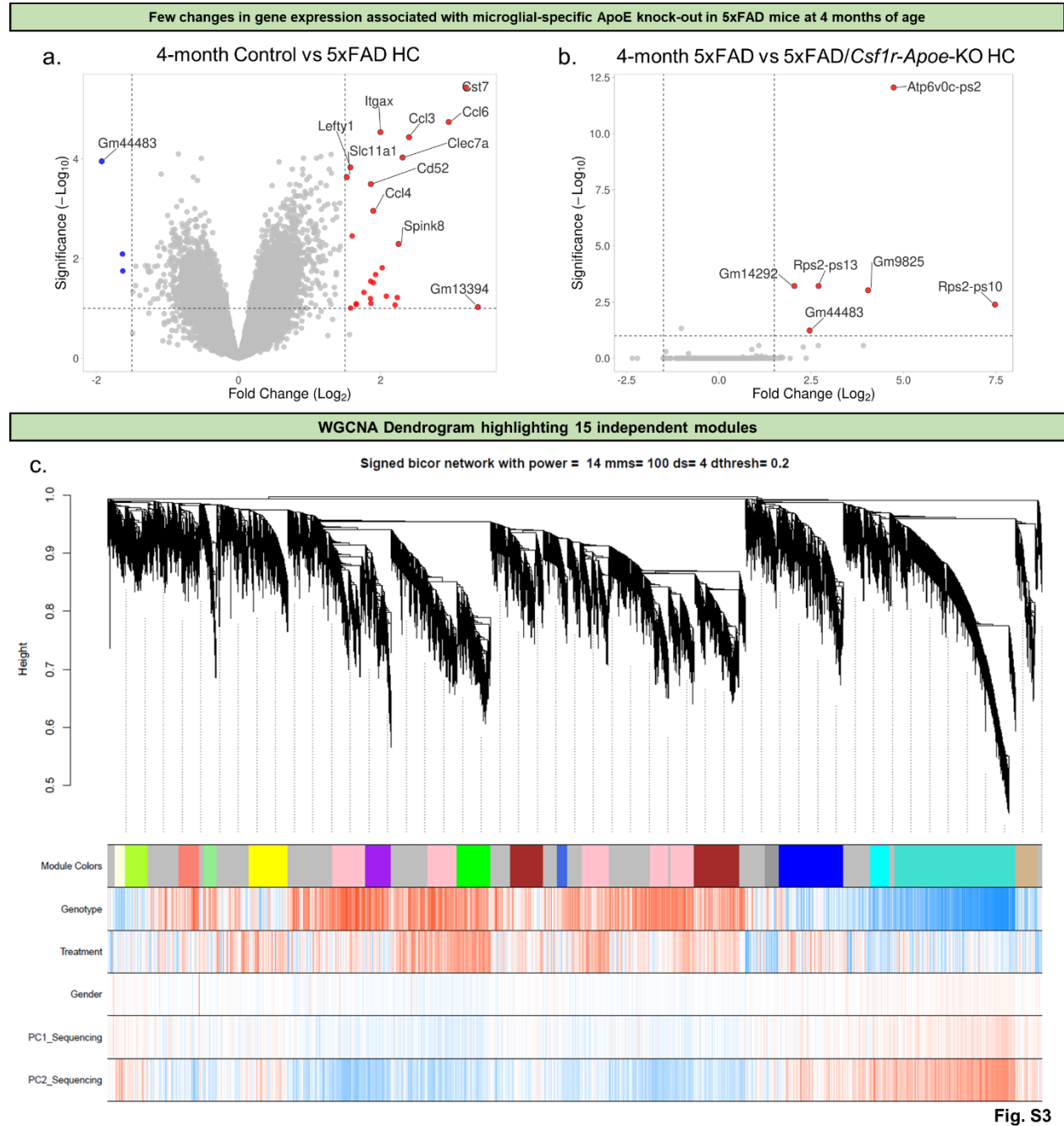


Fig. 5

**Figure 1.5: Few RNA changes associated with microglial-specific ApoE knock-out.** Volcano plot showing higher expression of inflammatory and other AD associated genes in the hippocampus of 5xFAD mice (n=7) compared to Control mice (n=3) at 12 months of age (a). Volcano plot showing very few changes in gene expression between 5xFAD (n=7) and 5xFAD/*Csf1r*-*Apoe*-KO (n=5) mice at 12 months of age (b). Correlation of modules generated by weighted gene correlation network analysis (WGCNA) to the AD genotype (Z-score cut-off: +/-0.4; \* = green module; # = turquoise module) (c). Correlation of modules

generated by WGCNA to *ApoE* genotype (Z-score cut-off:  $\pm 0.4$ ) (d). Cell-type enrichment heatmap displays genes associated with specific cell types within a given color module (e). Values provided indicate the number of genes within the network associated with that of a specific cell type. \*\*\* = 6+ genes. \*\* = 3+ genes. Module eigengene trajectory of gene expression value in *turquoise* (f) and *green* (g) modules. Interactive plot between hub genes extracted from the *turquoise* module showing a distinct AD signature (h). Interactive plot between hub genes extracted from the *green* module showing a distinct signature associated with *ApoE* knock-out (i).



**Supp. Figure 1.3: Few changes in gene expression associated with microglial-specific ApoE knock-out in 5xFAD mice at 4 months of age.** Volcano plot showing higher expression of inflammatory and other

AD associated genes in the hippocampus of 5xFAD (n=5) mice compared to Control (n=8) mice at 4 months of age **(a)**. Volcano plot showing very few changes in gene expression between 5xFAD (n=5) and 5xFAD/*Csf1r-Apoe*-KO (n=4) mice at 4 months of age **(b)**. WGCNA Dendrogram highlighting 15 independent modules **(c)**.

## **Discussion:**

In this study, we sought to determine the role of microglial-expressed ApoE in AD pathogenesis and homeostasis. Previous studies have utilized global ApoE knock-out mouse models to elucidate the role of ApoE in AD [11, 70, 99, 194]; however, these studies do not delineate the role of microglial-expressed ApoE from astrocytic-expressed ApoE. Astrocytes have the capacity to associate with A $\beta$  plaques in an ApoE-dependent fashion [98] and internalize A $\beta$  peptides [46, 127]. Therefore, there is a need to differentiate the roles of microglial- and astrocytic-*Apoe* in AD pathogenesis and homeostasis. To that end, we developed a mouse model that specifically eliminates microglial-*Apoe* expression. To accomplish this, we crossed *Csf1r-cre* mice with a 5xFAD mouse model and *Apoe<sup>fl/fl</sup>* mice. The resultant progeny had *Apoe* expression constitutively knocked-out of microglia.

A well-studied aspect of the role of ApoE in AD is its association with A $\beta$ . As previously noted, global ApoE knock-out has been shown to reduce the number A $\beta$  plaques [11, 70, 194], a finding that we found is recapitulated by elimination of microglia [184]. Importantly, our data indicate that plaque load is not diminished, and CAA load does not change with microglial-specific loss of ApoE. Total soluble and insoluble A $\beta$ 1-40 and A $\beta$ 1-42 also remained unchanged with microglial-specific ApoE knock-out. However, we do see a significant increase in average plaque size in the hippocampus. The increase in plaque size aligns with a previous study utilizing the APP/PS1 mouse model of AD, which found that global ApoE deficiency increased A $\beta$  plaque size, while decreasing amyloid burden

[194]. An increase in plaque size may indicate that microglial-expressed ApoE is necessary for microglial interaction with A $\beta$  plaques, in line with data indicating that microglia are necessary for plaque compaction [17, 27, 201]. Interestingly, reductions in ApoE signaling prior to plaque deposition was shown to prevent A $\beta$  accumulation in *APOE\* $\epsilon$ 4 knock in mice, whereas its reduction after the emergence of plaques had no impact on plaque load, but showed an increase in average plaque size [75], aligning directly with what we show following microglia-specific ApoE knock-out.*

With microglial-specific knock-out of ApoE we found no differences in microglial number nor in the number of microglia per  $\mu$ m of plaque diameter, indicating that microglial clustering around plaques is unaltered in this model. Additionally, we found that astrocytic number was unchanged with microglial-specific ApoE knock-out in 5xFAD mice. Previous studies have shown that global *Trem2* or *ApoE* knock-out decreases plaque-associated microgliosis in multiple mouse models of AD [11, 85, 99, 130, 201] which is not seen with the model used in this study. Additionally, the interaction between TREM2 and ApoE has been shown to drive the dysfunctional transcriptional phenotype of microglia in AD [99]. To explore whether this is recapitulated in our knockout model, we performed bulk-RNA sequencing on hippocampal tissue and observed very few changes in gene expression between 5xFAD mice and 5xFAD mice with microglial-specific ApoE intact. This included no changes in genes considered to be DAM associated (*Cst7*, *Trem2*, *Ctss*, *Itgax*, etc.). Additionally, there was no reduction in *ApoE* mRNA with microglial-specific ApoE knock-out in 5xFAD mice. Altogether, these data suggest microglial-expressed ApoE may not be necessary for the microglial transcriptional shift into a DAM state. It is important to clarify the limitations of bulk-tissue RNA sequencing as it reflects the averaged gene

expression across many different cell types in the hippocampus. Worth noting, we find that microglia may utilize ApoE produced by other cells in the brain, such as astrocytes, as we find evidence for ApoE protein within plaque associated microglia in 5xFAD/*Csf1r-Apoe*-KO mice.

In mouse models of AD, the absence of ApoE increases neuritic dystrophy [194] and synaptic loss [104, 123]. However, reductions in APOE signaling after initial plaque deposition in *APOE\** $\epsilon$ 4 APP/PS1-21 mice attenuate neuritic dystrophy, suggesting a time-specific role of ApoE in AD [75]. With microglial-specific knock-out of ApoE in 5xFAD mice, we found the ratio of dystrophic neurites to plaque volume trended downward ( $p=.076$ ), suggesting microglial-expressed ApoE may contribute to neuronal damage in AD.

To determine why there may be alterations in plaque size and neuritic dystrophy, we explored genetic network analysis, utilizing weighted gene co-expression analysis (WGCNA). We found 15 independent modules of which *turquoise* and *green* stood out. The *turquoise* module was highly correlated to AD genotype (5xFAD vs. non-5xFAD) while the *green* module was highly correlated to both AD and *Apoe* KO genotypes (microglial-ApoE intact vs microglial ApoE KO). Interestingly in the *green* module, eigengene expression for genes associated with this network were downregulated in 5xFAD mice but upregulated with microglial-specific ApoE knock-out. Go-term analysis revealed that these genes are involved in neuronal processes such as *axonogenesis*, *microtubule bundle formation*, and *chromatin remodeling*. This may indicate that microglial-specific ApoE possibly promotes these neuronal functions and could serve as

a reason why we see a downward trend in neuritic dystrophy in these mice compared to 5xFAD controls.

Reductions in synaptic proteins such as PSD95 have been observed in *APOE\**ε4 knock-in mice and *APOE\**ε4 postmortem human brain tissue [114, 117, 210]. We found both pre- and post- synaptic protein levels were reduced in microglial-specific ApoE knock-out mice and 5xFAD microglial-specific ApoE knock-out mice compared to ApoE intact controls at 12 months of age. Importantly, microglial-specific ApoE knock-out in 5xFAD mice did not further exacerbate synaptic marker loss seen in 5xFAD mice. To investigate further, we stained tissue with homeostatic microglial marker P2ry12 and found a loss in intensity associated with microglial-expressed ApoE knock-out, mirroring our synaptic protein findings (Fig. 5d-k). Recently, we have shown that dysregulation of homeostatic microglia through partial inhibition of *Csf1r* results in reduced P2ry12 expression and reduction in synaptic proteins [6]. In a similar manner, microglial-expressed ApoE knock-out may dysregulate microglial homeostasis potentially leading to changes in synapse maintenance and development outside of AD.

Collectively, our results indicate that microglial-expressed ApoE does not profoundly alter the course of AD pathogenesis, at least with regard to the microglial reaction to plaques and adoption of a disease-associated gene expression phenotype. However, while we explored the role of microglial-specific ApoE in AD in this study, it is worth mentioning that targeting ApoE in the mouse may have differential effects compared to studies targeting human *APOE* variants. Additionally, the involvement of microglial-expressed ApoE in the pathogenesis of tau pathology needs to be considered – *Trem2* knock-out studies have shown differential effects on inflammation in plaque vs. tau pathology developing mouse

models [87, 110, 201], while recent studies have highlighted the protective effects of both global ApoE knock-out and microglial depletion on brain atrophy induced by tau [179, 180]. Additionally, it was shown that the removal of APOE\* $\epsilon$ 4 from astrocytes stemmed neurodegeneration and lessened tau pathology and neurodegeneration in a P301S tauopathy mouse model [197]. These studies highlight the need to determine the role of microglial-specific knock-out of ApoE in tauopathy models.

## Chapter Two:

### Generation of a novel, inducible destabilized Cre mouse line to specifically target disease associated microglia

#### Highlights

- We have developed a novel mouse model which specifically targets disease associated microglia (DAMs) and can be used to manipulate DAM gene expression
- DAMs represent a subset of plaque associated microglia (PAMs), and DAM expression increases with disease progression
- Through spatial transcriptomic analyses, we find that DAMs have higher expression of disease and inflammatory genes compared to other PAMs

#### Summary

To explore the roles of microglia in the progression of Alzheimer's disease (AD), we need to develop models which specifically target diverse microglia subpopulations. Here, we develop a destabilized Cre recombinase (DD-Cre) mouse line knocked-in to the *Cst7* locus (*Cst7*<sup>DD-Cre</sup>) and crossed this line to the 5xFAD mouse model of AD and a tdTomato reporter line. We found that at early and aged disease timepoints, we can specifically label disease associated microglia (DAMs) that are around amyloid-beta (A $\beta$ ) plaques. Interestingly, the DAMs appear to be a subset of plaque-associated microglia (PAMs), and DAM expression appears to increase with age. Utilizing spatial transcriptomics approaches to identify tdTomato<sup>+</sup> cells, we found that DAMs specifically labelled by our model have increased disease and inflammatory gene expression compared to other microglial populations, including when compared to other PAMs that are not labelled. This



model can specifically target and manipulate DAMs and underlines the importance of targeted approaches when studying microglia in AD.

## **Introduction**

Alzheimer's disease (AD) is the most common neurodegenerative disease characterized by the appearance of amyloid-beta (A $\beta$ ) plaques and neurofibrillary Tau tangles (NFT). Microglia, the resident immune cells of the brain, cluster around A $\beta$  plaques in the brain parenchyma in what is theorized as an attempt to control and restrict plaques [17, 27]. Recently, targeting microglia in AD has become an emerging therapeutic avenue due to the identification via genome wide association studies (GWAS) of single nucleotide polymorphisms (SNPs) in genes highly enriched in microglia that confer a heightened risk of developing AD [72, 81, 101, 103, 188]. Our lab and others have shown that microglia are integral for plaque formation as well as responsible for downstream pathologies including synaptic, neuronal, and perineuronal net loss [30, 58, 184, 185], yet others have shown that the microglial response to plaques directly protects against disease progression. While we know microglia are key to disease pathologies and outcomes, the precise role of microglia in AD and neurodegeneration largely remains unknown, and there is considerable disagreement and contradiction in the literature that needs to be resolved (Table 1, 2, and 3).

For example, in exploring the role of microglia in AD, significant focus has been placed on triggering receptor expressed on myeloid cells 2 (TREM2), a transmembrane receptor known to be vital for the microglial transcriptional shift into a disease-associated microglia (DAM) state [94, 99, 126]. TREM2 is necessary for microglia to respond to and surround

plaques [86, 200]; studies targeting TREM2 have shown conflicting results as to whether the microglial response to A $\beta$  plaques, as well as tau pathology, is beneficial or harmful to various disease outcomes. Studies claiming that the microglia-A $\beta$  interaction is beneficial to AD outcomes have shown *Trem2* loss of function in AD mouse models is associated with a reduction in microglia clustering around A $\beta$  plaques which leads to worsening of neuritic dystrophy [200, 201, 212] and an increase in complement mediated synaptic loss [217]. Additionally, attempts to boost TREM2 signaling via overexpression/introduction of hTREM2 [105, 183], soluble TREM2 (sTREM2) [214, 218], or TREM2-promoting antibodies [196, 198] leads to increased microglial proliferation and metabolism, and improved disease outcomes in amyloid mouse models. To complement these studies in amyloidosis models, studies examining *Trem2* deficiency in tauopathy models observe exacerbation in tau pathology and spreading [14, 109]. While these studies indicate that the microglial response to plaques is beneficial, potential confounds and conflicting studies must be adequately considered. Firstly, loss of function mutations in genes expressed primarily in microglia such as *Trem2*, *Tyrobp*, and *Csf1r* are associated with distinct neurodegenerative diseases in humans, implicating microglial dysfunction in neurodegeneration [15, 182]. In the case of *Trem2*, the interpretation that *Trem2* knock-out worsens outcomes in AD models is clouded by its neurodegenerative disease-causing phenotype in humans [15]. Additionally, in contrast with the previously mentioned *Trem2* deficiency studies, other *Trem2* knock-out studies have shown reductions in A $\beta$  plaque deposition and inflammation, while maintaining reductions in microglial association with A $\beta$  plaques [85, 86]. In line with these data, knock-out of TREM2 downstream effector, TYROBP, reduces microglial-plaque interaction, neuritic

dystrophy, and behavioral deficits in AD mice [61]; although, studies targeting SYK, which directly binds TYROBP's ITAM domain, show SYK is neuroprotective in AD mouse models [36, 199]. Finally, microglial depletion in mouse models of tauopathy reduces tau pathology, and attenuates neurodegeneration [7, 122], while *Trem2* deficiency in a model of tauopathy similarly protects against neurodegeneration [110]. These discrepancies likely arise from caveats with the various animal models used in each study, as well as the disease-stage and brain-region specific effects of microglia in AD, and the complexity of targeting all microglia over discrete populations.

## TREM2 knock-out from amyloid or tau models:

Publication	Disease Model	Age	Microglial modulation	Effect on microglia	Effect on amyloid	Effect on tau	Other effects
Jay et al. 2015 (JEM)	AβPPS1	4 mo	Trem2 <sup>-/-</sup>	Reduce plaque-assoc. macs (CD45 <sup>hi</sup> /Ly6C <sup>+</sup> )	Reduce HC amyloid deposition, reduce insoluble Aβ	Reduce pMAPT (AT8 & AT180) associated with plaques	Reduce inflammation, Reduce astrogliosis
Wang et al. 2015 (Cell)	5xFAD	8.5 mo	Trem2 <sup>-/-</sup>	Fail to cluster around plaques	Increase Aβ accumulation in HC; Increase insoluble Aβ	-	Loss of layer-V neurons in HC
Wang et al. 2016 (JEM)	5xFAD + parabiosis	4 mo	Trem2 <sup>-/-</sup>	Plaques less enclosed by microglia; Plaque-associated are microglia	No change (more diffuse, less dense)	-	Increase neuritic dystrophy
Jay et al. 2017 (J Neurosci)	AβPPS1-21	2 & 8 mo	Trem2 <sup>-/-</sup>	No change (2 mo), Reduce Pu.1 and Tmem119 (8 mo) and CD45 <sup>hi</sup> , Reduce accumulation around plaques	Reduce plaque area (2 mo), No change (4 mo), Increase plaque area & size (8 mo)	-	Reduce amyloid internalization, Reduce astrogliosis; Reduce inflammatory genes
Leyns et al. 2017 (PNAS)	PS19	9 mo	Trem2 <sup>-/-</sup>	Reduce microgliosis	-	No change	Less atrophy; Reduce inflammatory cytokines; Reduce astrogliosis
Bemiller et al. 2017 (Mol Neurodegener)	hTau	6 mo	Trem2 <sup>-/-</sup>	Altered morphology and surface marker expression	-	Increase soluble and insoluble pTau (AT8, AT180, PHF-1) (not at 3 mo)	No difference in cytokines; Dysregulation in JNK/ERK
Leyns et al. 2019 (Nat. Neuro.)	NP tau injected model	Injected at 5.5 mo Sacrificed at 8.5 mo	TREM2 <sup>-/-</sup>	Reduce microgliosis	-	Exacerbate NP tau seeding and spreading	-

■ = microglia are beneficial  
■ = microglia are detrimental  
■ = nuanced

## TREM2 knock-out from amyloid + tau models, or TREM2 R47H knock-in:

Gratuzze et al. 2021 (JEM)	5xFAD + AD-tau inj	Inject at 6 mo, analyzed at 9 mo	PLX3397 (290 mg/kg) (3 wks before injection) +/- 14 wk repop +/- Trem2 <sup>-/-</sup>	Repopulated microglia show strong homeostatic gene signature	Repopulated microglia and Trem2 <sup>-/-</sup> increase amyloid plaques and plaque-associated ApoE	Trem2 <sup>-/-</sup> ; depletion and repopulated microglia elevate NP plaque pathology and NP-tau seeding	Increase neuritic dystrophy
Lee et al. 2021 (Neuron)	pR5-183 (P301L) TauPS2APP	6, 10, 18 mo 9 & 17 mo	Trem2 <sup>-/-</sup>	Blunted DAM activation (same as without amyloid)	Increased plaque diffuseness	Exacerbate tau accumulation and spreading (early age, with amyloid)	Promote brain atrophy (later stage, with amyloid)
Delizannis et al. 2021 (Acta Neuropath Comm)	5xFAD + AD-tau inj	4.5 mo	PLX3397 (1000 mg/kg + 290 mg/kg) Trem2 <sup>-/-</sup> Trem2 <sup>-/-</sup>	Reduction in PAMs Reduce DAMs	Reduction in cortical plaques Increased plaques (females)	Decrease in NP tau pathology Increase AT8 (more in Trem2 <sup>-/-</sup> )	Decrease in APP dystrophic processes
Yuan et al. 2016 (Neuron)	5xFAD AβPPS1-21 Human R47H	4 mo	Trem2 <sup>-/-</sup> Dap12 <sup>-/-</sup>	Abolish microglial barrier around plaque; no effect phagocytosis	Decrease plaque compaction	Increase tau hyperphosphorylation (human R47H)	Severe axonal dystrophy
Song et al. 2018 (JEM)	5xFAD	8.5 mo	Human CV or TREM2 <sup>R47H</sup> into mTrem2 <sup>-/-</sup>	Impair microgliosis; Reduce activation	No change	-	Soluble TREM2 shedding on neurons and plaques in CV, but not R47H (not impacted in vitro)
Gratuzze et al. 2020 (JCI)	PS19	3 & 9 mo	Human TREM2 <sup>R47H</sup>	Attenuate microglial reactivity; Decrease	-	Reduce p-tau	Attenuate brain atrophy and synapse loss

## Miscellaneous TREM2 studies:

Publication	Disease Model	Age	Microglial modulation	Effect on microglia	Effect on amyloid	Effect on tau	Other effects
Haure Mirande 2017 (ACTA Neuropathol.)	APPSP1	4 mo	TYROBP <sup>-/-</sup>	Reduce microglia activation and plaque association	Reduced circularity in plaques Decreased oligomeric A $\beta$	No effect in APPSP1 mice	Reduction in neuritic dystrophy (LAMP1) Improved spatial learning and memory
Ennerfelt et al. 2022 (Cell)	5xFAD	5 mo	SYK <sup>2;fl</sup>	Fail to cluster around plaques; reduced proliferation	Increase A $\beta$ accumulation in HC, Ctx, and thal	Increase in AT8 p-tau	Increase in dystrophic neurites (APP) Increased cell death Behavior deficits
Zhong et al. 2019 (Nature)	5xFAD	4 mo	Stereotactic injection or AAV mediated expression of sTREM2	Promotes microgliosis, phagocytosis, and migration	Reduction in hippocampal plaque load	-	Reduction in neuritic dystrophy
Wang et al. 2020 (JEM)	5xFAD; 5xFAD/ humanR47h	2 & 8 mo	hTREM2 mAb injection	Increased mg surveillance Expands metabolically active microglia	Reduces soluble A $\beta$ load	-	Ameliorates neuronal damage Reduces neuritic dystrophy
Lee et al. 2018 (Neuron)	5xFAD	4 & 7 mo	BAC-Trem2 overexpression	Increased microglial-plaque association	Reduced plaque levels at 4 mo	-	Reduced neuritic dystrophy
Van Lengerich et al. 2023 (Nat. Neuro.)	APP <sup>SAA</sup> , 5xFAD	5 mo	Trem2 activating antibody	Increase microglia metabolism and activation	-	-	Increased brain glucose metabolism

**Table 2.1: Conflicting reports of TREM2/microglial impact on AD.** A compilation of select studies knocking out TREM2 in amyloid, tau, and amyloid + tau models, studies using TREM2 R47H mutations, and studies manipulating TREM2 not via knock-out in various mouse models. Effects from these studies that support the assertion that TREM2, and thereby microglial reaction to pathology, is beneficial are colored in green, while data asserting the opposite are colored in red. Studies that show a more nuanced reaction are colored in both red and green.

The emergence of single-cell RNA sequencing has provided unprecedented insight into the heterogeneity of microglia, identifying transcriptionally distinct microglial subpopulations, including but not limited to: DAMs [94], Injury responsive microglia (IRM) [57], axon tract associated microglia (ATM) [57, 111, 124, 125], and white matter associated microglia (WAM) [165]. Of particular interest, DAMs are characterized by increased expression of inflammatory genes such as *Trem2*, *Cst7*, *Lpl*, *Axl*, *Clec7a*, *Itgax*, *Ccl6*, and others, and likely represent plaque associated microglia (PAMs) in the AD brain [94]; however, the exact relationship between DAMs and PAMs is unknown and the question of whether DAMs represent all, or just a subset of PAMs remains. Worth noting,

many of the gene changes that occur in DAMs are conserved in IRMs, ATMs, and WAMs [57, 94, 165]. These studies suggest that microglia have distinct signaling pathways and functions based on their location within the brain and their association with disease/injury. Previous data from our lab reinforces this idea, as CSF1R inhibition in a 5xFAD mouse model depleted a much higher percentage of non-plaque associated microglia (NPAM) versus PAMs, suggesting that PAMs may be less reliant on CSF1R signaling for survival [184]. With this in mind, we sought to develop tools which could be used to distinguish between these two populations.

Altogether, the role of microglia in AD and other neurodegenerative diseases is most-likely very nuanced, with population dependent effects. To complicate matters further, microglia have been shown to have age- and brain-region specific effects in the AD brain [39, 50, 82, 85, 159]. To begin to understand the role of microglia in AD, we first need to understand the contributions of PAMs/DAMs to disease pathology and outcomes, separately from other microglial populations. To that end, we have developed a novel, inducible Cre recombinase mouse line which has destabilized Cre (DD-Cre) knocked-in to the locus of a highly upregulated DAM gene, *Cst7*, allowing us to target DAMs with temporal specificity. Through this approach, we show that our model specifically targets DAMs, and through spatial transcriptomics, we find that these unique cells represent a subset of the entire PAM population, further highlighting the importance of determining the exact roles that these diverse microglial subsets have in AD.

## **Methods**

### **Animals**

All animal experiments performed in this study were approved by the UC Irvine Institutional Animal Care and Use Committee (IACUC) and were compliant with ethical regulations for animal research and testing. The 5xFAD mouse has previously been described in detail [144] and the following primers were used to genotype these animals: PS1 Forward 5' - AAT AGA GAA CGG CAG GAG CA – 3' and PS1 Reverse 5' - GCC ATG AGG GCA CTA ATC AT – 3'. For DAM-specific labelling, *Cst7*<sup>DD-cre</sup> (Transgenic Mouse Facility (TMF) at UCI), For genotyping *Cst7*<sup>DD-cre</sup> the following primers were used: WT *Cst7* F 5' – CCCAAGTCCTGAAGATGAAGCG - 3', WT *Cst7* R 5' – CCACCGCCTGATCTATGGTG – 3', and *ecDHFR* R 5' – GCATAGCGTTTTCCATCCCG – 3'. For genotyping *Ai14*<sup>tdTomato</sup> mice, the following primers were used: WT Forward 5' – AAGGGAGCTGCAGTGGAGTA – 3', WT Reverse 5' – CCGAAAATCTGTGGGAAGTC – 3', Mutant Reverse 5' – GGCATTAAGCAGCGTATCC - 3', and Mutant Forward 5' – CTGTTCTGTACGGCATGG – 3'.

### **Animal Treatments**

2.5- and 9.5-month-old 5xFAD/ *Cst7*<sup>DD-cre</sup>/*Ai14*<sup>tdTomato</sup> old mice were treated with trimethoprim (TMP; Sigma Aldrich, T0667-250mg) at 0.8mg/mL in drinking water for 1.5 months. At the end of treatment, mice were euthanized via CO<sub>2</sub> inhalation and transcardially perfused with 1X phosphate buffered saline (PBS). For all studies, brains were removed, and hemispheres separated along the midline. Brain halves were either flash frozen for subsequent biochemical analysis, or drop-fixed in 4% Paraformaldehyde (PFA; Thermo Fisher Scientific, Waltham, USA) for subsequent immunohistochemical

analysis. Half brains were collected into 4% PFA for 48 hrs and then transferred to a 30% sucrose solution with 0.02% sodium azide for another 48-72 hrs at 4C. Fixed half brains were sliced at 40  $\mu$ m using a Leica SM2000 R freezing microtome and sliced tissue was stored in 30% glycerol, 30% ethylene glycol, and 1xPBS solution at -20°C.

### *Cuprizone (CPZ) treatment*

10-month-old *Cst7<sup>DD-Cre</sup>/Ai14<sup>tdTomato</sup>* were fed 0.3% cuprizone chow (Envigo, Indianapolis, IN) and given 0.8mg/mL TMP through drinking water for 6 weeks. Weights of individual mouse and chow consumptions of each cage were recorded, and chow was changed every 7 days to monitor expected weight loss as well as ensuring freshness of cuprizone chow. Brains were collected and fixed in 4% paraformaldehyde for 24 h followed by cryoprotection by immersion in 5% sucrose for 24 h then 30% sucrose for 5 days, all at 4 °C before slicing.

### **Immunohistochemistry**

Fluorescent immunolabeling was performed using a standard indirect technique as described previously [67, 68] Primary antibodies and dilutions are used as follows: anti-ionized calcium-binding adapter molecule 1 (IBA1; 1:1000; 019–19741; Wako, Osaka, Japan), anti-CD11c (1:200, 50-112-2633; eBioscience), anti-CST7 (courtesy of Dr. Collin Watts, University of Dundee, UK). Thioflavin-S (Thio-S; 1892; Sigma-Aldrich) and Amylo-Glo (TR-300-AG; Biosensis, Thebarton, South Australia, AU) was used according to manufacturer's instructions to visualize A $\beta$  plaques.

For Amylo-Glo staining, tissue sections were washed in 70% ethanol 1X5 minutes, followed by a 1X2 minute wash in distilled water. Sections were then 1% Amylo-Glo solution for 1X10 minutes then washed with 0.9% saline for 1x5 minutes and distilled



water for 1X15 seconds. For Thio-S staining, tissue sections were placed for 1×10 min incubation in 0.5% Thio-S diluted in 50% ethanol. Sections were then washed 2×5 min each in 50% ethanol and one 10-min wash in 1xPBS before continuing with fluorescent immunolabelling. Sections were then briefly rinsed in 1XPBS and immersed in normal serum blocking solution (5% normal serum with 0.2% Triton-X100 in 1XPBS) for 60 minutes. Tissue was then incubated overnight in primary antibody at the dilutions described above in normal serum blocking solution at 4 degrees Celsius. The next day tissue sections were washed in 1XPBS 3X10 minutes before being placed in appropriate secondary antibody in normal serum blocking solution (1:200 for all species and wavelengths; Invitrogen) for 60 minutes. Tissue sections were then washed for 3X10 minutes in 1XPBS before tissue was mounted and coverslipped. High resolution fluorescent images were obtained using a Leica TCS SPE-II confocal microscope and LAS-X software. To capture whole brain stitches, automated slide scanning was performed using a Zeiss AxioScan.Z1 equipped with a Colibri fluorescence light source and Zen AxioScan 2.3 software.

### **Data Analysis and Statistics**

Both male and female mice were used in all statistical analyses. Statistical analysis was accomplished using Prism GraphPad (v9.0.0). To compare two groups, the unpaired Student's t-test was used. To compare 2 or more groups at a single timepoint or in a single brain region, one-way ANOVA with Tukey's multiple comparison correction was performed. To compare 2 or more groups at either different timepoints or brain regions, with multiple treatments/genotypes, two-way ANOVA with Tukey's multiple comparison

correction was used. For all analyses, statistical significance was accepted at  $p < 0.05$ . and significance expressed as follows: \* $p < 0.05$ , \*\* $p < 0.01$ , \*\*\* $p < 0.001$ .

### **Single-cell Spatial Transcriptomics**

Isopentane fresh-frozen brain hemispheres were embedded in optimal cutting temperature (OCT) compound (Fisher, 23-730-571), and 10 $\mu$ m thick coronal sections prepared using a cryostat (Leica CM1950). Six hemibrains were mounted directly onto VWR Superfrost Plus microscope slide (Avantor, 48311-703) and kept at  $-80^{\circ}\text{C}$  until fixation. 5xFAD/*Cst7*<sup>DD-Cre</sup>/*Ai14*<sup>tdTomato</sup> (n=3), and WT/*Cst7*<sup>DD-Cre</sup>/*Ai14*<sup>tdTomato</sup> (n=1) treated with TMP, and WT/*Cst7*<sup>DD-Cre</sup>/*Ai14*<sup>tdTomato</sup> treated with cuprizone (CPZ) and TMP (n=2) were used for transcriptomics. Tissues were processed according to the Nanostring CosMx fresh-frozen slide preparation manual (MAN-10159-01) for RNA assays.

### **Tissue preparation for spatial transcriptomics**

Briefly, slides were fixed in 10% neutral buffered formalin (NBF; EMS Diasum, 15740-04) for 2 hours at  $4^{\circ}\text{C}$ , followed by a series of washes in 1x PBS and dehydration with 50%, 70% and 100% ethanol. Antigen retrieval was performed at  $100^{\circ}\text{C}$  for 15 minutes with CosMx Target Retrieval Solution followed by tissue permeabilization for 30 minutes and fiducial application. After post-fixation with 10% NBF and NHS-Acetate (Fisher, 26777), in situ hybridization with the 1000-plex Mouse Neuro RNA panel and rRNA segmentation marker was done overnight for 16-18 hours in a hybridization oven at  $37^{\circ}\text{C}$ . Two stringent washes with 50% formamide and 4x saline-sodium citrate (SSC) solution at  $37^{\circ}\text{C}$  for 30 minutes each were done prior to nuclear DAPI stain for 15 minutes. Tissues were incubated in GFAP and histone cell segmentation markers for 1 hour before flow cells were assembled according to the CosMx manual. Once assembled, flow cells were

loaded into the CosMx machine with roughly 300 FOVs selected per slide, capturing the cortex and hippocampus. Slides were imaged in the machine for 7 days before the data were uploaded to the Nanostring AtoMx platform for further analysis and visualization. Pre-processed data was then exported as a Seurat object for further analysis in R v4.3.1.

### **Spatial transcriptomics data analysis**

Spatial transcriptomics datasets were filtered using the AtoMx RNA Quality Control module to flag poorly performing probes, cells, FOVs, and target genes. Datasets were then normalized and scaled using Seurat SCTransform to account for differences in library size across cell types [25, 55]. Principal component analysis (PCA) and uniform manifold approximation and projection (UMAP) analysis were performed to reduce dimensionality for downstream analysis. Unsupervised clustering at 1.0 resolution yielded 38 clusters for the dataset. Clusters were manually annotated based on gene expression and spatial location. Differential gene expression analysis per cell type between genotypes was performed using MAST to calculate the average difference, defined as the difference in average expression levels between two conditions [38]. Differential upregulation (DU) and differential downregulation (DD) scores were calculated by summing the product of the negative  $\log_{10}(\text{padj})$  and the average difference for each statistically significant gene ( $\text{padj} < 0.05$ ) with an absolute average difference greater than 0.3. Microglia were then subsetted and further subclustered for deeper analysis. Data visualizations were generated using ggplot2 [204].

## **Results**

### **Generation of a novel destabilized Cre (DD-Cre) mouse line to target DAMs**

To develop a mouse model which can selectively target and modulate DAMs, we screened for genes that were upregulated by microglia around plaques but were not expressed under homeostatic conditions. Utilizing previous data from microglia depleted 5xFAD mice via chronic CSF1R inhibitor administration [184], we identified 10 candidate genes that had upregulated RNA levels in 5xFAD mice, but nearly abolished levels with microglial depletion: *Ccl6*, *Clec7a*, *Cst7*, *Ctsd*, *Ctsz*, *C1qa*, *Hexb*, *Siglech*, *Sip1*, and *Itgax* [184]. From this list we analyzed which genes had undetectable expression in the wild-type brain and found *Cst7* to be a suitable candidate as it had high expression in 5xFAD mice, but essential no expression when microglia were eliminated, and zero expression in the WT brain [184]. Having identified *Cst7* as an appropriate driver, we wanted to develop a model in which gene expression in DAMs could be targeted inducibly, ideally allowing for long-term targeting and without utilization of tamoxifen, which is potentially toxic, poor at crossing the BBB, and has effects on macrophage populations [13, 74, 78, 168]. Furthermore, many other cell-type specific driver lines result in haploinsufficiency of the target gene, which itself becomes a confound. An alternative to tamoxifen inducible cre recombinase has been described that instead relies on the presence of the antibiotic trimethoprim, known as DD-Cre [168]. DD-Cre systems utilize destabilized bacterial dihydrofolate reductase (ecDHFR). ecDHFR is normally degraded through the proteasomal pathway, however, when in the presence of the antibiotic trimethoprim (TMP), its decay is blocked. This allows stabilization of the Cre protein and subsequent recombination at loxP sites. Not only is the use of trimethoprim safer for the mice, but it can also be dissolved into the animal's drinking water allowing for long term treatment, whereas tamoxifen can only safely be administered short-term. Hence, we have

developed a novel, inducible destabilized Cre recombinase (DD-Cre) mouse line in which DD-Cre was knocked into the *Cst7* locus (*Cst7*<sup>DD-Cre</sup>) (Fig. 2.1A).

Importantly, the DD-Cre genetic sequence is followed by a P2A linker, meaning there will be no knockout of endogenous *Cst7* gene expression in these mice, and instead, the Cre protein and CST7 should be produced independently of one another (Fig. 2.1A).

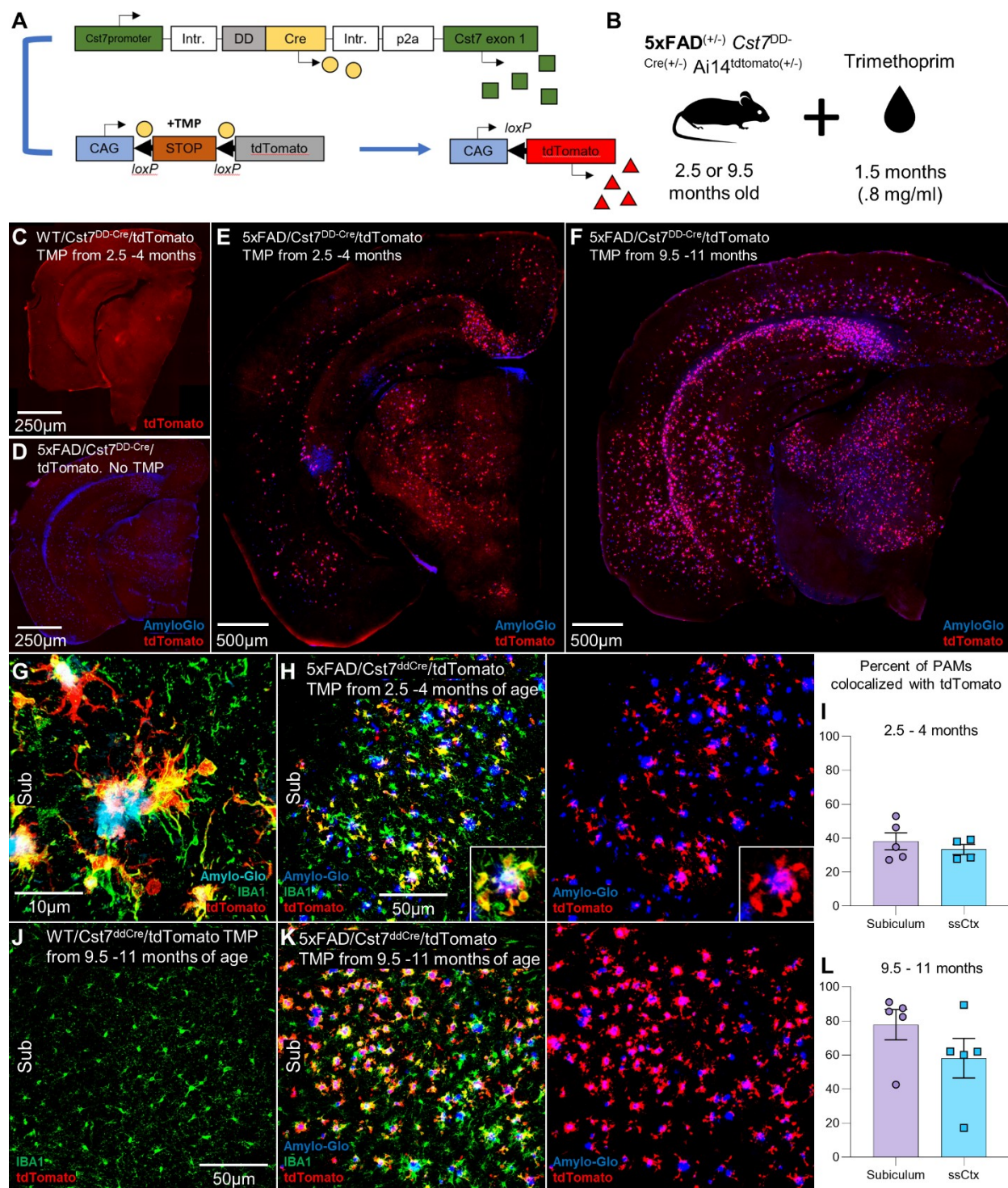


**Figure 2.1: Novel *Cst7*<sup>DD-Cre</sup> mouse line specifically targets plaque associated microglia (PAMs).**

(A) Diagram showing genetic paradigm. When trimethoprim (TMP) is administered, the DD-Cre cuts loxP sites flanking the STOP cassette preceding the tdTomato genetic sequence. tdTomato will then be expressed only in *Cst7* expressing cells.

(B) Schematic showing experimental paradigm. 2.5 and 9.5 month old 5x*FAD*/*Cst7*<sup>DD-Cre</sup>/*Ai14*<sup>tdtomato</sup>(+/-) mice were treated with TMP in their drinking water for 1.5 months before sacrifice.

(C-F) Representative 10x whole-slide scan images of WT/*Cst7*<sup>DD-Cre</sup>/*Ai14*<sup>tdtomato(+/-)</sup> mice treated with TMP (C), and 5xFAD/*Cst7*<sup>DD-Cre</sup>/*Ai14*<sup>tdtomato(+/-)</sup> mice not treated with TMP (D) show no expression of tdTomato. Meanwhile 4 month (E) and 11 month (F) 5xFAD/*Cst7*<sup>DD-Cre</sup>/*Ai14*<sup>tdtomato(+/-)</sup> mice treated with TMP show robust tdTomato expression.

(G) 63x Airyscan image in a 5xFAD/*Cst7*<sup>DD-Cre</sup>/*Ai14*<sup>tdtomato(+/-)</sup> mouse showing tdTomato colocalization with microglial marker, IBA1, and plaque stain, Amylo-Glo.

(H-I) 20x representative confocal microscopy image of 4 month 5xFAD/*Cst7*<sup>DD-Cre</sup>/*Ai14*<sup>tdtomato(+/-)</sup> mouse subiculum showing tdTomato proximity to plaques and microglial colocalization (H). Quantification of the percentage of PAMs that colocalize with tdTomato is 38% and 33% for the subiculum and somatosensory cortex, respectively (I).

(J) 20x confocal microscopy image showing no tdTomato expression in WT/*Cst7*<sup>DD-Cre</sup>/*Ai14*<sup>tdtomato(+/-)</sup>.

(K-L) 20x representative confocal microscopy image of 11 month 5xFAD/*Cst7*<sup>DD-Cre</sup>/*Ai14*<sup>tdtomato(+/-)</sup> mouse subiculum showcasing tdTomato proximity to plaques and microglial colocalization (K). Quantification of the percentage of PAMs that colocalize with tdTomato is 78% and 58% for the subiculum and somatosensory cortex, respectively (L).

### ***Cst7*<sup>DD-Cre</sup> specifically targets DAMs in the 5xFAD mouse model**

To investigate whether the *Cst7*<sup>DD-Cre</sup> line specifically and inducibly targets CST7 expressing cells, we bred these mice to the 5xFAD mouse model of AD and subsequently bred their offspring with a loxP-stop-loxP tdTomato reporter line knocked into the Rosa26 locus (*Ai14*<sup>tdTomato</sup>; Fig. 2.1A). Under normal conditions, the stop cassette ensures no transcription of the proceeding tdTomato sequence, as the cassette mediates transcriptional termination via repeated polyA signaling. However, upon stabilization of the DD-Cre protein via TMP, DD-Cre will cut at both loxP sites flanking the stop cassette. Once the stop cassette is excised, tdTomato can be expressed via the CAG promoter. In 5xFAD hemizygous mice, plaques begin to form in the thalamus and subiculum at around 3 months of age [144, 162] and synaptic and neuronal loss starting as early as 6 months of age [41, 84, 144]. To look at both early and late responses to plaques, we treated 2.5 and 9.5 month old 5xFAD/*Cst7*<sup>DD-Cre</sup>/*Ai14*<sup>tdTomato</sup> mice with TMP for 1.5 months at a concentration of 0.8mg/ml in their drinking water at which point mice were sacrificed at 4- and 11-months of age, respectively (Fig. 2.1B).

As expected, WT/*Cst7*<sup>DD-Cre</sup>/*Ai14*<sup>tdTomato</sup> mice treated with TMP show no tdTomato recombination in the brain (Fig. 2.1C) as there is no *Cst7* expression in the WT mouse brain. Additionally, we do not see tdTomato expression in 5xFAD<sup>+/-</sup>/*Cst7*<sup>DD-Cre</sup>/*Ai14*<sup>tdTomato</sup> mice that were not treated with TMP (Fig. 2.1D) indicating that there is no leakiness associated with the Cre line. Importantly, 5xFAD<sup>+/-</sup>/*Cst7*<sup>DD-Cre</sup>/*Ai14*<sup>tdTomato</sup> mice treated with TMP have brain-wide recombination of tdTomato in plaque associated areas in both the young (Fig. 2.1E) and aged (Fig. 2.1F) cohorts, but not in areas outside the vicinity of plaques. Further, using confocal microscopy, we find that, in our young cohort, tdTomato fluorescent signaling colocalizes only with IBA1+ PAMs in the brain (Fig. 2.1G, H) and labels ~38% and ~33% of PAMs in the subiculum and somatosensory cortex, respectively (Fig. 2.1I). In our aged cohort, we again find that tdTomato fluorescence colocalizes only with IBA+ PAMs (Fig. 2.1K), but to an even greater extent than in young mice, with ~78% and ~58% of PAMs colocalizing with tdTomato in the subiculum and somatosensory cortex, respectively (Fig. 2.1L). This is a dramatic increase in PAM targeting compared to the young cohort, indicating that DAM gene expression may increase with disease progression.

To further characterize these cells, we performed IHC staining for the DAM marker CD11c in young (Fig. 2.2A) and aged cohorts (Fig. 2.2b) and found that 84% and 86% of CD11c+ cells colocalized with tdTomato in the subiculum in young and aged cohort, respectively (Fig. 2.2C), indicating our mouse line targets cells that express or have expressed DAM genes. We previously found that MAC2/LGALS3 stains both infiltrating myeloid cells in the brain, as well as a small subset of PAMs [69]. Staining for MAC2 in young (Fig. 2.2D) and aged (Fig. 2.2E) cohorts and show that around 41% and 52% of MAC2+ cells



colocalized with tdTomato in the subiculum in young and aged cohort, respectively (Fig. 2.2F), indicating that a distinct subset of MAC2<sup>+</sup> PAMs that are not tdTomato/CD11c<sup>+</sup> exists. Ultimately, these results indicate that the novel *Cst7*<sup>DD-Cre</sup> mouse line can effectively target DAMs and asserts that even within microglia that cluster around plaques there may be functionally and transcriptionally different subsets of cells.

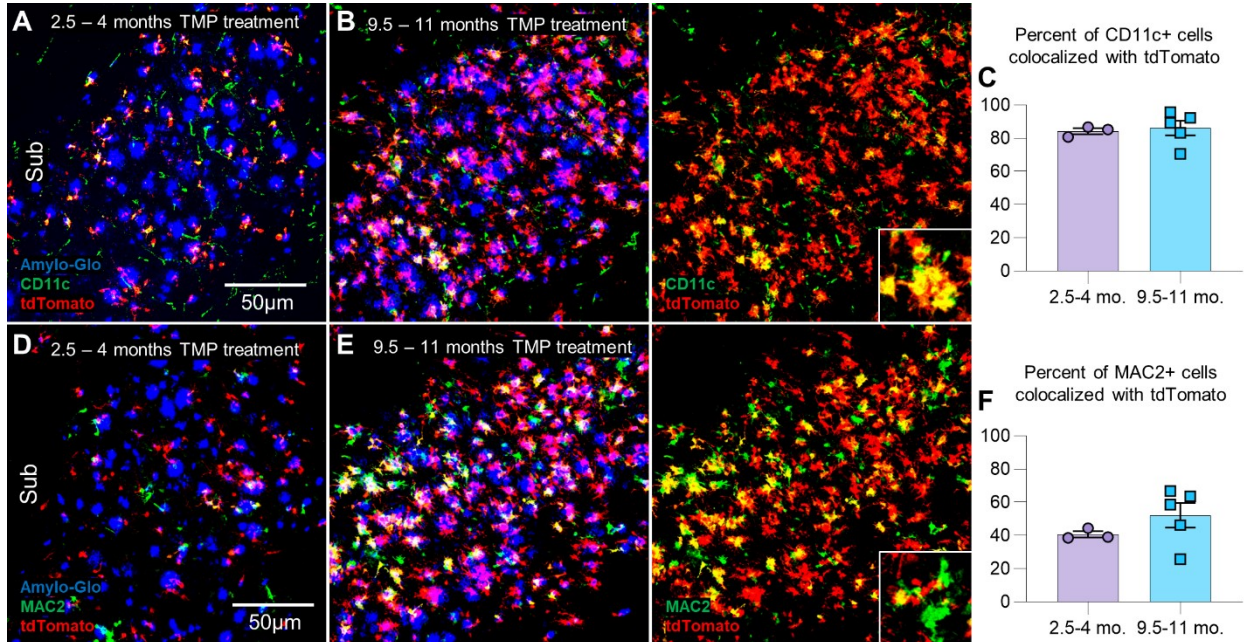


**Figure 2.2: tdTomato<sup>+</sup> cells colocalize more specifically to DAM markers.**

(A-C) 20x representative confocal microscopy images of 4 month (A) and 11 month (B) 5x*FAD*/*Cst7*<sup>DD-Cre</sup>/*Ai14*<sup>tdtomato(+/-)</sup> mice show colocalization of DAM marker CD11c with tdTomato. Roughly 84% and 86% of CD11c<sup>+</sup> cells are colocalized with tdTomato<sup>+</sup> cells at 4 month and 11 months of age, respectively (C). (D-F) 20x representative confocal microscopy images of 4 month (D) and 11 month (E) 5x*FAD*/*Cst7*<sup>DD-Cre</sup>/*Ai14*<sup>tdtomato(+/-)</sup> mice show colocalization of infiltrating macrophage marker MAC2 with tdTomato. Roughly 41% and 52% of MAC2<sup>+</sup> cells are colocalized with tdTomato<sup>+</sup> cells at 4 month and 11 months of age, respectively (F).

### ***Cst7*<sup>DD-Cre</sup> targets DAMs associated with white matter in an inducible demyelinating cuprizone mouse model**

While DAMs were first characterized in the 5x*FAD* mouse model [94], DAMs or DAM-like cells have since been found in other plaque models [43, 145], tauopathy models [43, 110], and other neurodegenerative/ demyelinating models [24, 83, 99, 126, 186]. We aimed to

see if our  $Cst7^{DD-Cre}/Ai14^{tdTomato}$  mouse model was capable of targeting DAMs in other disease models by utilizing cuprizone (CPZ) which is a copper-chelating chemical that causes oligodendrocytic cell death, demyelination, and brain wide neuroinflammation, particularly in white-matter areas [16]. 10-month  $Cst7^{DD-Cre}/Ai14^{tdTomato}$  mice were treated with TMP delivered via drinking water and a CPZ diet for 1.5 months (Fig. 2.3A).  $Cst7^{DD-Cre}/Ai14^{tdTomato}$  treated with CPZ and TMP exhibit robust tdTomato fluorescence around white-matter areas in the brain (Fig. 2.3B), and all tdTomato signal colocalizes with IBA1+ microglia particularly in white-matter regions such as the striatum (Fig. 2.3C), and the Corpus Callosum (Fig. 2.3D). Of note, tdTomato signal colocalizes with DAM marker CD11c (Fig. 2.3E) and infiltrating myeloid marker MAC2 (Fig. 2.3F). Ultimately, our model is able to target DAMs in both the 5xFAD model and an inducible demyelinating mouse model.

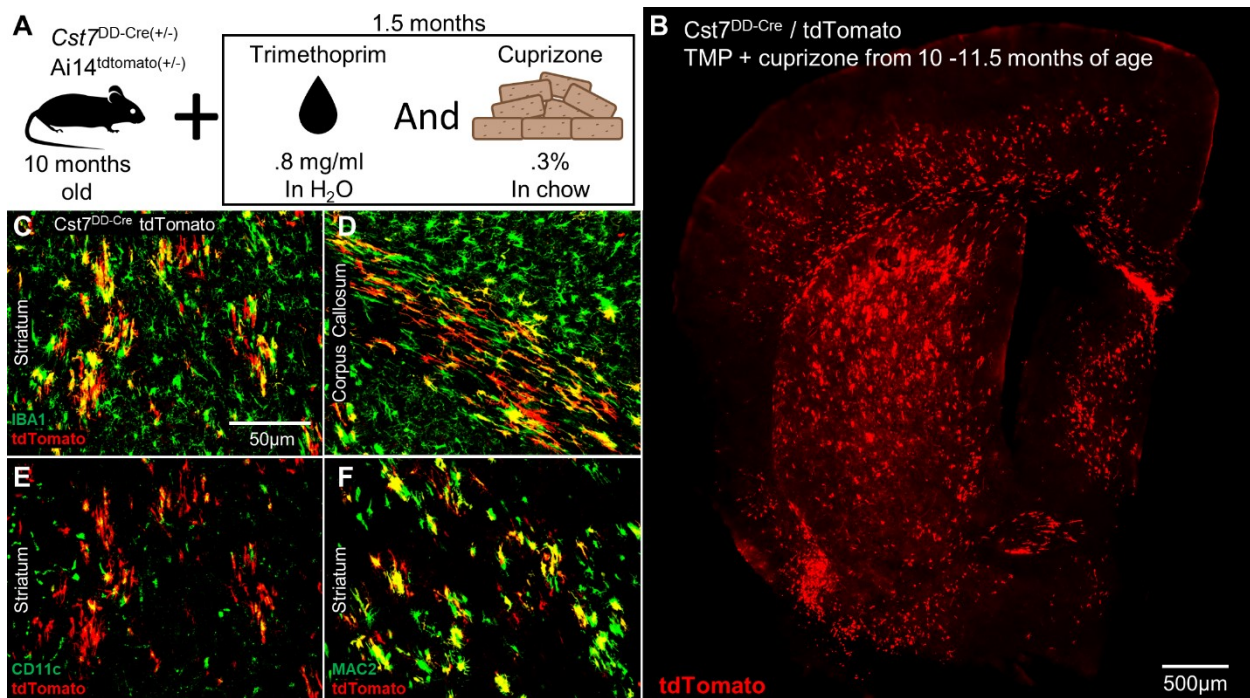


**Figure 2.3:** WT/ $Cst7^{DD-Cre}/Ai14^{tdTomato(+/-)}$  mice fed a demyelinating cuprizone diet and treated with TMP show tdTomato expression in white matter-associated microglia.

(A) Schematic showing experimental paradigm. 10 month WT/*Cst7*<sup>DD-Cre</sup>/*Ai14*<sup>tdtomato(+/-)</sup> were treated with TMP in their drinking water and fed a cuprizone diet for 1.5 months before sacrifice.  
(B) 10x whole-slide scan image of tdTomato expression shows robust expression in white-matter areas of the brain.  
(C-D) 20x confocal microscopy images of the white matter areas of the brain, the striatum (C), and the corpus callosum (D), show colocalization of tdTomato with microglia around white matter.  
(E,F) 20x confocal microscopy images of the white matter areas of the striatum showing tdTomato colocalization with CD11c (E) and MAC2(F)

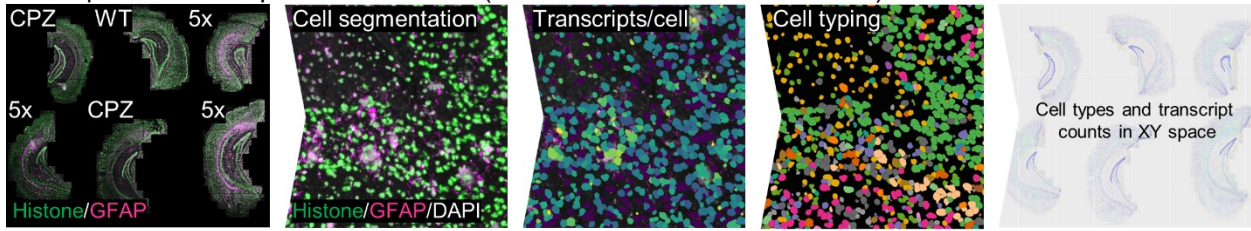
## **Spatial transcriptomics reveal tdTomato<sup>+</sup> microglia have higher DAM expression compared to other microglial populations**

Since the *Cst7*<sup>DD-Cre</sup> mouse line can specifically target DAMs while keeping other microglial cells, including other PAMs, unaffected, we next aimed to characterize the differences between these DAMs with other cells. To accomplish this, we utilized a novel spatial transcriptomics approach which can measure gene expression of 1000 different genes in every cell in a given brain section. In this experiment, a custom probe for tdTomato and other relevant microglial genes were added to the standard 1000 plex mouse neuroscience panel. First, the brain slices are hybridized by RNA probes and FOVs for area of interest are selected for each brain. In our case, we chose to analyze the hippocampus and cortex of three 11-month-old 5xFAD<sup>+/-</sup> *Cst7*<sup>DD-Cre</sup>/*Ai14*<sup>tdTomato</sup>, two 10-month-old CPZ/ *Cst7*<sup>DD-Cre</sup>/*Ai14*<sup>tdTomato</sup>, and one 11-month-old WT/ *Cst7*<sup>DD-Cre</sup>/*Ai14*<sup>tdTomato</sup> mice all treated with TMP (Fig. 2.4A). In each FOV, cells are identified and segmented using Histone, GFAP, and DAPI, then the transcripts of each gene per cell are measured, and data visualization and interpretation can proceed using Seurat.

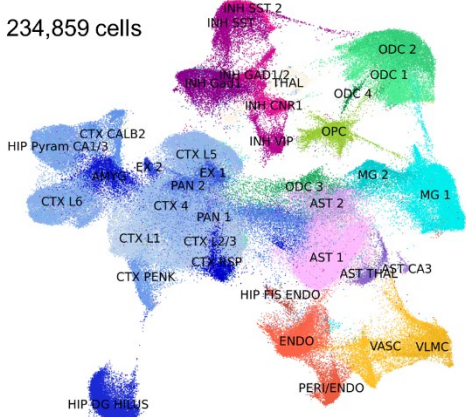
To visualize the data, we first clustered a total of 234,859 cells into a UMAP and found 38 different clusters of cells (Fig. 2.4B) that were annotated according to gene expression and spatial location (Fig. 2.4C). Based on the expression of *Csf1r* (Fig. 2.4D), *Cst7* (Fig. 2.4E), and *tdTomato* (Fig. 2.4F) on the UMAP, we found two clusters of microglia (MG 1

and MG 2) comprised of 19,568 cells. We then took the cells from MG 1 and MG 2, sorted them based in expression of tdTomato, and mapped each cell onto WT (Fig. 4G), CPZ (Fig. 2.4H), and 5xFAD (Fig. 2.4I) brains. As expected, very few tdTomato expressing cells are seen in the WT brain compared to the CPZ and 5xFAD brain, with the 5xFAD showing the most tdTomato signal, indicating that 5xFAD microglia have the highest DAM signature. These data are reinforced by the relative expression of DAM and homeostatic microglial genes, with WT having the lowest expression of DAM genes (e.g.: *Cst7*, *ApoE*, *Trem2*) and the highest expression of microglial homeostatic genes (e.g.: *Tmem119*, *P2ry12*), while the 5xFAD mice have the highest DAM gene expression and lowest homeostatic microglial gene expression (Fig. 2.4J). We next aimed to further characterize the difference between our tdTomato<sup>+</sup> DAM cells and all other microglia. As expected, the tdTomato<sup>+</sup> cells map onto areas of the brain where plaques are present (Fig. 2.4K). Differential gene expression (DGE) analysis comparing tdTomato<sup>+</sup> to tdTomato<sup>-</sup> microglia, shows that tdTomato<sup>+</sup> microglia have much higher expression of DAM genes, and lower expression of homeostatic microglial genes, indicating that we can utilize *Cst7*<sup>DD-Cre</sup> to target the most inflammatory microglial cells in the brain (Fig 2.4L).

# A Spatial Transcriptomics Workflow (CosMx 1000 Plex mRNA Panel)



**B** 234,859 cells



- Cell Types**
- AST 1
  - AST 2
  - AST CA3
  - AST THAL
  - ENDO
  - HIP FIS ENDO
  - PERI/ENDO
  - CTX L1
  - CTX L2/3
  - CTX 4
  - CTX L5
  - CTX L6
  - HIP Pyram CA1/3
  - CTX PENK
  - CTX CALB2
  - PAN 1
  - PAN 2
  - EX 1
  - EX 2
  - HIP DG HILUS
  - AMYG
  - CTX RSP
  - INH Gad1
  - INH SST
  - INH VIP
  - INH GAD1/2
  - INH CNR1
  - INH SST 2
  - MG 1
  - MG 2
  - ODC 1
  - ODC 2
  - ODC 3
  - ODC 4
  - OPC
  - THAL
  - VASC
  - VLNC

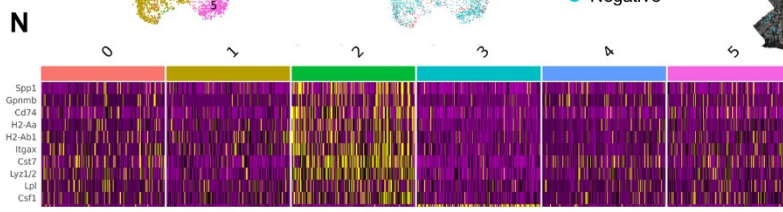
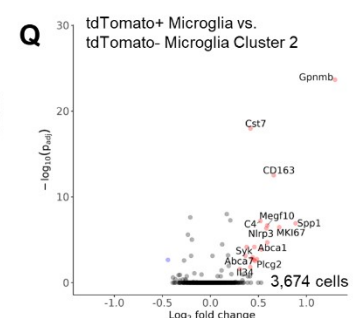
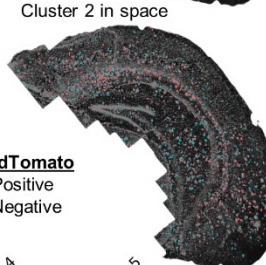
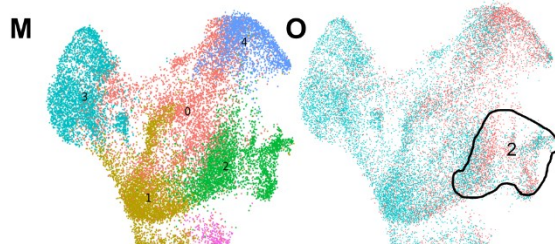
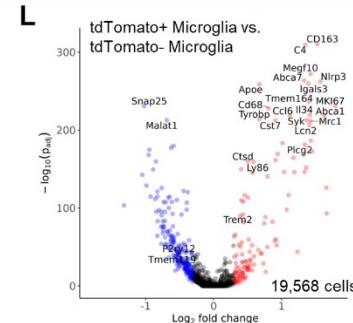
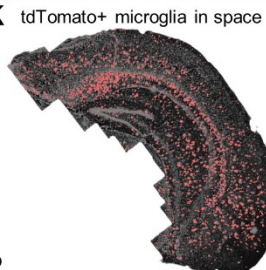
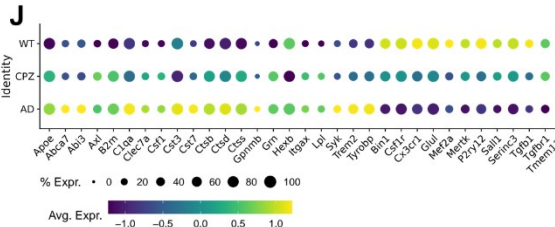
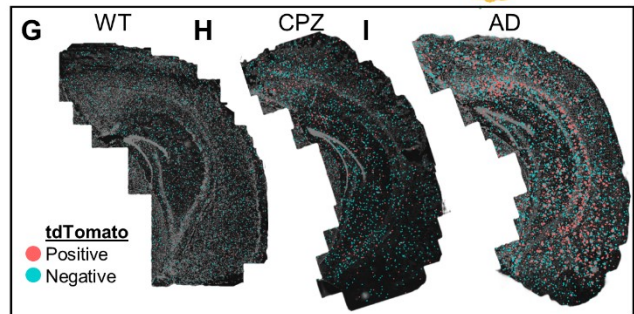
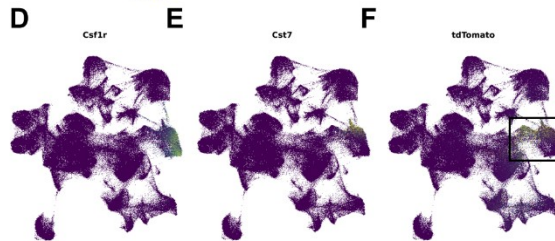
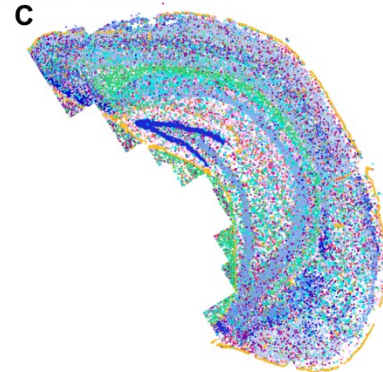


**Figure 2.4: Spatial transcriptomics analyses reveal increased DAM expression in tdTomato<sup>+</sup> PAMs vs tdTomato<sup>-</sup> PAMs.**

(A) Schematic of spatial transcriptomics workflow using the CosMx 1000 Plex mRNA Panel. Whole brains slices were mounted and FOVs of the hippocampus and cortex were selected. Cells are segmented using histone, GFAP, and DAPI and transcripts are then measured in each cell for further analysis.

(B-C) UMAP of 234,859 cells reveals 38 clusters distinct clusters (B) that can be mapped in space on each brain (C).

(D-F) UMAPs showing normalized expression of *Csf1r* (D), *Cst7* (E), and tdTomato (F), indicating these genes are expressed in MG 1 and MG 2 which are boxed in (F).

(G-I) Clusters MG 1 and MG 2 mapped in space on a WT (G), cuprizone (CPZ), and 5xFAD brain with tdTomato<sup>+</sup> cells represented in red, and tdTomato<sup>-</sup> cells represented in cyan.

(J) Dot Plot comparing microglial gene expression between WT, CPZ, and 5xFAD groups shows enriched DAM gene expression and diminished homeostatic microglial gene expression in CPZ and 5xFAD compared to WT.

(K) tdTomato<sup>+</sup> cells from MG 1 and MG 2 mapped onto a 5xFAD brain.

(L) Volcano plot comparing tdTomato<sup>+</sup> microglia vs tdTomato<sup>-</sup> microglia from MG 1 and MG 2 shows an upregulation in DAM gene expression (e.g.: *Trem2*, *Cst7*, *Apoe*), and a downregulation in homeostatic gene expression (e.g.: *Tmem119*, *Pr2ry12*).

(M-O) UMAP of 19,568 cells from MG 1 and MG 2 subclustered into 6 distinct clusters.

(N) Heatmap showing the 10 most upregulated genes in cluster 2 compared to the other microglial clusters. DAM genes such as *Gpnmb*, *Cst7*, *Itgax*, and *Lpl* are highly upregulated in cluster 2 indicating this cluster may be associated with A $\beta$  pathology.

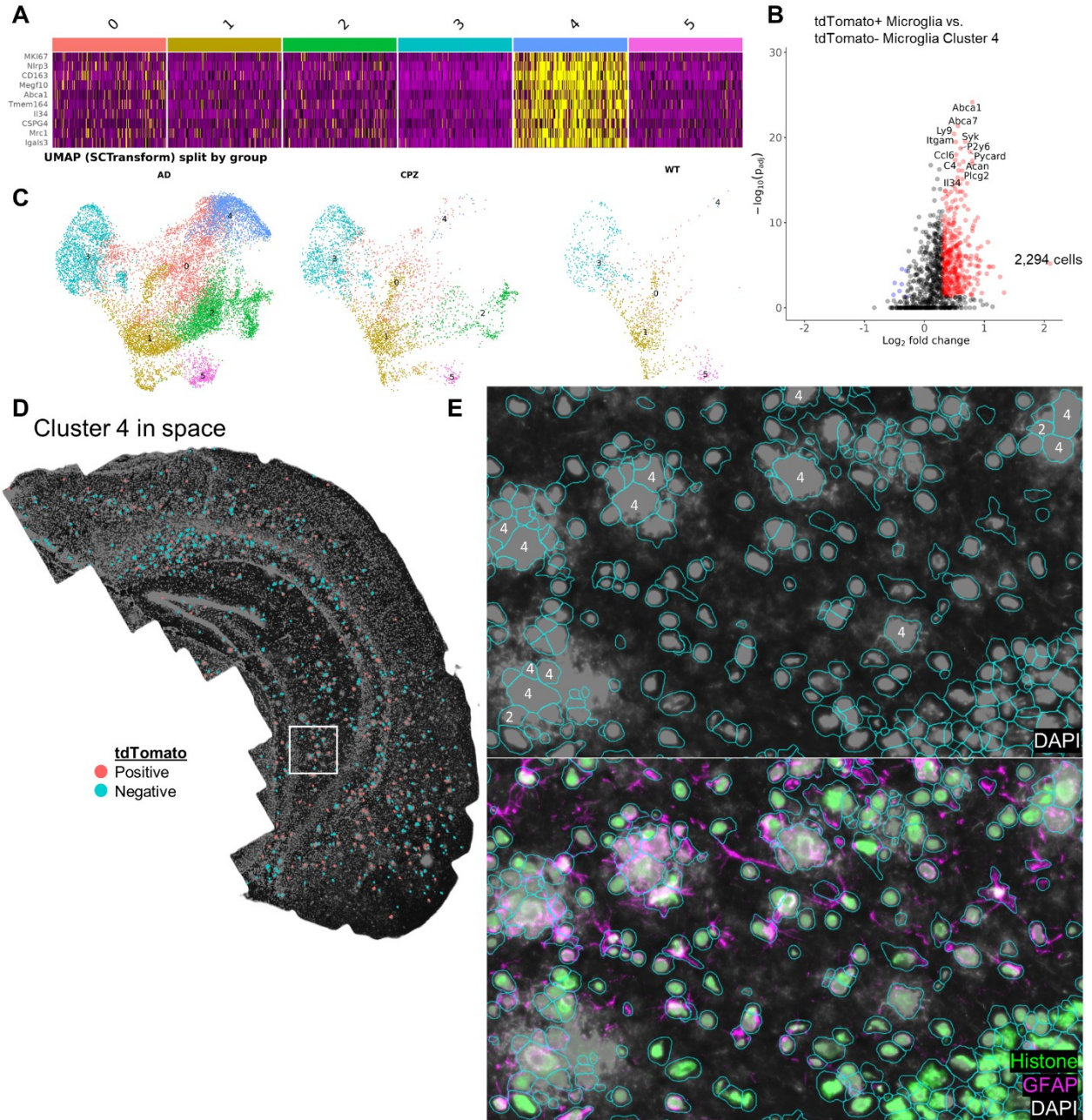
(O-P) UMAP showing tdTomato<sup>+</sup> and tdTomato<sup>-</sup> cells with cluster 2 encircled (O). tdTomato<sup>+</sup> and tdTomato<sup>-</sup> cells from cluster 2 mapped onto a 5xFAD brain shows that both types of cells are located directly around A $\beta$  plaques (P).

(Q) Volcano plot comparing tdTomato<sup>+</sup> microglia vs tdTomato<sup>-</sup> microglia from cluster 2 shows an upregulation in DAM gene expression (e.g.: *Cst7*, *Gpnmb*, *Spp1*, *Itgax*).

**tdTomato<sup>+</sup> microglia exhibit higher DAM gene expression compared to other PAMs**

So far, we have shown that the tdTomato<sup>+</sup> cells in our *Cst7*<sup>DD-Cre</sup>/*Ai14*<sup>tdTomato</sup> mice have higher DAM gene expression compared to all other microglia, however; it is unknown whether these cells have higher DAM gene expression compared to other PAMs that do not express tdTomato. To assess this, we further subclustered MG 1 and MG 2 into six distinct clusters (Fig. 2.4M). We found that out of these subclusters, subcluster 2, has the highest expression of DAM genes (e.g.: *Itgax*, *Cst7*, *Gpnmb*) compared to all other microglial subclusters (Fig. 2.4N). Subcluster 2 is also found to have a very high number of tdTomato<sup>+</sup> cells compared to other subclusters (Fig. 2.4O). Of note there appears to be a high number of tdTomato<sup>+</sup> cells in subcluster 4 as well, and this subcluster is

characterized by inflammation markers (e.g.: *CD163*, *Il34*, *Nlrp3*) (Supp. Fig. 2.1A). However, this subcluster appears to only be present in the 5xFAD group (Supp. Fig. 2.1C), and upon viewing the cell segmentation of the 5xFAD brain stained for DAPI, it appears that subcluster 4 cells may be A $\beta$  plaques themselves, which are stained by DAPI and contain many mRNA transcripts (Supp. Fig. 2.1D, E). Upon mapping the 3,674 subcluster 2 cells that are either tdTomato<sup>+</sup> or tdTomato<sup>-</sup> onto the 5xFAD brain, we observe that these cells are specifically located in plaque associated areas (Fig. 2.4P). Importantly, DGE analysis on tdTomato<sup>+</sup> vs tdTomato<sup>-</sup> cells from this subcluster, shows that tdTomato<sup>+</sup> cells have higher expression of DAM genes (e.g.: *Cst7*, *Gpnmb*, *Syk*, *Spp1*) (Fig. 2.4Q), indicating that the *Cst7*<sup>DD-Cre</sup> can specifically be used to target DAMs, while keeping other subsets of PAMs unaffected.



**Supplementary Fig 2.1: Microglia subcluster 4 is comprised of A $\beta$  plaques.**

(A) Heatmap showing 10 must upregulated genes in in cluster 4 compared to the other microglial clusters. (B) Volcano plot comparing tdTomato+ microglia vs tdTomato- microglia from cluster 2 shows an upregulation in inflammatory gene expression.

(C) UMAP split by 5xFAD, CPZ, and WT groups showing that cluster 4 is predominantly present in the 5xFAD group.

(D-E) Microglial subset cluster 4 tdTomato + and tdTomato- cells mapped onto a 5xFAD brain (D). White box indicates area of zoomed in FOV shown in (E).

(E) Cell segmentation image of a 5xFAD brain showing that some plaques stain positive by DAPI and are counted as cells which are subsequently grouped into microglial subset cluster 4.



## **Discussion**

Genetic data show that microglia can be disease driving and it is important to understand the exact mechanisms and contributions of involved microglial subpopulations to better determine their role in AD. To that end, we aimed to specifically target DAMs while leaving other microglia and cell types unaffected. This was undertaken in an effort to understand the specific contribution of these cells in AD, as the exact role of microglia in disease is currently unclear, as there are caveats with targeting all microglia/myeloid cells as demonstrated by *Trem2* knock-out studies. From our own studies and single cell RNA sequencing studies, it is evident that microglia exhibit differential functions based on their RNA expression [32, 57, 94, 111, 124, 125, 165, 184], and confusion about the role of microglia in AD may be a result of our inability to untangle the contribution of different microglial populations to AD.

Utilizing a novel DD-Cre mouse line knocked into the *Cst7* locus, we have created a model which effectively targets DAMs, while sparing other microglia and cell types in the brains of 5xFAD mice. Importantly, this suggests that DAM phenotypes are only induced next to plaques and these cells, and their progeny, do not migrate away from plaques after DAM expression, as has previously been hypothesized [45].

The *Cst7*<sup>DD-Cre</sup> line provides distinct advantages over other traditional and inducible microglia-specific Cre models. Widely used microglia Cre lines such as *Cx3cr1*<sup>CreER</sup> [209], *Tmem119*<sup>CreER</sup> [90], and *P2ry12*<sup>CreER</sup> [129] lines have been invaluable in efforts to understand microglial biology; however, these lines target all microglial cells and tamoxifen can only be administered as a short-term treatment. Particularly, in the *Cx3cr1*<sup>CreER</sup>, the Cre-ER fusion protein results in endogenous knock-out of CX3CR1 and

may have unintentional toxic effects that lead to microglial activation in mice [166, 209]. This line has also been shown to have Cre activity in the absence of tamoxifen [40]. The *Cst7*<sup>DD-Cre</sup> model avoids these potential confounds, while specifically targeting DAMs with no Cre leakiness. CST7 encodes for Cystatin F and is an endosomal/lysosomal cathepsin regulator and considered to be a DAM gene. Under normal conditions, CST7 is expressed by NK cells, T cells, and neutrophils in the periphery, with no expression found in the brain [120]. In disease, CST7 is upregulated in microglia in the white-matter during demyelination, and in microglia around plaques in amyloidosis models of disease [94, 120, 145]. Additionally, CST7 expression in the brain appears to be dependent on TREM2 signaling as CST7 expression is abolished in TREM2 knockout mice [33, 94, 110]. Although *Cst7* is highly upregulated in AD, little is known regarding its contribution to disease pathology. However, it has been shown that induction of its upstream kinase, RIPK1, increases CST7 levels and leads to impairment in lysosomal pathways [145].

In addition to showing enriched *Cst7* expression in PAMs, we observe an age-related increase in the proportion of tdTomato<sup>+</sup> PAMs at 11 months of age. Consistent with this, it has been shown that another DAM marker, CD11c, is elevated in 12-month-old 5xFAD mice compared to 4-month-old 5xFAD mice [192]. This suggests that some microglia may require more time or exposure to A $\beta$  to switch to a DAM gene profile, underlining the importance of studying the role of microglia at different stages of disease pathology. This is especially important at younger timepoints, as it appears there is more heterogeneity in PAMs at early timepoints when DAM expression is lower, versus later in disease when DAM expression appears higher. Additionally, the IHC and spatial transcriptomics data highlight the heterogeneity of PAMs themselves, and while in this study we did not look

at the average distance the tdTomato<sup>+</sup> and tdTomato<sup>-</sup> cells are from an A $\beta$  plaque, future studies will address whether there are differences in plaque-association between these groups of cells. Taken together, our data suggest that the dynamic expression of microglia at different disease stages and brain regions may have robust effects on therapeutic strategies targeting microglia, underlining the importance of studying the role of microglial subsets at different stages of disease pathology.

In conclusion, we have developed a powerful tool that will allow us to uncover the role of DAMs in AD and other diseases. Our DD-Cre/TMP system is an innovative treatment approach with safer, long-term efficacy compared traditional CreERT2/tamoxifen systems which may have detrimental effects on mouse safety and lead to increased activation of macrophages all while only having the potential for short term treatment [13, 74]. Importantly, we have shown that DAMs represent a subset of PAMs and are characterized by higher levels of disease and inflammatory gene expression compared to other populations of microglia, including other PAMs.

## Chapter Three:

### Selective targeting and modulation of plaque associated microglia via systemic dendrimer administration in an Alzheimer's disease mouse model

#### Introduction

Alzheimer's disease (AD) is a progressive, age-related neurodegenerative disorder that is triggered by the appearance and build-up of amyloid-beta ( $A\beta$ ) plaques in the cortex. Our lab and others have shown that microglia play an integral role in plaque formation and homeostasis, as well as downstream pathogenesis such as loss of synapses, perineuronal nets, and neurons [30, 58, 184, 185]. In addition to initiating the inflammatory response to disease pathology, phenotypically distinct microglia cluster around  $A\beta$  plaques and actively regulate plaque morphology (e.g., compaction) [17, 27]. Moreover, recent genome-wide association studies associated single nucleotide polymorphisms of genes highly enriched or exclusively expressed in myeloid cells (including *Trem2*, *Tyrobp*, *ApoE*, *Ms4a*, *Abca7*, *Abi3*, *Spi1*) with an altered risk of developing AD [58, 72, 81, 101, 188]. These data indicate microglia as a mediator of AD and a potential therapeutic target. Microglia surrounding plaques undergo significant physical and chemical changes, including the retraction of their processes and swelling of their cell bodies. These changes are mediated by extensive alterations in gene expression, which reprogram the microglia to mount inflammatory responses and remodel their metabolism and lipid handling [58]. As a result, they transition to a disease-associated microglia (DAM) phenotype, characterized by specific functional and molecular features. These changes in gene expression have been well studied by single cell RNA sequencing and find heterogeneous subsets of microglia in AD, demarcated by the expression of genes such as *Trem2* and *Tyrobp* that conventionally differentiate between disease- vs non-disease-associated

microglia, which in AD roughly correspond to plaque- and non-plaque-associated microglia (PAM and NPAM) respectively [94]. Currently, the role of PAMs in AD is unclear as brain wide microglial gene deletion and overexpression studies have shown contradicting results [51, 52, 85, 86, 105, 106, 153, 200]. Thus, there is a critical need to specifically target and modulate PAMs over NPAMs to determine this cell population's contribution to AD.

Dendranib precision nanomedicine is based on hydroxyl dendrimer (HD) technology. HDs consist of a hydrophobic core, repeating branches that expand outward, and hydrophilic functional groups at the outer surface. Importantly, the high density of surface hydroxyls provides a neutral charge allowing HDs to easily cross the blood brain barrier (BBB) in regions of inflammation and be selectively internalized by activated microglia and macrophages [133, 135, 138, 139, 143, 190].

Size and surface chemistry of dendrimers determine their toxicity and biodistribution [12]. More than 100 dendritic structures have been reported. Some dendrimers have been used clinically for nucleic acid and drug delivery in cancer, including many types of brain tumors [9, 92, 95, 131, 134, 205] and show potential application in gene therapy [4, 54, 119]. Notably, polyamidoamine (PAMAM) dendrimers have been shown to cross the BBB during times when pathological insults such as stroke, tumors, or traumatic brain injury compromise the BBB [169]. Traditional dendrimers alone do not bypass the BBB with high efficiency without resorting to invasive approaches such as carotid artery injections [187, 219]. Recently, however, systemic administration of HDs have shown promise in bypassing slightly impaired BBB and were shown to be taken up specifically by microglia and macrophages in regions of neuroinflammation in rodent models of cerebral palsy,

glioblastoma, Rett syndrome, AD, ALS, and multiple sclerosis (MS) [133, 135, 138, 139, 143, 177, 178, 190]. In the AD brain, PAMs are the primary phagocytic macrophages; therefore, HDs theoretically have the capacity to bypass the BBB and become specifically engulfed by PAMs.

Here, we sought to determine whether HDs can successfully bypass the BBB and be specifically phagocytosed by PAMs in the context of AD. To that end, we intraperitoneally injected HDs conjugated to a Cy5 fluorophore into an aggressive mouse model of amyloidosis; 5xFAD mice at 7 months of age. We find that one injection is sufficient for the dendrimers to cross the BBB and leads to brain-wide, PAM-specific engulfment of these HDs into the microglial lysosomal compartment. To therapeutically modulate PAM function, as proof of principle, we used D-45113, a dendranib that inhibits CSF1R tyrosine kinase. Our lab has previously shown that all microglia express CSF1R, and that inhibition of CSF1R leads to the indiscriminate death of the microglia [35], and that the elimination of microglia in 5xFAD mice can inhibit plaque development early in disease, and rescue synapse and neuronal number associated with late disease [184, 185]. Additionally, our lab and others have shown that low-dose inhibition of CSF1R can inhibit microglia-plaque association, attenuate neuroinflammation and rescue synaptic integrity and cognition in AD mouse models [31, 146]. Not to be overlooked, studies inhibiting CSF1R in tauopathy models show reduced levels of microglia which leads to reductions in tau levels, amelioration of inflammation, and synaptic, and neuronal loss [7, 88, 122]. Altogether, HDs represent a novel and nuanced approach for targeting PAMs and further studies should be undertaken with other microglial modulators to uncover the specific role of PAMs in AD. Establishing the effectiveness of these dendrimers in targeting and treating

PAMs will allow us to tailor appropriate therapies towards this subset of microglia and develop therapeutic treatments with greater precision.

## **Methods**

### **Synthesis of D-45113:**

D4-alkyne dendrimer (Lot# DP-07-85-3) was dissolved in 20 mL of anhydrous dimethylacetamide (DMA). A CSF1R tyrosine kinase inhibitor with a terminal azide was added to a stirring solution of D4-alkyne. Copper bromide and Pentamethyldiethylenetriamine (PMDTA) were then added to the solution. The stirring solution was placed in a 95°C oil bath overnight. The reaction mixture was then dialyzed against DMA followed by water (membrane cut-off at 1000 Da). The aqueous solution was then lyophilized to obtain D-45113.

### **Mice:**

All animal experiments performed in this study were approved by the UC Irvine Institutional Animal Care and Use Committee (IACUC) and were compliant with ethical regulations for animal research and testing. Mice were mixed sex C57BL/6 (000664) mice. Animals were housed with open access to food and water under 12h/12h light-dark cycles. All mice were aged to 5 or 12 months unless otherwise indicated. The 5xFAD mouse expresses five familial AD genes (APP Swedish, Florida, and London; PSEN1 M146L+L286V; [144] and is characterized by aggressive amyloid pathology throughout the brain and synaptic and neuronal loss in the subiculum. For 5xFAD genotyping, the primer sequences used were PS1 Forward 5' - AAT AGA GAA CGG CAG GAG CA – 3' and PS1 Reverse 5' - GCC ATG AGG GCA CTA ATC AT – 3'.

### **Animal treatments:**

All rodent experiments were performed in accordance with animal protocols approved by the Institutional Animal Care and Use Committee (IACUC) at the University of California, Irvine. 7-month-old wild-type (WT) or 5xFAD mice were intraperitoneally (IP) injected with 55mg/kg G4 PAMAM hydroxyl dendrimers conjugated to a Cy5 fluorophore followed by euthanasia 48 hours post injection. For time course D-Cy5 experiments, 7–9-month-old mice were treated as above, but euthanized either 48 hours, 15 days, or 21 days post injection. For D-45113 experiments, 4 month and 11-month-old mice were IP injected with 200mg/kg of D-45113 twice per week for four weeks. At the end of treatments, mice were euthanized via CO<sub>2</sub> inhalation and transcardially perfused with 1X phosphate buffered saline (PBS). For all studies, brains were removed, and hemispheres separated along the midline. Brain halves were either flash frozen for subsequent biochemical analysis, or drop-fixed in 4% Paraformaldehyde (PFA; Thermo Fisher Scientific, Waltham, USA) for subsequent immunohistochemical analysis. Half brains collected into 4% PFA for 48 hrs and then transferred to a 30% sucrose solution with 0.02% sodium azide for another 48-72 hrs at 4C. Fixed half brains were sliced at 40 µm using a Leica SM2000 R freezing microtome.

### **Histology and confocal microscopy:**

Fluorescent immunolabeling was performed using a standard indirect technique as described previously [67]. Brain sections were stained with primary antibodies against: ionized calcium binding adaptor molecule 1 (IBA1; 1:1000; 019-19741, Wako and ab5076, Abcam), CD68 (1:200; BioRad) glial fibrillary protein (GFAP; 1:1000; Abcam), NeuN (1:1000; Millipore), OLIG2 (1:200; Abcam), A $\beta$ 1-16 (6E10; 1:1000; Biolegend), and anti-lysosomal associated membrane protein 1 (LAMP1; 1:200; Santa Cruz



Biotechnologies). For Amylo-Glo staining (TR-300-AG; Biosensis), tissue sections were washed in 70% ethanol 1X5 minutes, followed by a 1×2 minute wash in distilled water. Sections were then placed in a 1% Amylo-Glo solution for 1×10 minutes then washed with .9% saline for 1×5 minutes and distilled water for 1×15 seconds before continuing fluorescent immunolabelling. For Thioflavin-S (Thio-S) staining, tissue sections were placed for 1×10 min incubation in 0.5% Thio-S (1892; Sigma-Aldrich) diluted in 50% ethanol. Sections were then washed 2×5 min each in 50% ethanol and one 10-min wash in 1xPBS before continuing with fluorescent immunolabelling.

High resolution fluorescent images were obtained using a Leica TCS SPE-II confocal microscope and LAS-X software. For confocal imaging, one field of view (FOV) per brain region was captured per mouse unless otherwise indicated.

### **A $\beta$ and NfL ELISA**

To isolate protein for the ELISA, flash-frozen brain hemispheres were microdissected into cortical, hippocampal, and thalamic regions and grounded to a powder. Hippocampal tissue was then homogenized in Tissue Protein Extraction Reagent (TPER (Life Technologies, Grand Island, NY)) with protease and phosphatase inhibitors present. Samples were centrifuged at 100,000 g for 1 hour at 4 °C to generate TPER-soluble fractions. To generate formic acid fractions, protein pellets from the TPER-soluble fraction were then homogenized in 70% formic acid and centrifuged at 100,000 g for 1 hour at 4 °C, the formic acid fraction is then neutralized. Quantification of soluble and insoluble fractions of both A $\beta$  and NfL was performed as previously described [192].

### **RNA Sequencing**

Whole transcriptome RNA sequencing (RNA-Seq) libraries were produced from hippocampal tissue of WT/Veh, WT/D-45113, 5xFAD/Veh, and 5xFAD/D-45113 mice sacrificed at 12 months of age. RNA was isolated with an RNA Plus Universal Mini Kit (Qiagen, Valencia, USA) according to the manufacturer's instructions. Library preparation, RNA-seq, and read mapping analysis were performed by Novogene Co. Gene expression was analyzed using Limma, edgeR, and org.Mm.eg.db packages [163] with expression values normalized into FPKM (fragments per kilobase of transcript per million mapped reads). Differentially-expressed genes were selected by using false discovery rate (FDR) <0.05. Heatmaps were created using Morpheus (Morpheus, <https://software.broadinstitute.org/morpheus>) and volcano plots were created using VolcanoR [49].

Weighted correlation network analysis: Network analysis was performed using weighted gene co-expression analysis (WGCNA) package in R [213]. First, bi-weighted mid-correlations were calculated for all gene pairs, and then used to generate an eigengene network matrix, which reflects the similarity between genes according to their expression profiles. This matrix was then raised to power  $\beta$  ( $\beta=16$ ). Modules were defined using specific module cutting parameters (minimum module size = 100 genes, deepSplit = 4 and threshold of correlation = 0.2). Modules with a correlation greater than 0.8 were merged. We used first principal component of the module, called signed bicor network, to correlate 5xFAD genotype, sex, and treatment. Hub genes were defined using intra-modular connectivity (kME) parameter of the WGCNA package. Gene enrichment analysis: Gene-set enrichment analysis was done using enrichR [100].

## **Data analysis and statistics**

Both male and female mice were used in all statistical analyses. ThioS, IBA1, NeuN, and OLIG2 counts were measured via the spots function and 6E10, LAMP1, and GFAP volume were measured via the surfaces function on Imaris version 9.6. The number of dendrimer<sup>+</sup> cells / FOV in the subiculum and somatosensory cortex were manually counted for all sections via ImageJ

Statistical analysis was performed with Prism Graph Pad (v.8.0.1; La Jolla, USA). To compare two groups, the unpaired or paired Student's t-test was used. Time-course data was analyzed using One-way ANOVA (48 hours, 15 days, and 21 days), while D-45113 data with more than two groups used Two-way ANOVA (Treatment: Vehicle vs. D-45113 and Genotype: WT vs. 5xFAD) using GraphPad Prism Version 8. Tukey's post hoc tests were employed to examine biologically relevant interactions from the two-way ANOVA regardless of statistical significance of the interaction. For all analyses, statistical significance was accepted at  $p < 0.05$ . and significance expressed as follows: \* $p < 0.05$ , \*\* $p < 0.01$ , \*\*\* $p < 0.001$ . n is given as the number of mice within each group. Statistical trends are accepted at  $p < 0.10$  (#). Data are presented as raw means and standard error of the mean (SEM).

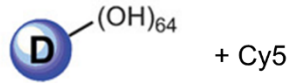
## **Results**

### **Hydroxyl dendrimers are phagocytosed exclusively by PAMs in the 5xFAD mouse brain.**

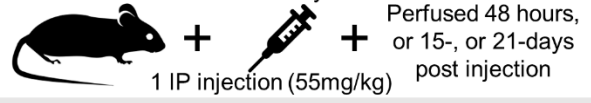
To determine whether HDs can be used as a pharmacological tool to target PAMs in an AD mouse model, we utilized HDs conjugated to a Cy5 fluorophore (referred to as D-Cy5) as previously described [133, 135, 138, 139, 143, 190] (Fig. 3.1a). 7-month-old 5xFAD mice were intraperitoneally injected with D-Cy5 or saline and subsequently

perfused 48 hours, 15 days, or 21 days post injection (Fig. 3.1b). Cy5 signal is seen in the brain of 5xFAD, with a marked abundance of Cy5 around dense core plaques stained with Amylo-Glo (Fig. 3.1c), while control 5xFAD mice show no Cy5 signal in the brain (Fig. 3.1d). Upon closer inspection, D-Cy5 colocalizes with microglia (IBA1) and microglial lysosomes (CD68), in both the hippocampus (Fig. 3.1e, e1) and somatosensory cortex (Fig. 3.1g, g1), clustered around plaques, indicating that PAMs may phagocytose D-Cy5. Importantly, wild-type (WT) mice treated with D-Cy5 show very little Cy5 signal in the hippocampus (Fig. 3.1k) and somatosensory cortex (Fig. 3.1l); however, signal that is present colocalizes with microglia and their lysosomes. Quantification shows that 55% and 60% of PAMs as well as 20% and 15% of NPAMs contain D-Cy5 in the hippocampus and somatosensory cortex, respectively in 5xFAD mice (Fig. 3.1f, 3.1h), showing a preferential targeting of PAMs vs NPAMs. Further, D-Cy5 is present in 5xFAD brains at 48 hours, 15 days, and 21 days post injection in both the subiculum (Fig. 3.1j) and somatosensory cortex (Fig. 3.1j). To determine if any other cell types in the 5xFAD brain take up D-Cy5 we stained for astrocytes (GFAP; Fig. 3.1m, m1), neurons (NeuN; Fig. 3.1n), and oligodendrocytes (OLIG2; Fig. 3.1o, o1) and find virtually no D-cy5 signal in any of these cell types in the subiculum (Fig. 3.1p) nor somatosensory cortex (Fig. 3.1q).

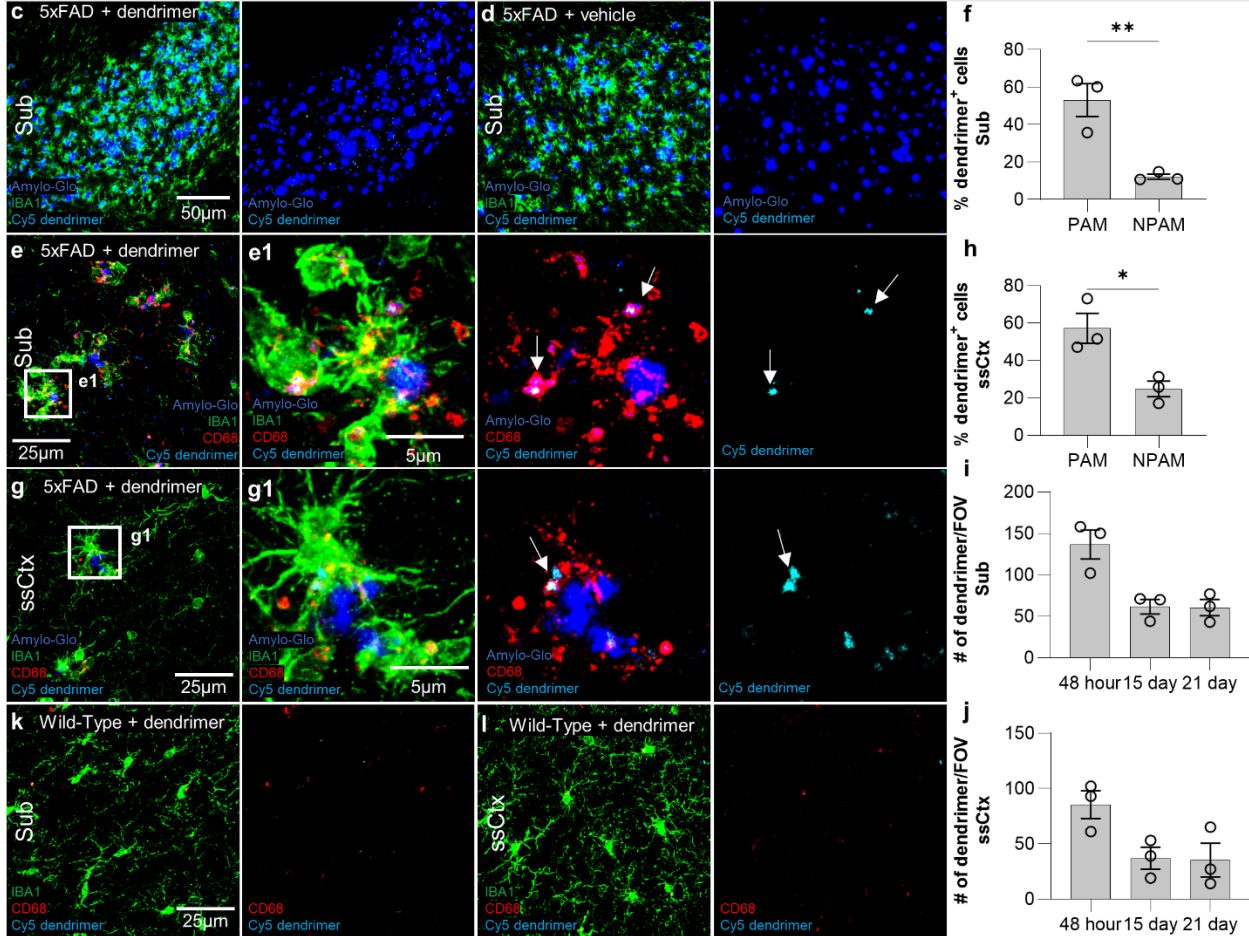
a



b 7 mo 5xFAD+ or WT Dendrimer tagged with Cy5



**PAMAM hydroxyl dendrimers are phagocytosed by PAMs in 5xFAD mice**



**PAMAM hydroxyl dendrimers are not taken up by other cell types in the brain**

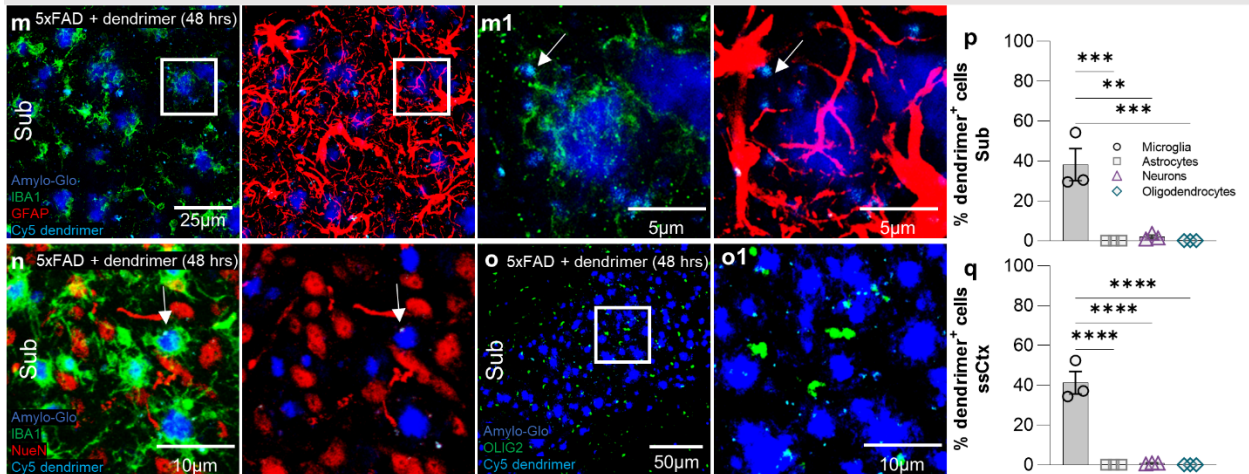


**Figure 3.1: G4 HDs are phagocytosed by plaque associated microglia (PAM).** Schematic of HD conjugated to a Cy5 fluorophore (a). Experimental paradigm: 5xFAD mice were IP injected with dendrimer conjugated to a Cy5 fluorophore and perfused either 48 hours, 15 days, or 21 days post injection (b). Representative 20x confocal microscopy images of the subiculum (c) show dendrimer localization in plaque-heavy areas, while 5xFAD mice injected with vehicle do not show Cy5 signal (d). 63x (e, g) and inset images (e1, g1) of the hippocampus (e) and somatosensory cortex (g) highlight dendrimer colocalization within microglial lysosomes (CD68). Arrows indicate areas where dendrimers colocalize with CD68. Quantification of the percentage of plaque-associated microglia (PAM) and non-plaque-associated microglia (NPAM) containing dendrimer reveal that dendrimers are taken up primarily by PAM and to a lesser extent by NPAM in the subiculum (f) and somatosensory cortex (h). Quantification of the number of dendrimer puncta present in a 20x FOV at 48 hours, 15 days, and 21 days post injection in the hippocampus and somatosensory cortex indicate that dendrimers persist in the brain through 21 days in the subiculum (i) and somatosensory cortex (j). Representative 20x images of WT mice injected with dendrimer show small amounts of dendrimer present in the subiculum (k) and somatosensory cortex (l). 63x representative images (m) and zoomed in images (m1) of GFAP (astrocytes) and IBA1 staining, 63x images of IBA1 and NeuN (neurons) staining (n), and 20x (o) and zoomed in images of OLIG2 (oligodendrocytes) staining show virtually no uptake of Cy5 dendrimer in any of these cell types in the subiculum (p) nor somatosensory cortex (q). Statistical analysis for (f, h) used a two-tailed t-test; (i, j, p, q) used a one-way ANOVA with Tukey's multiple comparison test. Significance indicated as \*  $p < 0.05$ ; \*\*  $p < 0.01$ ; \*\*\*  $p < 0.001$ .

### **PAMAM hydroxyl dendrimers conjugated to tyrosine kinase inhibitor, rescues Elevated Plus Maze (EPM) performance and A $\beta$ burden in 12-month-old 5xFAD mice.**

Having confirmed that HDs can pass the BBB and preferentially target PAMs in 5xFAD mice, we sought to determine the therapeutic potential of these dendrimers through a proof of principle experiment. To that end, we used D-45113, a dendranib that inhibits CSF1R tyrosine kinase (D-45113) (Fig 3.2a) which has a Kd of 0.04nM against CSF1R (Fig. 3.2b). D-45113 or vehicle dendrimer was administered to 4- and 11-month-old 5xFAD and WT mice (IP) twice weekly for 4 weeks (Fig 3.2c), giving the following 4 groups: **WT/Veh**, **WT/D-45113**, **5xFAD/Veh**, and **5xFAD/D-45113** (Fig. 3.2d). Mice were assessed with the elevated plus maze (EPM) task 24 hours after the last injection and subsequently perfused 24 hours later at which point, they were analyzed via immunohistochemistry (IHC), protein, and RNA analyses.

Anxiety behavior in mice was evaluated using the EPM, where performance of 5-month-old mice was similar across all groups regardless of genotype or treatment, as evidenced by their comparable time spent in the open arm of the maze (Fig. 3.2e). However, the distance travelled by 5xFAD/Veh mice was lower than that of both WT/D45113 and 5xFAD/D-45113 mice, indicating that D-45113 may increase hyperexcitability in mice (Fig. 3.2f). At 4 months of age, there were no apparent changes in behavior. At 12 months of age, 5xFAD/Veh and 5xFAD/D-45113 mice spent significantly more time in the open arm of the EPM compared to WT/Veh and WT/D45113 mice (Fig. 3.2g), as expected [41]. Time spent in the open arm was rescued in 5xFAD/D45113 mice compared to 5xFAD/Veh mice, suggesting that D-45113 injection may improve behavioral outcomes in these mice (Fig. 3.2g). Notably, there was no significant difference in total distance travelled between any of the four groups (Fig. 3.2h).

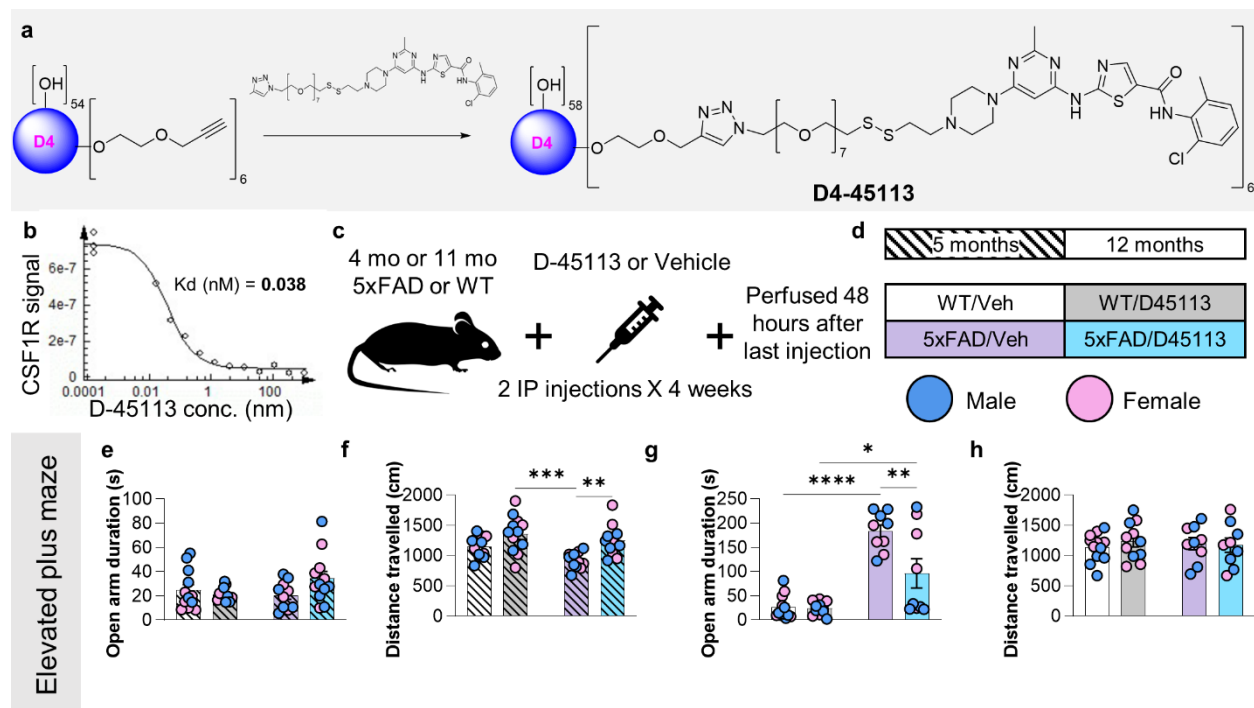


**Figure 3.2: Intraperitoneal administration D-45113 rescues elevated plus maze performance in 5xFAD mice.** Schematic of D-45113, a dendranib that inhibits CSF1R tyrosine kinase (a). Graph measuring the amount of CSF1R kinase plotted against D-45113 concentration ( $K_d = 0.04$ ) (b). Experimental paradigm schematic revealing that 4- and 11-month-old 5xFAD and wild-type (WT) mice were injected with D-45113 or a vehicle for a total of 8 injections over the course of a month, at which point animals were perfused at either 5- or 12-months of age (c). All subsequent analysis and images of the 5-month timepoint are indicated by diagonal hatch lines while the 12-month timepoint is solidly filled, with male data-points filled with blue, and female data-points filled with pink (d). Elevated plus maze data at the 5-month timepoint indicate no changes are seen in the amount of time spent in the open maze arms with dendrimer treatment nor with 5xFAD genotype (e), however; WT/D45113 and 5xFAD/D-45113 mice traveled a greater distance over the course of the 5-minute trial compared to 5xFAD/Veh mice (f). In the 12-month timepoint, the 5xFAD groups both showed a significant increase in the duration of time spent in the open arms of the maze, as expected, but strikingly, 5xFAD/D45113 mice showed a significant rescue in behavior when compared to 5xFAD/Veh mice (g). Importantly, no groups in the 12-month timepoint significantly differed in total distance travelled during the trial (h). All analyses performed on this figure used a two-way ANOVA with Tukey's multiple comparison test. Significance indicated as \*  $p < 0.05$ ; \*\*  $p < 0.01$ ; \*\*\*  $p < 0.001$ .

To investigate whether D-45113 treatment induces pathological changes in the brains of 5xFAD mice, we performed IHC using Thio-S, an amyloid-specific dye for dense core plaques, and 6E10, an antibody against  $A\beta$  and APP. At 5 months of age in the somatosensory cortex, 5xFAD/D-45113 mice exhibited a trending reduction in the number of Thio-S dense core plaques ( $p=0.057$ ; Fig. 3.3a, b) and a significant reduction in extracellular 6E10 staining ( $p=0.0034$ ; Fig. 3.3e, f) compared to 5xFAD/Veh mice. However, in the plaque-heavy subiculum, no significant differences were observed between the two 5xFAD groups in the number of ThioS+ plaques (Fig. 3.3c, d) or 6E10 staining (Fig. 3.3g, h). At the 12-month time point, a trending reduction in ThioS+ plaque number ( $p=0.11$ ; Fig. 3.3i, j) and a significant reduction in 6E10 staining ( $p=0.032$ ; Fig. 3.3m, n) were observed in the 5xFAD/D-45113 group compared to the 5xFAD/Veh group in the somatosensory cortex. In the subiculum, no differences were observed in the number of ThioS+ dense core plaques (Fig. 3.3k, l); however, a significant reduction in



extracellular 6E10 volume was observed in 5xFAD/D-45113 mice compared to 5xFAD/Veh controls ( $p=0.0025$ ; Fig. 3.3o, p).

We measured the levels of insoluble and soluble A $\beta$ 40 and -42 in the hippocampal tissue from 5xFAD/D-45113 and 5xFAD/Veh brains. As expected, the amount of soluble and insoluble A $\beta$ 40 was significantly higher at the 12-month time point compared to the 5-month time point. However, D-45113 administration had no effect on the concentration of A $\beta$ 40 in the hippocampus (Fig. 3.3q, r). Similarly, an age-dependent increase in soluble and insoluble A $\beta$ 42 was observed, but no changes in concentration were observed due to D-45113 administration (Fig. 3.3s, t).

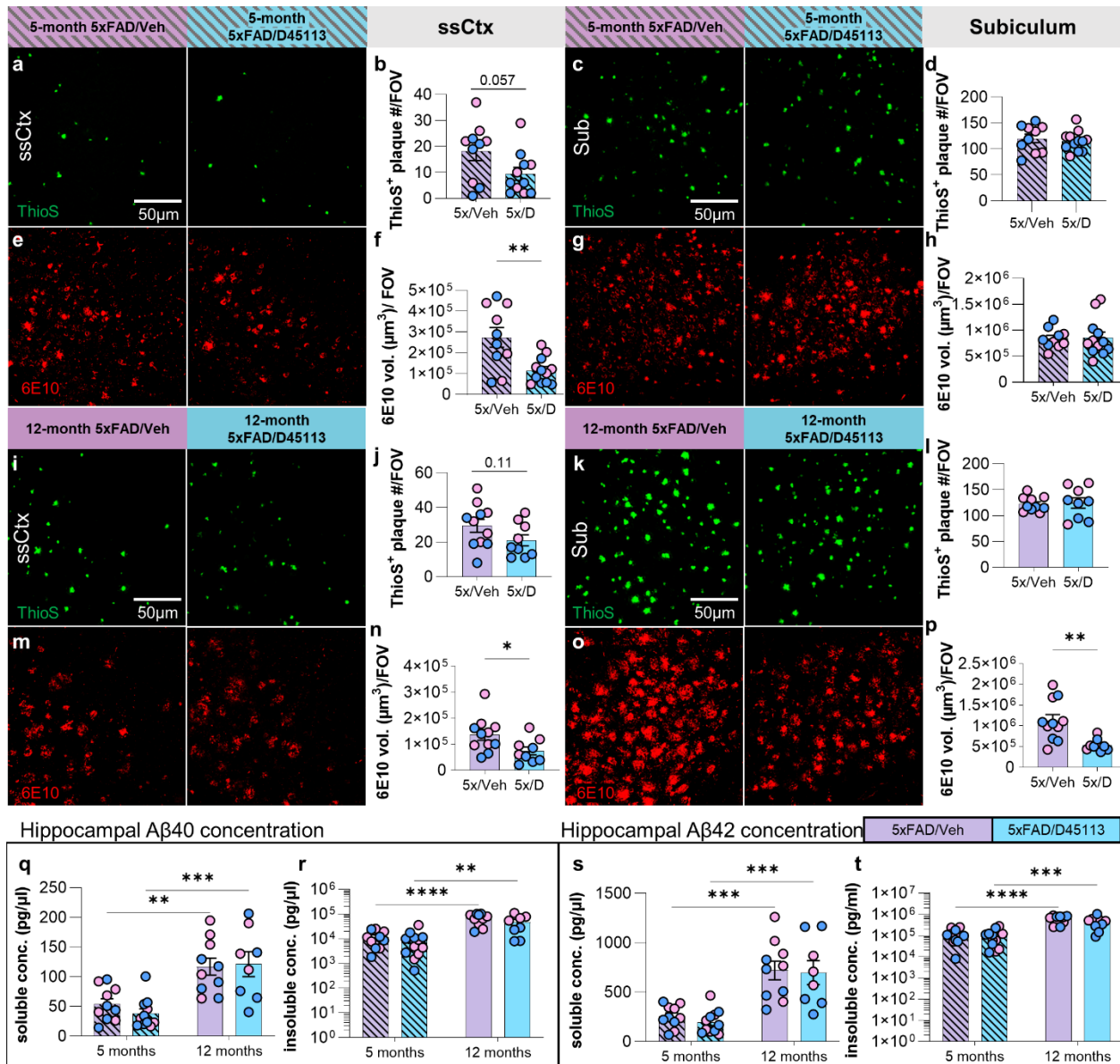


**Figure 3.3: D-45113 treatment reduces Aβ plaque volume but not soluble and insoluble Aβ levels in the brains of 5xFAD mice.** Representative 20x images of Thioflavin S (ThioS) staining in the somatosensory cortex (a) and subiculum (c) in 5-month 5xFAD groups, showing a nearly significant decrease in ThioS<sup>+</sup> dense-core plaques in the somatosensory cortex (b), but no change in the subiculum (d). 20x images of 6E10 staining for Aβ in the somatosensory cortex (e) and subiculum (g) in 5-month 5xFAD/Veh and 5xFAD/D45113 groups reveal a significant reduction in 6E10 in the somatosensory cortex (f) of 5xFAD/D45113 mice, but no change in the subiculum (h). Representative 20x images of ThioS staining in 12-month-old 5xFAD/veh and 5xFAD/D45113 groups in the somatosensory cortex (i) and subiculum (k) and corresponding analysis shows a trending reduction in ThioS<sup>+</sup> plaques in the somatosensory cortex (j), but not subiculum (l). 20x images of 6E10 staining in the somatosensory cortex (m) and subiculum (o) show striking reductions in 6E10 total volume in 5xFAD/D45113 mice compared to 5xFAD/Veh controls in both brain regions (n, p). Hippocampal Aβ40 concentration measured via MSD assay shows an increase in soluble (q) and insoluble (r) Aβ40 levels in 12-month-old 5xFAD groups compared to 5-month-old 5xFAD groups, but no effects due to D45113 treatment are observed. Similarly,

soluble (**s**) and insoluble (**t**) hippocampal A $\beta$ 42 concentrations increase with age, but no changes are seen due to D45113 treatment. Statistical analysis for (b, d, f, h, j, l, n, p) used a two-tailed t-test; (q-t) used a two-way ANOVA with Tukey's multiple comparison test. Significance indicated as \*  $p < 0.05$ ; \*\*  $p < 0.01$ ; \*\*\*  $p < 0.001$ .

### **D-45113 treatment reduces the number of microglia in aged 5xFAD mice.**

Having shown that HDs selectively target PAMs, we next investigated the effect of D-45113 treatment on microglia. We performed IHC on brain sections from 5- and 12-month-old WT/Veh, WT/D-45113, 5xFAD/Veh, and 5xFAD/D-45113 mice with the microglial marker, IBA1, and the dense core plaque stain, Amylo-Glo (Fig. 3.4a, d). At 5 months of age, we observed an increase in the number of IBA1+ microglia in both 5xFAD groups compared to the WT groups, as expected. However, no differences were observed due to dendrimer treatment in either the WT or 5xFAD mice (Fig. 3.4b, c). Exploring the 12-month time-point, significant reductions in IBA1+ microglial densities are induced by D-45113 treatment in both brain regions in 5xFAD mice, but not WT mice (Fig. 3.4e).

We next investigated whether D-45113 treatment affected other cell types in the brain. We stained 12-month-old WT/Veh, WT/D-45113, 5xFAD/Veh, and 5xFAD/D-45113 mouse brain slices with the reactive astrocyte marker GFAP and Amylo-Glo (Fig. 3.4i) and measured GFAP+ staining in the somatosensory cortex and subiculum. In both regions, we observed an increase in the GFAP+ signal in both 5xFAD groups compared to both WT groups, consistent with previous literature [41]. However, no changes were observed due to D-45113 administration (Fig. 3.4j, k). We also stained 12-month-old mouse brains with oligodendrocyte marker, OLIG2 (Fig. 3.4l). In the somatosensory

cortex, no differences in the number of OLIG2+ cells were observed between the WT/Veh, WT/D-45113, 5xFAD/Veh, and 5xFAD/D-45113 groups (Fig. 3.4m). However, in the subiculum, WT/D-45113 and 5xFAD/D-45113 mice had fewer OLIG2+ cells compared to WT/Veh mice, suggesting that D-45113 treatment may indirectly affect oligodendrocytes in the brain.

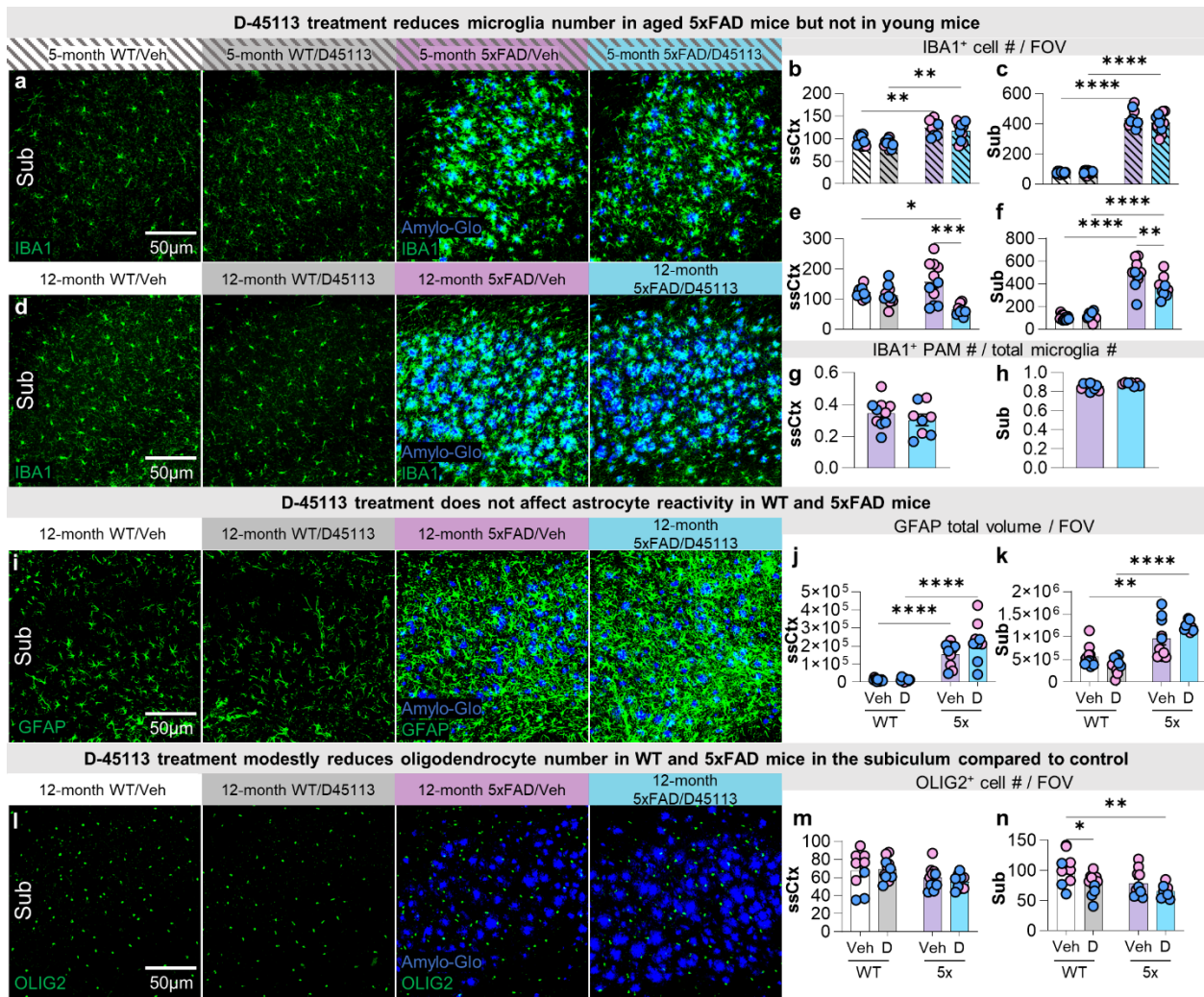


**Figure 3.4: D-45113 treatment reduces the number of microglia in aged 5xFAD mice.** Representative 20x images of the subiculum of 5-month-old WT/Veh, WT/D45113, 5xFAD/Veh, and 5xFAD/D45113 stained for IBA1 and Amylo-Glo (a). In both the somatosensory cortex (b) and subiculum (c), the number of IBA<sup>+</sup> cells increase in the 5xFAD groups compared to the WT groups, however, no changes are observed due to dendrimer treatment. 20x images in the subiculum of 12-month-old groups stained for IBA1 (d) show a significant reduction in the number of IBA<sup>+</sup> cells in the 5xFAD/D45113 group compared to the 5xFAD/Veh group in both the somatosensory cortex (e) and subiculum (f). At 12-months of age, the percentage of

IBA1<sup>+</sup> cells that are plaque associated remains unchanged between the 5xFAD/Veh and 5xFAD/D45113 groups in the somatosensory cortex (**g**) and subiculum (**h**). Representative 20x images of the subiculum of all four groups stained with reactive astrocyte marker, GFAP, and Amylo-Glo (**i**). In the somatosensory cortex (**j**) and subiculum (**k**) there is more GFAP volume in the 5xFAD groups compared to the WT groups, however, no changes occur with D45113 treatment. Representative 20x images of all four groups stained with oligodendrocyte marker, OLIG2, and Amylo-Glo (**l**) reveal no differences between groups in the somatosensory cortex (**m**), however; in the subiculum, the number of OLIG2<sup>+</sup> cells are reduced in WT/D45113 and 5xFAD/D45113 mice compared to WT/Veh mice (**n**). Statistical analysis for (g, h) used a two-tailed t-test; (b, c, e, f, j, k, m, n) used a two-way ANOVA with Tukey's multiple comparison test. Significance indicated as \*  $p < 0.05$ ; \*\*  $p < 0.01$ ; \*\*\*  $p < 0.001$ .

### **D-45113 treatment in aged mice reduces microglial and inflammatory gene expression in 5xFAD mice.**

To confirm the IHC changes due to D-45113 treatment, we performed bulk RNA sequencing (RNA-seq) on microdissected hippocampi from WT/Veh, WT/D-45113, 5xFAD/Veh, and 5xFAD/D-45113 mice. We first compared differentially expressed genes (DEGs) between WT/D-45113 and WT/Veh and found no significantly changed genes between the two groups, indicating that D-45113 does not have an effect on hippocampal gene expression in the WT mice (Fig. 3.5a). Consistent with literature [41], the expression of inflammatory genes was higher in 5xFAD/Veh mice compared to WT/Veh, with genes such as *Cst7*, *Itgax*, and *Clec7a* being highly upregulated (Fig. 3.5b). In contrast, 5xFAD/D45113 mice had robust gene expression changes compared to 5xFAD/Veh mice, with a marked downregulation of genes associated with microglia and inflammation such as *Itgam*, *Itgax*, and *Cxcl9* (Fig. 3.5c). We generated a clustered heatmap from the fragments per kilobase of exon per million mapped fragments (FPKM) values for the 777 DEGs identified between 5xFAD/D-45113 and 5xFAD/Veh mice (Fig. 3.5d) and identified three clusters: genes that are downregulated with D-45113 treatment, genes that are upregulated in 5xFAD/Veh mice but rescued in 5xFAD/D-45113 mice, and genes that are

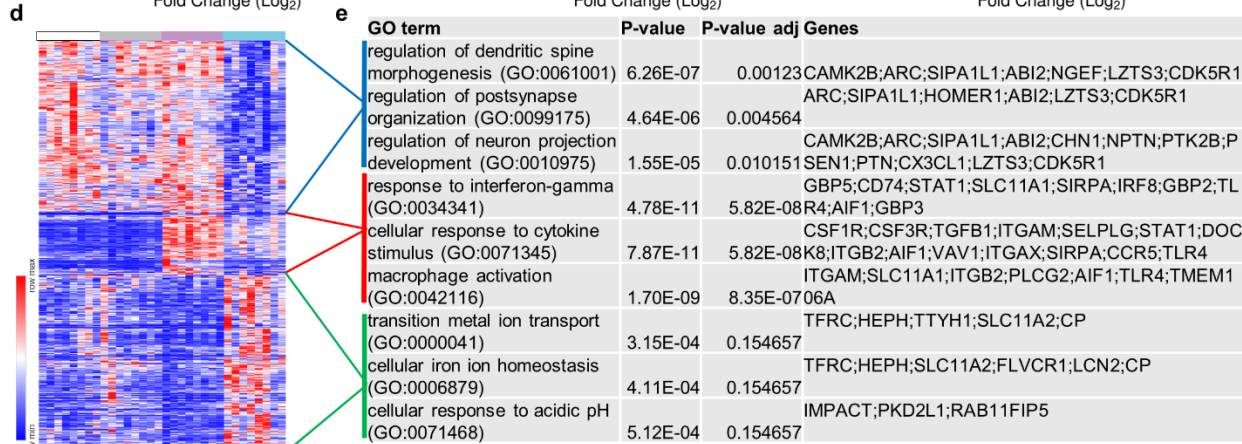
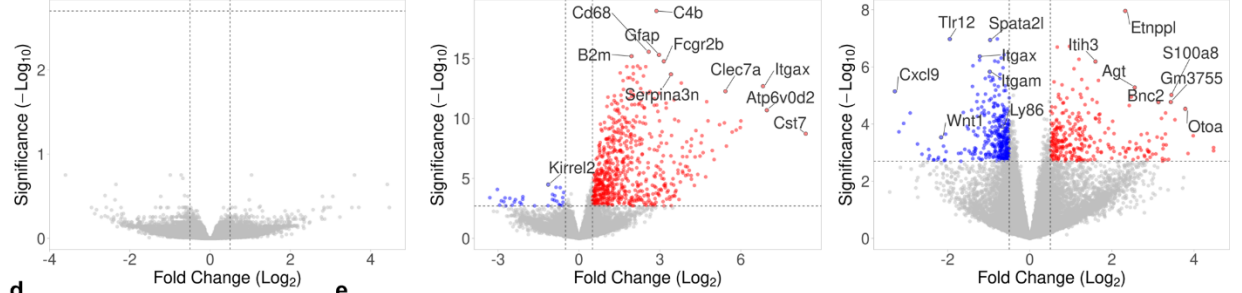
upregulated with D-45113 treatment. We performed pathway analysis on the three clusters of genes through gene ontology (GO) analysis and listed the GO terms, P-value, adjusted P-value, and genes associated with the term in a table (Fig. 3.5e). The GO terms associated with the group of genes that are downregulated with D-45113 treatment are generally linked to synapses and neurons, with the top GO term being related to the regulation of dendritic spine morphogenesis. In the second group of genes, which are upregulated in 5xFAD/Veh mice but downregulated in 5xFAD/D-45113, the top GO terms are all linked to inflammation, with response to interferon-gamma being the top GO term. Finally, the third group, which contains genes that are upregulated with dendrimer administration, has GO terms linked to ion transport and homeostasis, but the adjusted P-values of the top GO terms are not significant. Overall, it appears that D-45113 treatment may impact inflammatory and dendritic and neuronal gene expression in the hippocampi of these mice.

To explore the effect dendrimer treatment has on networks of genes, we performed weighted gene co-expression network analysis (WGCNA) on the gene expression dataset and identified 48 independent modules (Supp. Fig. 3.1a). Correlation of each module to either D-45113 treatment (Fig. 3.5f) or 5xFAD genotype status (Fig. 3.5g) was undertaken of which 16 modules were graphed. The *blue* module is very highly correlated to 5xFAD genotype, while the *darkturquoise* and *pink* modules are correlated with D-45113 treatment. *Blue*, *darkturquoise*, and *pink* eigengene expression was counted and plotted (Fig. 3.5h, i, j) and genes from each module displayed as a heatmap (Fig. 3.5k, l, m). The *blue* module consists of 1294 genes and is highly upregulated in the 5xFAD/Veh and 5xFAD/D-45113 groups, and the GO terms associated with this module are associated

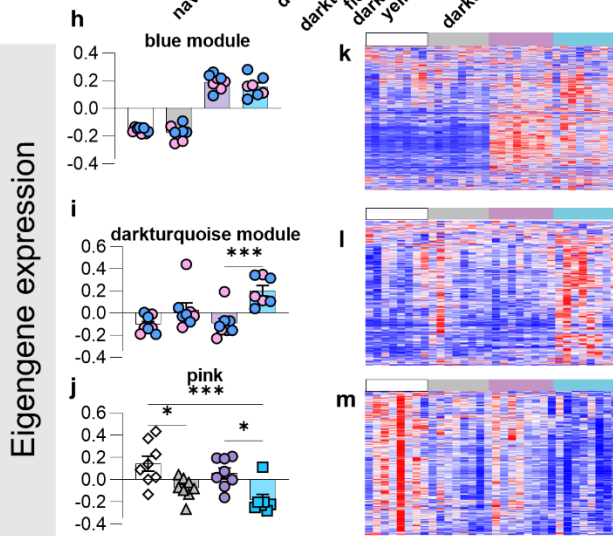
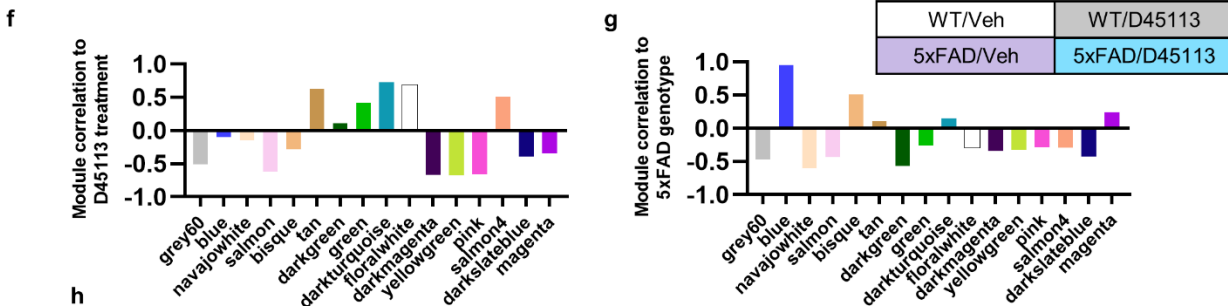
with inflammation (Fig. 3.5n). Additionally, the *blue* module displays gene network changes associated with microglia (Supp. Fig. 3.1b). The *darkturquoise* module consists of 520 genes and is highly upregulated in 5xFAD/D-45113, and the GO terms associated with this module are neutrophil activation and degranulation (Fig. 3.5o). Finally, the *pink* module consists of 500 genes and is downregulated in 5xFAD/D45113 mice, and the GO terms associated with this module are associated with synaptic transmission (Fig. 3.5p), reinforcing the potential link between D-45113 treatment and changes in neurons and synapses.

D-45113 treatment in aged 5xFAD mice results in a reduction of microglial gene expression

a 12-month WT/D-45113 vs WT/Veh    b 12-month 5x/Veh vs. WT/Veh    c 12-month 5x/D-45113 vs. 5x/Veh



WGCNA



GO term	P-value
neutrophil mediated immunity (GO:0002446)	2.96E-34
neutrophil degranulation (GO:0043312)	3.82E-34
neutrophil activation involved in immune response (GO:0002283)	8.28E-34
fatty acid oxidation (GO:0019395)	7.31E-05
neutrophil degranulation (GO:0043312)	9.35E-05
neutrophil activation involved in immune response (GO:0002283)	1.07E-04
chemical synaptic transmission (GO:0007268)	6.16E-13
anterograde trans-synaptic signaling (GO:0098916)	1.52E-11
adenylate cyclase-inhibiting G protein-coupled receptor signaling pathway (GO:0007193)	3.94E-09

Eigengene expression



**Figure 3.5: Bulk RNA-seq inflammatory gene expression is downregulated in 5xFAD mice treated with D45113.** Volcano plot looking at differentially expressed genes (DEGs) between WT/D45113 and WT/Veh groups show no changes in gene expression between the groups **(a)**. Volcano plot examining the DEGs between 12-month-old 5xFAD/Veh mice compared to WT/Veh mice reveals upregulation of classical AD inflammatory genes (*Clec7a*, *Itgax*, *Cst7*, etc.) **(b)**. Volcano plot examining the DEGs between 12-month-old 5xFAD/D45113 mice and 5xFAD/Veh mice reveals downregulation of microglial and inflammatory genes (*Itgax*, *Itgam*, *Cxcl9*, etc.) **(c)**. Heatmap of individual FPKM values of the DEGs between the 12-month-old 5xFAD/D45113 group and 5xFAD/Veh group for all mice analyzed via bulk RNA-seq **(d)**. Gene ontology analysis on three distinct populations of DEGs **(e)**. Sixteen weighted gene connectivity network analysis (WGCNA) modules graphed according to correlation to D45113 treatment **(f)** and 5xFAD genotype **(g)**. Module eigengene expression trajectory of gene expression value in *blue* **(h)**, *darkturquoise* **(i)**, and *pink* **(j)**. Heatmap of genes within its respective module **(k-m)** and subsequent GO analysis terms and p-value for the *blue* **(n)**, *darkturquoise* **(o)**, and *pink* **(p)** modules. Statistical analysis for (h-j) used a one-way ANOVA with Tukey's multiple comparison test. Significance indicated as \* p < 0.05; \*\* p < 0.01; \*\*\* p < 0.001.



**Supp. Figure 3.1:** WGCNA dendrogram highlighting 48 modules (a). Interactive plot between hub genes extracted from the *blue* (b), *darkturquoise* (c), and *pink* (d) modules. Cell-type enrichment heatmap which displays gene network associations with different cell-types (e).

### **Axonal and neuritic damage are not rescued with D-45113 treatment.**

To explore synaptic and neuronal network differences between 5xFAD/Veh and 5xFAD/D-45113 mice, we stained 5- and 12-month-old 5xFAD/Veh and 5xFAD/D-45113 mouse brain tissue with the neuritic dystrophy marker, LAMP1, and Amylo-Glo (Fig. 3.6a). At 5-months of age in the somatosensory cortex, there is no significant difference between the 5xFAD/Veh and 5xFAD/D-45113 groups (Fig. 3.6b). However, in the subiculum, 5xFAD/D-45113 mice have higher LAMP1 staining adjusted for plaque load than 5xFAD/Veh mice (Fig. 3.6c). At 12-months of age, there are no differences in LAMP1 staining adjusted for plaque load in the somatosensory cortex (Fig. 3.6d) and subiculum (Fig. 3.6e). Neurofilament light chain (NfL) found in blood plasma has emerged as a potential biomarker for AD, with higher levels of NfL associated with higher axonal damage [108]. We measured plasma NfL levels of 5- and 12-month 5xFAD/Veh and 5xFAD/D-45113 mice. At the 5-month timepoint, there is an elevation in plasma NfL in both 5xFAD groups compared to WT groups but no differences with D-45113 treatment (Fig. 3.6f). At 12-months of age, 5xFAD/D45113 mice have higher plasma NfL levels than 5xFAD/Veh mice (Fig. 3.6g). Measurements of NfL in the insoluble brain fraction reveal increases in 5-month-old 5xFAD groups compared to WT, but no changes are observed due to D-45113 treatment (Fig. 3.6h). In the soluble fraction, NfL in the WT/D-45113 group is elevated compared to the other three groups (Fig. 3.6i). Similar to the 5-month data, the 12-month timepoint shows an increase in insoluble hippocampal NfL in 5xFAD groups and no differences with D-45113 treatment (Fig. 3.6j), however, no changes in the soluble fraction are observed (Fig. 3.6k).

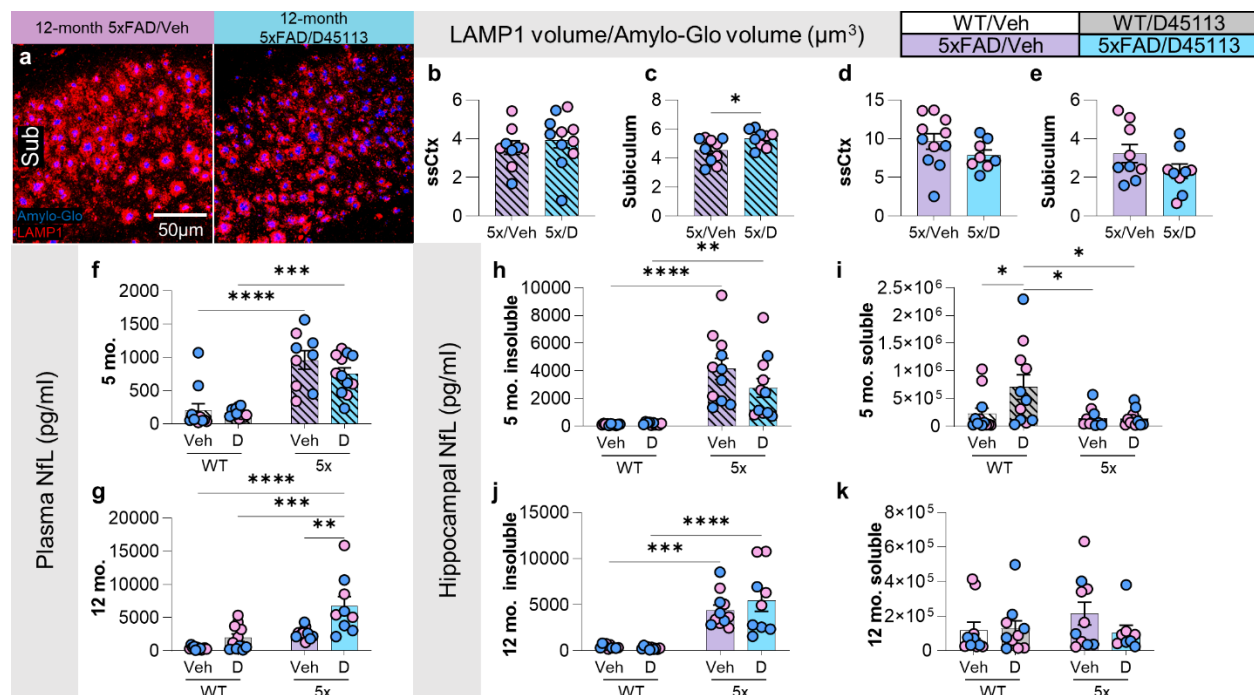


**Figure 3.6: Axonal damage in 5xFAD mice is not rescued with D45113 treatment.** Representative 20x images of the subiculum of 12-month-old 5xFAD/Veh and 5xFAD/D45113 mice stained with a marker for dystrophic neurites, LAMP1, and Amylo-Glo (a). There are no differences at 4-months of age in the somatosensory cortex between 5xFAD/Veh and 5xFAD/D45113 mice in LAMP1 volume/Amylo-Glo volume (b), however, in the subiculum, 5xFAD/D45113 show a higher level of dystrophic neurites (c). At 12-months of age, however, there are no differences in LAMP1 volume/Amylo-Glo volume levels in the somatosensory cortex (d) and the subiculum (e). Plasma neurofilament light chain (NfL) levels, which is a peripheral marker for axonal damage, increase in 5-month-old 5xFAD groups compared to WT groups but not with D45113 treatment (f). At 12-months of age, D45113 treatment in 5xFAD mice exacerbates plasma NfL levels (g). MSD assays measuring soluble and insoluble hippocampal NfL reveal an increase in insoluble NfL in 5xFAD groups compared to WT groups but no difference due to D45113 treatment (h). In the soluble fraction, there is an increase in NfL in the WT/D45113 group compared to the other three groups (i). At 12-months of age, both 5xFAD groups have higher hippocampal insoluble NfL levels compared to WT groups, but no changes are observed due to D45113 treatment (j). No changes are observed in soluble NfL at 12-months of age (k). Statistical analysis for (b-e) used a two-tailed t-test; (f-k) used a two-way ANOVA with Tukey's multiple comparison test. Significance indicated as \*  $p < 0.05$ ; \*\*  $p < 0.01$ ; \*\*\*  $p < 0.001$ .

## Discussion

Dendrimers are dynamic nanomolecules which have been utilized for drug delivery in cancer and in the brain when the BBB has been severely compromised [169]. Factors determining dendrimer biodistribution and toxicity are chemical composition, architecture,

size, and surface properties. Traditional PAMAM dendrimers have trouble passing intact or slightly impaired BBB [219]. Currently, there exist few ways to deliver therapeutics past the BBB and into the brain. One approach is through cerebrospinal fluid (CSF), intracerebral, and intracerebroventricular injection, however, while this is an efficient means to get therapeutics in the brain, these injections are very invasive procedures [34, 150]. Other non-invasive delivery methods such as nasal drug administration, exosome delivery, and nanoparticle delivery represent promising avenues for drug delivery to the brain, but these methods have their own caveats as well such as toxicity problems, dosing limitations, and drug conjugation problems [34, 64, 148, 170]. Previous research has shown that HDs can bypass a partially impaired blood-brain barrier and be phagocytosed by activated microglia and macrophages [133, 135, 138, 139, 143, 190]. However, to our knowledge, this is the first study to assess the ability of HDs to target and treat PAMs specifically in the context of AD. With this in mind, we aimed to address two main objectives: first, to investigate whether HDs can selectively target PAMs in the brains of 5xFAD mice; and second, to evaluate the potential of these HDs for biological modulation of PAMs in the brain.

To clarify the precise role of microglia in AD pathogenesis, it is critical to target specific subsets of microglia, particularly PAMs. Among the key regulators of microglial-plaque association in AD, the most extensively studied is triggering receptor expressed on myeloid cells 2 (TREM2). Previous research that involved knocking out, knocking down, or overexpressing TREM2 or its downstream effectors has emphasized the crucial role of TREM2 in promoting microglial association with plaques [51, 52, 85, 86, 105, 106, 153, 200]. Nevertheless, the impact of this association on the brain remains uncertain. This

may be due to the fact that the vast majority of these studies have targeted all cells in the brain and periphery starting *in utero* in mouse models. In humans, TREM2 is essential for maintaining normal brain homeostasis [47, 71, 137, 189], and *TREM2* mutations resulting in loss of function are associated with a distinct neurodegenerative condition, Nasu-Hakola disease [206]. This represents a confound in the current literature and highlights the importance of developing therapies which target subsets of diverse cells with temporal specificity. HDs, which target only the most phagocytic microglia in AD, appear to be very promising in this regard. HDs have the ability to therapeutically modulate PAM in regions of inflammation while sparing other cell types of potential off-target effects. Furthermore, AD progresses at different rates in different brain regions, resulting in varying microglial responses throughout the disease's course. These dendrimers may be beneficial in that they may target microglia only when needed in disease.

Here, we show proof of principle that HDs are specifically internalized by PAMs and can have a biological effect when conjugated to a CSF1R inhibitor (D-45113) in a mouse model of AD. While we find that dendrimer is only colocalizes with microglia in the brain, it is possible that other cell types may take up levels of dendrimers that are undetectable via IHC. Also worth noting is the fact that PAMs are more resistant to CSF1R inhibition-mediated depletion compared to NPAMs in 5xFAD mice and a mouse A/T/N model [116, 184], perhaps indicating that CSF1R may not be the ideal target to robustly modulate PAMs. Regardless, D-45113 administration in 5xFAD mice reduces microglia number, similar to previous studies which pharmacologically inhibit CSF1R [31, 35, 185]. Interestingly, with reductions in microglia number in 5xFAD mice treated with dendrimer, there is also a reduction in diffuse plaque volume (6E10); however, no difference in

dense-core plaque volume (ThioS) is observed. This could in-part be due to the timing of treatment, as dense-core plaques are present in 5xFAD mice as early as 2 months of age [144]. Additionally, D-45113 treatment results in less microglia-plaque interaction and an increase in plasma NfL levels in 5xFAD mice. This falls in line with previous studies suggesting that microglia-plaque interaction is beneficial in limiting the amount of damage caused by A $\beta$  plaques [36, 51, 184, 198, 201, 218]. These effects are much more prominent in older mice, as evidenced by behavioral, plaque, microglial, and RNA differences observed in 12-month-old 5xFAD mice treated with D-45113. Previous data from our lab indicate that PAMs show much higher levels of DAM marker CD11c (ITGAX) at 12- versus 4-months of age [192], perhaps suggesting that microglia in our older cohort of mice may be more prone to dendrimer uptake. Surprisingly, while treatment with D-45113 led to a rescue in EPM behavior and A $\beta$  levels, and a lowering of inflammatory gene expression, there is no rescue in dystrophic neurite or NfL levels. A few reasons we may not see a rescue include: 1. We treated mice that are mid-late stage in disease pathogenesis and perhaps treating earlier and for longer than 28 days will lead to a rescue; 2. The partial reduction of PAMs is not sufficient to rescue the damage apparent in 5xFAD mice; and 3. D-45113 treatment may have independent effects on the brain of these mice. Our findings suggest that while D-45113 treatment may have therapeutic benefits, further investigation is needed to determine the mechanisms behind synaptic damage and rescue with treatment.

Here, we have shown that HDs have the capacity to target and treat PAMs with temporal precision through systemic administration. We were also able to show proof of principle that D-45113, a dendranib that inhibits the CSF1R has biological activity in the AD mouse

brain, specifically in PAMs. Previous studies have shown successful conjugation of dendrimers with siRNAs, antisense oligonucleotides, and other commercially available drugs [23, 34], making these tools essential for delivering therapeutics across the BBB and directly to PAMs. Microglia have been increasingly implicated in tau hyperphosphorylation [14, 51, 106, 109, 110, 172], and future studies employing dendrimers in plaque + tau mouse models will be crucial to understand the interaction between microglia and the two primary histopathological hallmarks of AD. Overall, however, these results demonstrate that systemically administered HD's can be conjugated to effector molecules and enact a biological effect on their target microglial population.

### **Conclusions:**

Our results indicate that hydroxyl dendrimers (HDs) can cross a slightly impaired BBB and preferentially target PAMs in the brains of 5xFAD mice while leaving other cell types unaffected. Additionally, we show proof of principle that HDs conjugated to a CSF1R inhibitor (D-45113) can have effects on AD plaque pathology microglial number, plaque association, and transcription in 5xFAD mice. Ultimately, we show that HDs conjugated to effector molecules can have modulating effects on PAMs and further studies utilizing HDs should be undertaken to therapeutically target the PAM cell population.



## Concluding Remarks

Since the first reports of Alzheimer's disease (AD) more than 100 years ago [3], there has been a lack of transformative, mechanistic cures for the disease. Current disease-modifying therapeutics targeting amyloid-beta ( $A\beta$ ) have shown promising, but subtle, benefits on disease outcomes; however, better understanding of the AD brain is needed to understand how to effectively treat patients. Microglia have been shown to change morphologically in AD [77, 128], and recently have emerged as key contributors to disease pathogenesis and outcomes [17, 27, 184, 185]. Although much research has been performed examining the roles of microglia in AD, it is unclear whether these cells overall contribute positively or negatively to disease outcomes. While studies targeting microglial CSF1R or TAM receptors (AXL, MERTK) indicate that the microglial response to  $A\beta$  may be harmful [31, 73, 146, 184, 185], studies targeting *Trem2*, a gene responsible for microglial association with  $A\beta$  plaques, provide conflicting results [51, 52, 85, 86, 105, 153, 174, 196, 200].

One reason for these discrepancies could be due to the morphologic and transcriptomic heterogeneity of microglia found in AD. One such population of microglia, disease-associated microglia (DAMs), directly respond to  $A\beta$  in the AD brain and are characterized by the expression of neuroinflammatory genes such as *Cst7*, *Trem2*, *Apoe*, and *Itgax* [94]. As such, my thesis investigates the role of PAMs in AD and provides tools with which to: 1. explore their mechanisms in disease and 2. therapeutically target these cells. All of this is done with the goal of determining this specific population's role in disease hallmarks and outcomes.

First, we explored the role of microglial-specific Apolipoprotein E (ApoE) in disease pathogenesis. ApoE is a glycoprotein normally involved in lipid transport; however, in humans, *APOE* is considered a major genetic risk determinant in late-onset AD [29, 48, 103] and can bind A $\beta$  in brain [102]. Previous ApoE knock-out studies demonstrated a reduction in A $\beta$  plaque load and synaptic proteins [11, 70, 114, 194, 210], as well as a rescue in the microglial homeostatic signature [99], although these knock-out studies affected all cell types' ability to produce ApoE which does not indicate what cellular sources are important for plaque production. Under normal conditions, astrocytes are the main supplier of ApoE and microglia produce very little, but upon exposure to A $\beta$  plaques, microglia enter a DAM state and dramatically upregulate ApoE production. To determine the impact of ApoE expressed by PAMs, I knocked *ApoE* out of all myeloid cells while leaving other sources of ApoE unaffected. Our results indicate that microglial-expressed ApoE is not essential to induce the microglial transcriptional shift associated with 5xFAD pathology, nor for plaque formation. While seemingly unnecessary for plaque formation, we found microglial-expressed ApoE may be needed for proper plaque homeostasis in AD, as plaques were slightly larger in mice that had ApoE from microglia knocked-out. Additionally, microglial-expressed ApoE may have a role in synapse maintenance. Our lab has previously shown that dysregulation of homeostatic microglia through partial inhibition of CSF1R results in reduced P2RY12 expression and reduction in synaptic proteins [6]. Similarly, microglia lacking ApoE express reduced levels of P2RY12 which indicate some level of microglial dysregulation which ultimately impacts synapse maintenance and development. Importantly, while *ApoE* mRNA was knocked out from all microglia, ApoE protein was still present within microglia, suggesting that these cells can

uptake ApoE from other sources in the brain such as astrocytes. Altogether, these data indicate that microglial-ApoE interaction has an effect on plaque size in 5xFAD mice; however, in the absence of microglial-expressed ApoE, other sources of ApoE supplied may be sufficient for microglia to induce changes in the 5xFAD brain. Also worth noting, this work highlights the importance of examining compensatory mechanisms in cell-specific knock-out models, particularly when targeting genes that are expressed in multiple cell types which are translated into secreted proteins that ultimately function outside of the cell.

To examine the role of PAMs more precisely in AD, we developed both a genetic and pharmacological approach to target and manipulate these cells with temporal specificity. In our genetic approach, we developed a novel and inducible destabilized Cre system knocked-in to the *Cst7* locus. Previous data indicate that CST7 is solely expressed in PAMs and our genetic model can efficiently and specifically target a subset of these cells, DAMs, in 5xFAD mice. This new technology can be used in a variety of way, including in lineage tracing studies. For example, newly FDA A $\beta$  immunotherapies will soon be performed worldwide, however; it is unknown what happens to the microglia around the plaques once A $\beta$  is cleared from the brain. It stands to reason that these cells will either stay in a disease-associated state, or revert back to some form of homeostatic function. The *Cst7*<sup>DD-Cre</sup> mouse line crossed with tdTomato and 5xFAD mice will be used to label DAMs prior to A $\beta$  immunization, which will then be subsequently followed to determine their plasticity in function once plaques are depleted from the brain. Other future studies will address the role of this specific cell population in AD through specific knock-out of TREM2 or SYK from PAMs. This approach represents a unique and nuanced way to

modulate any specific gene only in DAMs and will hopefully contribute to our understanding of the exact role of microglia in AD.

While the genetic approach utilized in Chapter Two will help to define the role of DAMs in disease progression, we need to develop methods to therapeutically target these cells while sparing other homeostatic populations. To that end we explored the potential of a pharmacological approach utilizing polyamidoamine (PAMAM) hydroxyl dendrimers which are preferentially phagocytosed by PAMs in the AD brain [177, 178]. Using these dendrimers conjugated to colony stimulating factor 1 receptor (CSF1R), we observe reductions in microglial number, inflammatory gene expression, and A $\beta$  immunohistochemical staining in 5xFAD mice. Overall, these dendrimers show the potential to cross the blood-brain barrier (BBB), specifically modulate PAMs, and affect disease outcomes. PAMAM hydroxyl dendrimers represent an emerging therapeutic that can target PAMs in AD.

Importantly, my thesis highlights the necessity of targeted approaches when determining the role of microglia in neurodegenerative disease. AD is a vastly nuanced disease, with multiple pathological hallmarks and a mosaic of disease expression that is age- and brain region-dependent. Similarly, the microglial response to the pathological hallmarks of AD is nuanced, with age- and brain region-dependent morphological and transcriptional responses. My work sheds insight into how we can begin to target specific subsets of microglia in AD through precise, complementary approaches. Our work demonstrates the utility of nuanced approaches that specifically target microglia, or microglia directly involved with amyloid plaques, allowing us to investigate and begin to develop therapeutics combating the mechanisms behind AD pathogenesis.

## References

- 1 Akiyama H, Barger S, Barnum S, Bradt B, Bauer J, Cole GM, Cooper NR, Eikelenboom P, Emmerling M, Fiebich B et al (2000) Inflammation and Alzheimer's disease. *Neurobiol Aging* 21: 383-421 Doi 10.1016/s0197-4580(00)00124-x
- 2 Albert M, Mairet-Coello G, Danis C, Lieger S, Caillierez R, Carrier S, Skrobala E, Landrieu I, Michel A, Schmitt M et al (2019) Prevention of tau seeding and propagation by immunotherapy with a central tau epitope antibody. *Brain* 142: 1736-1750 Doi 10.1093/brain/awz100
- 3 Alzheimer A, Stelzmann RA, Schnitzlein HN, Murtagh FR (1995) An English translation of Alzheimer's 1907 paper, "Über eine eigenartige Erkrankung der Hirnrinde". *Clin Anat* 8: 429-431 Doi 10.1002/ca.980080612
- 4 Amreddy N, Babu A, Muralidharan R, Panneerselvam J, Srivastava A, Ahmed R, Mehta M, Munshi A, Ramesh R (2018) Recent Advances in Nanoparticle-Based Cancer Drug and Gene Delivery. *Adv Cancer Res* 137: 115-170 Doi 10.1016/bs.acr.2017.11.003
- 5 Arendt T, Schindler C, Bruckner MK, Eschrich K, Bigl V, Zedlick D, Marcova L (1997) Plastic neuronal remodeling is impaired in patients with Alzheimer's disease carrying apolipoprotein epsilon 4 allele. *J Neurosci* 17: 516-529
- 6 Arreola MA, Soni N, Crapser JD, Hohsfield LA, Elmore MRP, Matheos DP, Wood MA, Swarup V, Mortazavi A, Green KN (2021) Microglial dyshomeostasis drives perineuronal net and synaptic loss in a CSF1R(+/-) mouse model of ALSP, which can be rescued via CSF1R inhibitors. *Sci Adv* 7: Doi 10.1126/sciadv.abg1601
- 7 Asai H, Ikezu S, Tsunoda S, Medalla M, Luebke J, Haydar T, Wolozin B, Butovsky O, Kugler S, Ikezu T (2015) Depletion of microglia and inhibition of exosome synthesis halt tau propagation. *Nat Neurosci* 18: 1584-1593 Doi 10.1038/nn.4132
- 8 Atagi Y, Liu CC, Painter MM, Chen XF, Verbeeck C, Zheng H, Li X, Rademakers R, Kang SS, Xu H et al (2015) Apolipoprotein E Is a Ligand for Triggering Receptor Expressed on Myeloid Cells 2 (TREM2). *J Biol Chem* 290: 26043-26050 Doi 10.1074/jbc.M115.679043
- 9 Bae Y, Green ES, Kim GY, Song SJ, Mun JY, Lee S, Park JI, Park JS, Ko KS, Han J et al (2016) Dipeptide-functionalized polyamidoamine dendrimer-mediated apoptin gene delivery facilitates apoptosis of human primary glioma cells. *Int J Pharm* 515: 186-200 Doi 10.1016/j.ijpharm.2016.09.083
- 10 Bailey CC, DeVaux LB, Farzan M (2015) The Triggering Receptor Expressed on Myeloid Cells 2 Binds Apolipoprotein E. *J Biol Chem* 290: 26033-26042 Doi 10.1074/jbc.M115.677286
- 11 Bales KR, Verina T, Cummins DJ, Du Y, Dodel RC, Saura J, Fishman CE, DeLong CA, Piccardo P, Petegnief V et al (1999) Apolipoprotein E is essential for amyloid deposition in the APP(V717F) transgenic mouse model of Alzheimer's disease. *Proc Natl Acad Sci U S A* 96: 15233-15238 Doi 10.1073/pnas.96.26.15233
- 12 Balogh LP (2007) Dendrimer 101. *Adv Exp Med Biol* 620: 136-155 Doi 10.1007/978-0-387-76713-0\_11
- 13 Behjati S, Frank MH (2009) The effects of tamoxifen on immunity. *Curr Med Chem* 16: 3076-3080 Doi 10.2174/092986709788803042
- 14 Bemiller SM, McCray TJ, Allan K, Formica SV, Xu G, Wilson G, Kokiko-Cochran ON, Crish SD, Lasagna-Reeves CA, Ransohoff RM et al (2017) TREM2 deficiency exacerbates tau pathology through dysregulated kinase signaling in a mouse model of tauopathy. *Mol Neurodegener* 12: 74 Doi 10.1186/s13024-017-0216-6

- 15 Bianchin MM, Martin KC, de Souza AC, de Oliveira MA, Rieder CR (2010) Nasu-Hakola disease and primary microglial dysfunction. *Nat Rev Neurol* 6: 2 p following 523 Doi 10.1038/nrneurol.2010.17-c1
- 16 Blakemore WF (1973) Demyelination of the superior cerebellar peduncle in the mouse induced by cuprizone. *J Neurol Sci* 20: 63-72 Doi 10.1016/0022-510x(73)90118-4
- 17 Bolmont T, Haiss F, Eicke D, Radde R, Mathis CA, Klunk WE, Kohsaka S, Jucker M, Calhoun ME (2008) Dynamics of the microglial/amyloid interaction indicate a role in plaque maintenance. *J Neurosci* 28: 4283-4292 Doi 10.1523/JNEUROSCI.4814-07.2008
- 18 Bornemann KD, Wiederhold KH, Pauli C, Ermini F, Stalder M, Schnell L, Sommer B, Jucker M, Staufenbiel M (2001) Abeta-induced inflammatory processes in microglia cells of APP23 transgenic mice. *Am J Pathol* 158: 63-73 Doi 10.1016/s0002-9440(10)63945-4
- 19 Boutajangout A, Quartermain D, Sigurdsson EM (2010) Immunotherapy targeting pathological tau prevents cognitive decline in a new tangle mouse model. *J Neurosci* 30: 16559-16566 Doi 10.1523/JNEUROSCI.4363-10.2010
- 20 Boyles JK, Pitas RE, Wilson E, Mahley RW, Taylor JM (1985) Apolipoprotein E associated with astrocytic glia of the central nervous system and with nonmyelinating glia of the peripheral nervous system. *J Clin Invest* 76: 1501-1513 Doi 10.1172/JCI112130
- 21 Budd Haeberlein S, Aisen PS, Barkhof F, Chalkias S, Chen T, Cohen S, Dent G, Hansson O, Harrison K, von Hehn C et al (2022) Two Randomized Phase 3 Studies of Aducanumab in Early Alzheimer's Disease. *J Prev Alzheimers Dis* 9: 197-210 Doi 10.14283/jpad.2022.30
- 22 Castellano JM, Kim J, Stewart FR, Jiang H, DeMattos RB, Patterson BW, Fagan AM, Morris JC, Mawuenyega KG, Cruchaga C et al (2011) Human apoE isoforms differentially regulate brain amyloid-beta peptide clearance. *Sci Transl Med* 3: 89ra57 Doi 10.1126/scitranslmed.3002156
- 23 Chauhan AS (2018) Dendrimers for Drug Delivery. *Molecules* 23: Doi 10.3390/molecules23040938
- 24 Chiu IM, Morimoto ET, Goodarzi H, Liao JT, O'Keeffe S, Phatnani HP, Muratet M, Carroll MC, Levy S, Tavazoie S et al (2013) A neurodegeneration-specific gene-expression signature of acutely isolated microglia from an amyotrophic lateral sclerosis mouse model. *Cell Rep* 4: 385-401 Doi 10.1016/j.celrep.2013.06.018
- 25 Choudhary S, Satija R (2022) Comparison and evaluation of statistical error models for scRNA-seq. *Genome Biol* 23: 27 Doi 10.1186/s13059-021-02584-9
- 26 Chung H, Brazil MI, Soe TT, Maxfield FR (1999) Uptake, degradation, and release of fibrillar and soluble forms of Alzheimer's amyloid beta-peptide by microglial cells. *J Biol Chem* 274: 32301-32308 Doi 10.1074/jbc.274.45.32301
- 27 Condello C, Yuan P, Schain A, Grutzendler J (2015) Microglia constitute a barrier that prevents neurotoxic protofibrillar Abeta42 hotspots around plaques. *Nat Commun* 6: 6176 Doi 10.1038/ncomms7176
- 28 Corder EH, Saunders AM, Risch NJ, Strittmatter WJ, Schmechel DE, Gaskell PC, Jr., Rimmler JB, Locke PA, Conneally PM, Schmechel KE et al (1994) Protective effect of apolipoprotein E type 2 allele for late onset Alzheimer disease. *Nat Genet* 7: 180-184 Doi 10.1038/ng0694-180
- 29 Corder EH, Saunders AM, Strittmatter WJ, Schmechel DE, Gaskell PC, Small GW, Roses AD, Haines JL, Pericak-Vance MA (1993) Gene dose of apolipoprotein E type 4 allele and the risk of Alzheimer's disease in late onset families. *Science* 261: 921-923 Doi 10.1126/science.8346443
- 30 Crapser JD, Spangenberg EE, Barahona RA, Arreola MA, Hohsfield LA, Green KN (2020) Microglia facilitate loss of perineuronal nets in the Alzheimer's disease brain. *EBioMedicine* 58: 102919 Doi 10.1016/j.ebiom.2020.102919
- 31 Dagher NN, Najafi AR, Kayala KM, Elmore MR, White TE, Medeiros R, West BL, Green KN (2015) Colony-stimulating factor 1 receptor inhibition prevents microglial plaque association and

- improves cognition in 3xTg-AD mice. *J Neuroinflammation* 12: 139 Doi 10.1186/s12974-015-0366-9
- 32 Deczkowska A, Keren-Shaul H, Weiner A, Colonna M, Schwartz M, Amit I (2018) Disease-Associated Microglia: A Universal Immune Sensor of Neurodegeneration. *Cell* 173: 1073-1081 Doi 10.1016/j.cell.2018.05.003
- 33 Delizannis AT, Nonneman A, Tsering W, De Bondt A, Van den Wyngaert I, Zhang B, Meymand E, Olufemi MF, Koivula P, Maimaiti Set al (2021) Effects of microglial depletion and TREM2 deficiency on Abeta plaque burden and neuritic plaque tau pathology in 5XFAD mice. *Acta Neuropathol Commun* 9: 150 Doi 10.1186/s40478-021-01251-1
- 34 Dong Y, Yu T, Ding L, Laurini E, Huang Y, Zhang M, Weng Y, Lin S, Chen P, Marson Det al (2018) A Dual Targeting Dendrimer-Mediated siRNA Delivery System for Effective Gene Silencing in Cancer Therapy. *J Am Chem Soc* 140: 16264-16274 Doi 10.1021/jacs.8b10021
- 35 Elmore MR, Najafi AR, Koike MA, Dagher NN, Spangenberg EE, Rice RA, Kitazawa M, Matusow B, Nguyen H, West BLet al (2014) Colony-stimulating factor 1 receptor signaling is necessary for microglia viability, unmasking a microglia progenitor cell in the adult brain. *Neuron* 82: 380-397 Doi 10.1016/j.neuron.2014.02.040
- 36 Ennerfelt H, Frost EL, Shapiro DA, Holliday C, Zengeler KE, Voithofer G, Bolte AC, Lammert CR, Kulas JA, Ulland TKet al (2022) SYK coordinates neuroprotective microglial responses in neurodegenerative disease. *Cell* 185: 4135-4152 e4122 Doi 10.1016/j.cell.2022.09.030
- 37 Farrer LA, Cupples LA, Haines JL, Hyman B, Kukull WA, Mayeux R, Myers RH, Pericak-Vance MA, Risch N, van Duijn CM (1997) Effects of age, sex, and ethnicity on the association between apolipoprotein E genotype and Alzheimer disease. A meta-analysis. APOE and Alzheimer Disease Meta Analysis Consortium. *JAMA* 278: 1349-1356
- 38 Finak G, McDavid A, Yajima M, Deng J, Gersuk V, Shalek AK, Slichter CK, Miller HW, McElrath MJ, Prlic Met al (2015) MAST: a flexible statistical framework for assessing transcriptional changes and characterizing heterogeneity in single-cell RNA sequencing data. *Genome Biol* 16: 278 Doi 10.1186/s13059-015-0844-5
- 39 Floden AM, Combs CK (2011) Microglia demonstrate age-dependent interaction with amyloid-beta fibrils. *J Alzheimers Dis* 25: 279-293 Doi 10.3233/JAD-2011-101014
- 40 Fonseca MI, Chu SH, Hernandez MX, Fang MJ, Modarresi L, Selvan P, MacGregor GR, Tenner AJ (2017) Cell-specific deletion of C1qa identifies microglia as the dominant source of C1q in mouse brain. *J Neuroinflammation* 14: 48 Doi 10.1186/s12974-017-0814-9
- 41 Forner S, Kawauchi S, Balderrama-Gutierrez G, Kramar EA, Matheos DP, Phan J, Javonillo DI, Tran KM, Hingco E, da Cunha Cet al (2021) Systematic phenotyping and characterization of the 5xFAD mouse model of Alzheimer's disease. *Sci Data* 8: 270 Doi 10.1038/s41597-021-01054-y
- 42 Frautschy SA, Yang F, Irrizarry M, Hyman B, Saido TC, Hsiao K, Cole GM (1998) Microglial response to amyloid plaques in APPsw transgenic mice. *Am J Pathol* 152: 307-317
- 43 Friedman BA, Srinivasan K, Ayalon G, Meilandt WJ, Lin H, Huntley MA, Cao Y, Lee SH, Haddick PCG, Ngu Het al (2018) Diverse Brain Myeloid Expression Profiles Reveal Distinct Microglial Activation States and Aspects of Alzheimer's Disease Not Evident in Mouse Models. *Cell Rep* 22: 832-847 Doi 10.1016/j.celrep.2017.12.066
- 44 Fu AK, Hung KW, Yuen MY, Zhou X, Mak DS, Chan IC, Cheung TH, Zhang B, Fu WY, Liew FYet al (2016) IL-33 ameliorates Alzheimer's disease-like pathology and cognitive decline. *Proc Natl Acad Sci U S A* 113: E2705-2713 Doi 10.1073/pnas.1604032113
- 45 Fuger P, Hefendehl JK, Veeraraghavalu K, Wendeln AC, Schlosser C, Obermuller U, Wegenast-Braun BM, Neher JJ, Martus P, Kohsaka Set al (2017) Microglia turnover with aging and in an Alzheimer's model via long-term in vivo single-cell imaging. *Nat Neurosci* 20: 1371-1376 Doi 10.1038/nn.4631

- 46 Funato H, Yoshimura M, Yamazaki T, Saido TC, Ito Y, Yokofujita J, Okeda R, Ihara Y (1998) Astrocytes containing amyloid beta-protein (Abeta)-positive granules are associated with Abeta40-positive diffuse plaques in the aged human brain. *Am J Pathol* 152: 983-992
- 47 Gawish R, Martins R, Bohm B, Wimberger T, Sharif O, Lakovits K, Schmidt M, Knapp S (2015) Triggering receptor expressed on myeloid cells-2 fine-tunes inflammatory responses in murine Gram-negative sepsis. *FASEB J* 29: 1247-1257 Doi 10.1096/fj.14-260067
- 48 Genin E, Hannequin D, Wallon D, Sleegers K, Hiltunen M, Combarros O, Bullido MJ, Engelborghs S, De Deyn P, Berr Cet al (2011) APOE and Alzheimer disease: a major gene with semi-dominant inheritance. *Mol Psychiatry* 16: 903-907 Doi 10.1038/mp.2011.52
- 49 Goedhart J, Luijsterburg MS (2020) VolcanoR is a web app for creating, exploring, labeling and sharing volcano plots. *Sci Rep* 10: 20560 Doi 10.1038/s41598-020-76603-3
- 50 Grabert K, Michoel T, Karavolos MH, Clohisey S, Baillie JK, Stevens MP, Freeman TC, Summers KM, McColl BW (2016) Microglial brain region-dependent diversity and selective regional sensitivities to aging. *Nat Neurosci* 19: 504-516 Doi 10.1038/nn.4222
- 51 Gratuze M, Chen Y, Parhizkar S, Jain N, Strickland MR, Serrano JR, Colonna M, Ulrich JD, Holtzman DM (2021) Activated microglia mitigate Abeta-associated tau seeding and spreading. *J Exp Med* 218: Doi 10.1084/jem.20210542
- 52 Gratuze M, Leyns CEG, Holtzman DM (2018) New insights into the role of TREM2 in Alzheimer's disease. *Mol Neurodegener* 13: 66 Doi 10.1186/s13024-018-0298-9
- 53 Gustin A, Kirchmeyer M, Koncina E, Felten P, Losciuto S, Heurtaux T, Tardivel A, Heuschling P, Dostert C (2015) NLRP3 Inflammasome Is Expressed and Functional in Mouse Brain Microglia but Not in Astrocytes. *PLoS One* 10: e0130624 Doi 10.1371/journal.pone.0130624
- 54 Haensler J, Szoka FC, Jr. (1993) Polyamidoamine cascade polymers mediate efficient transfection of cells in culture. *Bioconjug Chem* 4: 372-379 Doi 10.1021/bc00023a012
- 55 Hafemeister C, Satija R (2019) Normalization and variance stabilization of single-cell RNA-seq data using regularized negative binomial regression. *Genome Biol* 20: 296 Doi 10.1186/s13059-019-1874-1
- 56 Hamelin L, Lagarde J, Dorothee G, Leroy C, Labit M, Comley RA, de Souza LC, Corne H, Dauphinot L, Bertoux Met al (2016) Early and protective microglial activation in Alzheimer's disease: a prospective study using 18F-DPA-714 PET imaging. *Brain* 139: 1252-1264 Doi 10.1093/brain/aww017
- 57 Hammond TR, Dufort C, Dissing-Olesen L, Giera S, Young A, Wysoker A, Walker AJ, Gergits F, Segel M, Nemesh Jet al (2019) Single-Cell RNA Sequencing of Microglia throughout the Mouse Lifespan and in the Injured Brain Reveals Complex Cell-State Changes. *Immunity* 50: 253-271 e256 Doi 10.1016/j.immuni.2018.11.004
- 58 Hansen DV, Hanson JE, Sheng M (2018) Microglia in Alzheimer's disease. *J Cell Biol* 217: 459-472 Doi 10.1083/jcb.201709069
- 59 Hardy J (2009) The amyloid hypothesis for Alzheimer's disease: a critical reappraisal. *J Neurochem* 110: 1129-1134 Doi 10.1111/j.1471-4159.2009.06181.x
- 60 Hardy J, Selkoe DJ (2002) The amyloid hypothesis of Alzheimer's disease: progress and problems on the road to therapeutics. *Science* 297: 353-356 Doi 10.1126/science.1072994
- 61 Haure-Mirande JV, Audrain M, Fanutza T, Kim SH, Klein WL, Glabe C, Readhead B, Dudley JT, Blitzer RD, Wang Met al (2017) Deficiency of TYROBP, an adapter protein for TREM2 and CR3 receptors, is neuroprotective in a mouse model of early Alzheimer's pathology. *Acta Neuropathol* 134: 769-788 Doi 10.1007/s00401-017-1737-3
- 62 Hebert LE, Scherr PA, Bienias JL, Bennett DA, Evans DA (2003) Alzheimer disease in the US population: prevalence estimates using the 2000 census. *Arch Neurol* 60: 1119-1122 Doi 10.1001/archneur.60.8.1119



- 63 Hebert LE, Weuve J, Scherr PA, Evans DA (2013) Alzheimer disease in the United States (2010-2050) estimated using the 2010 census. *Neurology* 80: 1778-1783 Doi 10.1212/WNL.0b013e31828726f5
- 64 Heidarzadeh M, Gursoy-Ozdemir Y, Kaya M, Eslami Abriz A, Zarebkohan A, Rahbarghazi R, Sokullu E (2021) Exosomal delivery of therapeutic modulators through the blood-brain barrier; promise and pitfalls. *Cell Biosci* 11: 142 Doi 10.1186/s13578-021-00650-0
- 65 Hellwig S, Masuch A, Nestel S, Katzmarski N, Meyer-Luehmann M, Biber K (2015) Forebrain microglia from wild-type but not adult 5xFAD mice prevent amyloid-beta plaque formation in organotypic hippocampal slice cultures. *Sci Rep* 5: 14624 Doi 10.1038/srep14624
- 66 Heneka MT, Kummer MP, Stutz A, Delekate A, Schwartz S, Vieira-Saecker A, Griep A, Axt D, Remus A, Tzeng TC et al (2013) NLRP3 is activated in Alzheimer's disease and contributes to pathology in APP/PS1 mice. *Nature* 493: 674-678 Doi 10.1038/nature11729
- 67 Henningfield CM, Arreola MA, Soni N, Spangenberg EE, Green KN (2022) Microglia-specific ApoE knock-out does not alter Alzheimer's disease plaque pathogenesis or gene expression. *Glia* 70: 287-302 Doi 10.1002/glia.24105
- 68 Henningfield CM, Soni N, Lee RW, Sharma R, Cleland JL, Green KN (2024) Selective targeting and modulation of plaque associated microglia via systemic hydroxyl dendrimer administration in an Alzheimer's disease mouse model. *Alzheimers Res Ther* 16: 101 Doi 10.1186/s13195-024-01470-3
- 69 Hohsfield LA, Tsourmas KI, Ghorbanian Y, Syage AR, Jin Kim S, Cheng Y, Furman S, Inlay MA, Lane TE, Green KN (2022) MAC2 is a long-lasting marker of peripheral cell infiltrates into the mouse CNS after bone marrow transplantation and coronavirus infection. *Glia* 70: 875-891 Doi 10.1002/glia.24144
- 70 Holtzman DM, Fagan AM, Mackey B, Tenkova T, Sartorius L, Paul SM, Bales K, Ashe KH, Irizarry MC, Hyman BT (2000) Apolipoprotein E facilitates neuritic and cerebrovascular plaque formation in an Alzheimer's disease model. *Ann Neurol* 47: 739-747
- 71 Hsieh CL, Koike M, Spusta SC, Niemi EC, Yenari M, Nakamura MC, Seaman WE (2009) A role for TREM2 ligands in the phagocytosis of apoptotic neuronal cells by microglia. *J Neurochem* 109: 1144-1156 Doi 10.1111/j.1471-4159.2009.06042.x
- 72 Huang KL, Marcora E, Pimenova AA, Di Narzo AF, Kapoor M, Jin SC, Harari O, Bertelsen S, Fairfax BP, Czajkowski J et al (2017) A common haplotype lowers PU.1 expression in myeloid cells and delays onset of Alzheimer's disease. *Nat Neurosci* 20: 1052-1061 Doi 10.1038/nn.4587
- 73 Huang Y, Happonen KE, Burrola PG, O'Connor C, Hah N, Huang L, Nimmerjahn A, Lemke G (2021) Microglia use TAM receptors to detect and engulf amyloid beta plaques. *Nat Immunol*: Doi 10.1038/s41590-021-00913-5
- 74 Huh WJ, Khurana SS, Geahlen JH, Kohli K, Waller RA, Mills JC (2012) Tamoxifen induces rapid, reversible atrophy, and metaplasia in mouse stomach. *Gastroenterology* 142: 21-24 e27 Doi 10.1053/j.gastro.2011.09.050
- 75 Huynh TV, Liao F, Francis CM, Robinson GO, Serrano JR, Jiang H, Roh J, Finn MB, Sullivan PM, Esparza T et al (2017) Age-Dependent Effects of apoE Reduction Using Antisense Oligonucleotides in a Model of beta-amyloidosis. *Neuron* 96: 1013-1023 e1014 Doi 10.1016/j.neuron.2017.11.014
- 76 Iaccarino HF, Singer AC, Martorell AJ, Rudenko A, Gao F, Gillingham TZ, Mathys H, Seo J, Kritskiy O, Abdurrob F et al (2016) Gamma frequency entrainment attenuates amyloid load and modifies microglia. *Nature* 540: 230-235 Doi 10.1038/nature20587
- 77 Itagaki S, McGeer PL, Akiyama H, Zhu S, Selkoe D (1989) Relationship of microglia and astrocytes to amyloid deposits of Alzheimer disease. *J Neuroimmunol* 24: 173-182 Doi 10.1016/0165-5728(89)90115-x

- 78 Iusuf D, Teunissen SF, Wagenaar E, Rosing H, Beijnen JH, Schinkel AH (2011) P-glycoprotein (ABCB1) transports the primary active tamoxifen metabolites endoxifen and 4-hydroxytamoxifen and restricts their brain penetration. *J Pharmacol Exp Ther* 337: 710-717 Doi 10.1124/jpet.110.178301
- 79 Jack CR, Jr., Holtzman DM (2013) Biomarker modeling of Alzheimer's disease. *Neuron* 80: 1347-1358 Doi 10.1016/j.neuron.2013.12.003
- 80 Jankowsky JL, Slunt HH, Gonzales V, Savonenko AV, Wen JC, Jenkins NA, Copeland NG, Younkin LH, Lester HA, Younkin S et al (2005) Persistent amyloidosis following suppression of Abeta production in a transgenic model of Alzheimer disease. *PLoS Med* 2: e355 Doi 10.1371/journal.pmed.0020355
- 81 Jansen IE, Savage JE, Watanabe K, Bryois J, Williams DM, Steinberg S, Sealock J, Karlsson IK, Hagg S, Athanasiu L et al (2019) Genome-wide meta-analysis identifies new loci and functional pathways influencing Alzheimer's disease risk. *Nat Genet* 51: 404-413 Doi 10.1038/s41588-018-0311-9
- 82 Janssen L, Dubbelaar ML, Holtman IR, de Boer-Bergsma J, Eggen BJ, Boddeke HW, De Deyn PP, Van Dam D (2017) Aging, microglia and cytoskeletal regulation are key factors in the pathological evolution of the APP23 mouse model for Alzheimer's disease. *Biochim Biophys Acta Mol Basis Dis* 1863: 395-405 Doi 10.1016/j.bbadis.2016.11.014
- 83 Jauregui C, Blanco-Luquin I, Macias M, Roldan M, Caballero C, Pagola I, Mendioroz M, Jerico I (2023) Exploring the Disease-Associated Microglia State in Amyotrophic Lateral Sclerosis. *Biomedicines* 11: Doi 10.3390/biomedicines11112994
- 84 Jawhar S, Trawicka A, Jenneckens C, Bayer TA, Wirths O (2012) Motor deficits, neuron loss, and reduced anxiety coinciding with axonal degeneration and intraneuronal Abeta aggregation in the 5XFAD mouse model of Alzheimer's disease. *Neurobiol Aging* 33: 196 e129-140 Doi 10.1016/j.neurobiolaging.2010.05.027
- 85 Jay TR, Hirsch AM, Broihier ML, Miller CM, Neilson LE, Ransohoff RM, Lamb BT, Landreth GE (2017) Disease Progression-Dependent Effects of TREM2 Deficiency in a Mouse Model of Alzheimer's Disease. *J Neurosci* 37: 637-647 Doi 10.1523/JNEUROSCI.2110-16.2016
- 86 Jay TR, Miller CM, Cheng PJ, Graham LC, Bemiller S, Broihier ML, Xu G, Margevicius D, Karlo JC, Sousa G et al (2015) TREM2 deficiency eliminates TREM2+ inflammatory macrophages and ameliorates pathology in Alzheimer's disease mouse models. *J Exp Med* 212: 287-295 Doi 10.1084/jem.20142322
- 87 Jiang T, Zhang YD, Chen Q, Gao Q, Zhu XC, Zhou JS, Shi JQ, Lu H, Tan L, Yu JT (2016) TREM2 modifies microglial phenotype and provides neuroprotection in P301S tau transgenic mice. *Neuropharmacology* 105: 196-206 Doi 10.1016/j.neuropharm.2016.01.028
- 88 Johnson NR, Yuan P, Castillo E, Lopez TP, Yue W, Bond A, Rivera BM, Sullivan MC, Hirouchi M, Giles K et al (2023) CSF1R inhibitors induce a sex-specific resilient microglial phenotype and functional rescue in a tauopathy mouse model. *Nat Commun* 14: 118 Doi 10.1038/s41467-022-35753-w
- 89 Joly-Amado A, Davtyan H, Serraneau K, Jules P, Zitnyar A, Pressman E, Zagorski K, Antonyan T, Hovakimyan A, Paek H et al (2020) Active immunization with tau epitope in a mouse model of tauopathy induced strong antibody response together with improvement in short memory and pSer396-tau pathology. *Neurobiol Dis* 134: 104636 Doi 10.1016/j.nbd.2019.104636
- 90 Kaiser T, Feng G (2019) Tmem119-EGFP and Tmem119-CreERT2 Transgenic Mice for Labeling and Manipulating Microglia. *eNeuro* 6: Doi 10.1523/ENEURO.0448-18.2019
- 91 Kanekiyo T, Xu H, Bu G (2014) ApoE and Abeta in Alzheimer's disease: accidental encounters or partners? *Neuron* 81: 740-754 Doi 10.1016/j.neuron.2014.01.045

- 92 Katare YK, Daya RP, Sookram Gray C, Luckham RE, Bhandari J, Chauhan AS, Mishra RK (2015) Brain Targeting of a Water Insoluble Antipsychotic Drug Haloperidol via the Intranasal Route Using PAMAM Dendrimer. *Mol Pharm* 12: 3380-3388 Doi 10.1021/acs.molpharmaceut.5b00402
- 93 Kawanishi K, Sawada A, Ochi A, Moriyama T, Mitobe M, Mochizuki T, Honda K, Oda H, Nishikawa T, Nitta K (2013) Glomerulopathy with homozygous apolipoprotein e2: a report of three cases and review of the literature. *Case Rep Nephrol Urol* 3: 128-135 Doi 10.1159/000356849
- 94 Keren-Shaul H, Spinrad A, Weiner A, Matcovitch-Natan O, Dvir-Szternfeld R, Ulland TK, David E, Baruch K, Lara-Astaiso D, Toth Bet al (2017) A Unique Microglia Type Associated with Restricting Development of Alzheimer's Disease. *Cell* 169: 1276-1290 e1217 Doi 10.1016/j.cell.2017.05.018
- 95 Klajnert B, Wasiaik T, Ionov M, Fernandez-Villamarin M, Sousa-Herves A, Correa J, Riguera R, Fernandez-Megia E (2012) Dendrimers reduce toxicity of Abeta 1-28 peptide during aggregation and accelerate fibril formation. *Nanomedicine* 8: 1372-1378 Doi 10.1016/j.nano.2012.03.005
- 96 Koenigsknecht-Talboo J, Landreth GE (2005) Microglial phagocytosis induced by fibrillar beta-amyloid and IgGs are differentially regulated by proinflammatory cytokines. *J Neurosci* 25: 8240-8249 Doi 10.1523/JNEUROSCI.1808-05.2005
- 97 Koenigsknecht J, Landreth G (2004) Microglial phagocytosis of fibrillar beta-amyloid through a beta1 integrin-dependent mechanism. *J Neurosci* 24: 9838-9846 Doi 10.1523/JNEUROSCI.2557-04.2004
- 98 Koistinaho M, Lin S, Wu X, Esterman M, Koger D, Hanson J, Higgs R, Liu F, Malkani S, Bales KRet al (2004) Apolipoprotein E promotes astrocyte colocalization and degradation of deposited amyloid-beta peptides. *Nat Med* 10: 719-726 Doi 10.1038/nm1058
- 99 Krasemann S, Madore C, Cialic R, Baufeld C, Calcagno N, El Fatimy R, Beckers L, O'Loughlin E, Xu Y, Fanek Zet al (2017) The TREM2-APOE Pathway Drives the Transcriptional Phenotype of Dysfunctional Microglia in Neurodegenerative Diseases. *Immunity* 47: 566-581 e569 Doi 10.1016/j.immuni.2017.08.008
- 100 Kuleshov MV, Jones MR, Rouillard AD, Fernandez NF, Duan Q, Wang Z, Koplev S, Jenkins SL, Jagodnik KM, Lachmann Aet al (2016) Enrichr: a comprehensive gene set enrichment analysis web server 2016 update. *Nucleic Acids Res* 44: W90-97 Doi 10.1093/nar/gkw377
- 101 Kunkle BW, Grenier-Boley B, Sims R, Bis JC, Damotte V, Naj AC, Boland A, Vronskaya M, van der Lee SJ, Amlie-Wolf Aet al (2019) Genetic meta-analysis of diagnosed Alzheimer's disease identifies new risk loci and implicates Abeta, tau, immunity and lipid processing. *Nat Genet* 51: 414-430 Doi 10.1038/s41588-019-0358-2
- 102 LaDu MJ, Falduto MT, Manelli AM, Reardon CA, Getz GS, Frail DE (1994) Isoform-specific binding of apolipoprotein E to beta-amyloid. *J Biol Chem* 269: 23403-23406
- 103 Lambert JC, Ibrahim-Verbaas CA, Harold D, Naj AC, Sims R, Bellenguez C, DeStafano AL, Bis JC, Beecham GW, Grenier-Boley Bet al (2013) Meta-analysis of 74,046 individuals identifies 11 new susceptibility loci for Alzheimer's disease. *Nat Genet* 45: 1452-1458 Doi 10.1038/ng.2802
- 104 Lane-Donovan C, Wong WM, Durakoglugil MS, Wasser CR, Jiang S, Xian X, Herz J (2016) Genetic Restoration of Plasma ApoE Improves Cognition and Partially Restores Synaptic Defects in ApoE-Deficient Mice. *J Neurosci* 36: 10141-10150 Doi 10.1523/JNEUROSCI.1054-16.2016
- 105 Lee CYD, Daggett A, Gu X, Jiang LL, Langfelder P, Li X, Wang N, Zhao Y, Park CS, Cooper Yet al (2018) Elevated TREM2 Gene Dosage Reprograms Microglia Responsivity and Ameliorates Pathological Phenotypes in Alzheimer's Disease Models. *Neuron* 97: 1032-1048 e1035 Doi 10.1016/j.neuron.2018.02.002
- 106 Lee SH, Meilandt WJ, Xie L, Gandham VD, Ngu H, Barck KH, Rezzonico MG, Imperio J, Lalehzadeh G, Huntley MAet al (2021) Trem2 restrains the enhancement of tau accumulation and neurodegeneration by beta-amyloid pathology. *Neuron* 109: 1283-1301 e1286 Doi 10.1016/j.neuron.2021.02.010

- 107 Leinenga G, Gotz J (2015) Scanning ultrasound removes amyloid-beta and restores memory in an Alzheimer's disease mouse model. *Sci Transl Med* 7: 278ra233 Doi 10.1126/scitranslmed.aaa2512
- 108 Lewczuk P, Ermann N, Andreasson U, Schultheis C, Podhorna J, Spitzer P, Maler JM, Kornhuber J, Blennow K, Zetterberg H (2018) Plasma neurofilament light as a potential biomarker of neurodegeneration in Alzheimer's disease. *Alzheimers Res Ther* 10: 71 Doi 10.1186/s13195-018-0404-9
- 109 Leyns CEG, Gratuze M, Narasimhan S, Jain N, Koscal LJ, Jiang H, Manis M, Colonna M, Lee VMY, Ulrich JDet al (2019) TREM2 function impedes tau seeding in neuritic plaques. *Nat Neurosci* 22: 1217-1222 Doi 10.1038/s41593-019-0433-0
- 110 Leyns CEG, Ulrich JD, Finn MB, Stewart FR, Koscal LJ, Remolina Serrano J, Robinson GO, Anderson E, Colonna M, Holtzman DM (2017) TREM2 deficiency attenuates neuroinflammation and protects against neurodegeneration in a mouse model of tauopathy. *Proc Natl Acad Sci U S A* 114: 11524-11529 Doi 10.1073/pnas.1710311114
- 111 Li Q, Cheng Z, Zhou L, Darmanis S, Neff NF, Okamoto J, Gulati G, Bennett ML, Sun LO, Clarke LEet al (2019) Developmental Heterogeneity of Microglia and Brain Myeloid Cells Revealed by Deep Single-Cell RNA Sequencing. *Neuron* 101: 207-223 e210 Doi 10.1016/j.neuron.2018.12.006
- 112 Li R, Shen Y, Yang LB, Lue LF, Finch C, Rogers J (2000) Estrogen enhances uptake of amyloid beta-protein by microglia derived from the human cortex. *J Neurochem* 75: 1447-1454 Doi 10.1046/j.1471-4159.2000.0751447.x
- 113 Liddel SA, Guttenplan KA, Clarke LE, Bennett FC, Bohlen CJ, Schirmer L, Bennett ML, Munch AE, Chung WS, Peterson TCet al (2017) Neurotoxic reactive astrocytes are induced by activated microglia. *Nature* 541: 481-487 Doi 10.1038/nature21029
- 114 Liraz O, Boehm-Cagan A, Michaelson DM (2013) ApoE4 induces Abeta42, tau, and neuronal pathology in the hippocampus of young targeted replacement apoE4 mice. *Mol Neurodegener* 8: 16 Doi 10.1186/1750-1326-8-16
- 115 Liu CC, Zhao N, Fu Y, Wang N, Linares C, Tsai CW, Bu G (2017) ApoE4 Accelerates Early Seeding of Amyloid Pathology. *Neuron* 96: 1024-1032 e1023 Doi 10.1016/j.neuron.2017.11.013
- 116 Lodder C, Scheyltjens I, Stancu IC, Botella Lucena P, Gutierrez de Rave M, Vanherle S, Vanmierlo T, Cremers N, Vanrusselt H, Brone Bet al (2021) CSF1R inhibition rescues tau pathology and neurodegeneration in an A/T/N model with combined AD pathologies, while preserving plaque associated microglia. *Acta Neuropathol Commun* 9: 108 Doi 10.1186/s40478-021-01204-8
- 117 Love S, Siew LK, Dawbarn D, Wilcock GK, Ben-Shlomo Y, Allen SJ (2006) Premorbid effects of APOE on synaptic proteins in human temporal neocortex. *Neurobiol Aging* 27: 797-803 Doi 10.1016/j.neurobiolaging.2005.04.008
- 118 Lull ME, Block ML (2010) Microglial activation and chronic neurodegeneration. *Neurotherapeutics* 7: 354-365 Doi 10.1016/j.nurt.2010.05.014
- 119 Luong D, Kesharwani P, Deshmukh R, Mohd Amin MCI, Gupta U, Greish K, Iyer AK (2016) PEGylated PAMAM dendrimers: Enhancing efficacy and mitigating toxicity for effective anticancer drug and gene delivery. *Acta Biomater* 43: 14-29 Doi 10.1016/j.actbio.2016.07.015
- 120 Ma J, Tanaka KF, Shimizu T, Bernard CC, Kakita A, Takahashi H, Pfeiffer SE, Ikenaka K (2011) Microglial cystatin F expression is a sensitive indicator for ongoing demyelination with concurrent remyelination. *J Neurosci Res* 89: 639-649 Doi 10.1002/jnr.22567
- 121 Majumdar A, Cruz D, Asamoah N, Buxbaum A, Sohar I, Lobel P, Maxfield FR (2007) Activation of microglia acidifies lysosomes and leads to degradation of Alzheimer amyloid fibrils. *Mol Biol Cell* 18: 1490-1496 Doi 10.1091/mbc.e06-10-0975

- 122 Mancuso R, Fryatt G, Cleal M, Obst J, Pipi E, Monzon-Sandoval J, Ribe E, Winchester L, Webber C, Nevado A et al (2019) CSF1R inhibitor JNJ-40346527 attenuates microglial proliferation and neurodegeneration in P301S mice. *Brain* 142: 3243-3264 Doi 10.1093/brain/awz241
- 123 Masliah E, Mallory M, Ge N, Alford M, Veinbergs I, Roses AD (1995) Neurodegeneration in the central nervous system of apoE-deficient mice. *Exp Neurol* 136: 107-122 Doi 10.1006/exnr.1995.1088
- 124 Masuda T, Sankowski R, Staszewski O, Bottcher C, Amann L, Sagar, Scheiwe C, Nessler S, Kunz P, van Loo Get al (2019) Spatial and temporal heterogeneity of mouse and human microglia at single-cell resolution. *Nature* 566: 388-392 Doi 10.1038/s41586-019-0924-x
- 125 Matcovitch-Natan O, Winter DR, Giladi A, Vargas Aguilar S, Spinrad A, Sarrazin S, Ben-Yehuda H, David E, Zelada Gonzalez F, Perrin Pet al (2016) Microglia development follows a stepwise program to regulate brain homeostasis. *Science* 353: aad8670 Doi 10.1126/science.aad8670
- 126 Mathys H, Davila-Velderrain J, Peng Z, Gao F, Mohammadi S, Young JZ, Menon M, He L, Abdurrob F, Jiang X et al (2019) Single-cell transcriptomic analysis of Alzheimer's disease. *Nature* 570: 332-337 Doi 10.1038/s41586-019-1195-2
- 127 Matsunaga W, Shirokawa T, Isobe K (2003) Specific uptake of Abeta1-40 in rat brain occurs in astrocyte, but not in microglia. *Neurosci Lett* 342: 129-131 Doi 10.1016/s0304-3940(03)00240-4
- 128 McGeer PL, Itagaki S, Tago H, McGeer EG (1987) Reactive microglia in patients with senile dementia of the Alzheimer type are positive for the histocompatibility glycoprotein HLA-DR. *Neurosci Lett* 79: 195-200 Doi 10.1016/0304-3940(87)90696-3
- 129 McKinsey GL, Lizama CO, Keown-Lang AE, Niu A, Santander N, Larphaveesarp A, Chee E, Gonzalez FF, Arnold TD (2020) A new genetic strategy for targeting microglia in development and disease. *Elife* 9: Doi 10.7554/eLife.54590
- 130 Meilandt WJ, Ngu H, Gogineni A, Lalehzadeh G, Lee SH, Srinivasan K, Imperio J, Wu T, Weber M, Kruse AJ et al (2020) Trem2 Deletion Reduces Late-Stage Amyloid Plaque Accumulation, Elevates the Abeta42:Abeta40 Ratio, and Exacerbates Axonal Dystrophy and Dendritic Spine Loss in the PS2APP Alzheimer's Mouse Model. *J Neurosci* 40: 1956-1974 Doi 10.1523/JNEUROSCI.1871-19.2019
- 131 Mignani S, Rodrigues J, Tomas H, Zablocka M, Shi X, Caminade AM, Majoral JP (2018) Dendrimers in combination with natural products and analogues as anti-cancer agents. *Chem Soc Rev* 47: 514-532 Doi 10.1039/c7cs00550d
- 132 Mintun MA, Larossa GN, Sheline YI, Dence CS, Lee SY, Mach RH, Klunk WE, Mathis CA, DeKosky ST, Morris JC (2006) [11C]PIB in a nondemented population: potential antecedent marker of Alzheimer disease. *Neurology* 67: 446-452 Doi 10.1212/01.wnl.0000228230.26044.a4
- 133 Mishra MK, Beaty CA, Lesniak WG, Kambhampati SP, Zhang F, Wilson MA, Blue ME, Troncoso JC, Kannan S, Johnston MV et al (2014) Dendrimer brain uptake and targeted therapy for brain injury in a large animal model of hypothermic circulatory arrest. *ACS Nano* 8: 2134-2147 Doi 10.1021/nn404872e
- 134 Mishra V, Kesharwani P (2016) Dendrimer technologies for brain tumor. *Drug Discov Today* 21: 766-778 Doi 10.1016/j.drudis.2016.02.006
- 135 Modi HR, Wang Q, Olmstead SJ, Khoury ES, Sah N, Guo Y, Gharibani P, Sharma R, Kannan RM, Kannan S et al (2022) Systemic administration of dendrimer N-acetyl cysteine improves outcomes and survival following cardiac arrest. *Bioeng Transl Med* 7: e10259 Doi 10.1002/btm2.10259
- 136 Morris JC, Storandt M, Miller JP, McKeel DW, Price JL, Rubin EH, Berg L (2001) Mild cognitive impairment represents early-stage Alzheimer disease. *Arch Neurol* 58: 397-405 Doi 10.1001/archneur.58.3.397

- 137 N'Diaye EN, Branda CS, Branda SS, Nevarez L, Colonna M, Lowell C, Hamerman JA, Seaman WE (2009) TREM-2 (triggering receptor expressed on myeloid cells 2) is a phagocytic receptor for bacteria. *J Cell Biol* 184: 215-223 Doi 10.1083/jcb.200808080
- 138 Nance E, Kambhampati SP, Smith ES, Zhang Z, Zhang F, Singh S, Johnston MV, Kannan RM, Blue ME, Kannan S (2017) Dendrimer-mediated delivery of N-acetyl cysteine to microglia in a mouse model of Rett syndrome. *J Neuroinflammation* 14: 252 Doi 10.1186/s12974-017-1004-5
- 139 Nance E, Zhang F, Mishra MK, Zhang Z, Kambhampati SP, Kannan RM, Kannan S (2016) Nanoscale effects in dendrimer-mediated targeting of neuroinflammation. *Biomaterials* 101: 96-107 Doi 10.1016/j.biomaterials.2016.05.044
- 140 Nelson PT, Braak H, Markesbery WR (2009) Neuropathology and cognitive impairment in Alzheimer disease: a complex but coherent relationship. *J Neuropathol Exp Neurol* 68: 1-14 Doi 10.1097/NEN.0b013e3181919a48
- 141 Nelson PT, Pious NM, Jicha GA, Wilcock DM, Fardo DW, Estus S, Rebeck GW (2013) APOE-epsilon2 and APOE-epsilon4 correlate with increased amyloid accumulation in cerebral vasculature. *J Neuropathol Exp Neurol* 72: 708-715 Doi 10.1097/NEN.0b013e31829a25b9
- 142 Nimmerjahn A, Kirchhoff F, Helmchen F (2005) Resting microglial cells are highly dynamic surveillants of brain parenchyma in vivo. *Science* 308: 1314-1318 Doi 10.1126/science.1110647
- 143 Nino DF, Zhou Q, Yamaguchi Y, Martin LY, Wang S, Fulton WB, Jia H, Lu P, Prindle T, Jr., Zhang Fet al (2018) Cognitive impairments induced by necrotizing enterocolitis can be prevented by inhibiting microglial activation in mouse brain. *Sci Transl Med* 10: Doi 10.1126/scitranslmed.aan0237
- 144 Oakley H, Cole SL, Logan S, Maus E, Shao P, Craft J, Guillozet-Bongaarts A, Ohno M, Disterhoft J, Van Eldik Let al (2006) Intraneuronal beta-amyloid aggregates, neurodegeneration, and neuron loss in transgenic mice with five familial Alzheimer's disease mutations: potential factors in amyloid plaque formation. *J Neurosci* 26: 10129-10140 Doi 10.1523/JNEUROSCI.1202-06.2006
- 145 Ofengeim D, Mazzitelli S, Ito Y, DeWitt JP, Mifflin L, Zou C, Das S, Adiconis X, Chen H, Zhu Het al (2017) RIPK1 mediates a disease-associated microglial response in Alzheimer's disease. *Proc Natl Acad Sci U S A* 114: E8788-E8797 Doi 10.1073/pnas.1714175114
- 146 Olmos-Alonso A, Schettters ST, Sri S, Askew K, Mancuso R, Vargas-Caballero M, Holscher C, Perry VH, Gomez-Nicola D (2016) Pharmacological targeting of CSF1R inhibits microglial proliferation and prevents the progression of Alzheimer's-like pathology. *Brain* 139: 891-907 Doi 10.1093/brain/awv379
- 147 Ostendorf BN, Bilanovic J, Adaku N, Tafreshian KN, Tavora B, Vaughan RD, Tavazoie SF (2020) Common germline variants of the human APOE gene modulate melanoma progression and survival. *Nat Med* 26: 1048-1053 Doi 10.1038/s41591-020-0879-3
- 148 Ozsoy Y, Gungor S, Cevher E (2009) Nasal delivery of high molecular weight drugs. *Molecules* 14: 3754-3779 Doi 10.3390/molecules14093754
- 149 Pan XD, Zhu YG, Lin N, Zhang J, Ye QY, Huang HP, Chen XC (2011) Microglial phagocytosis induced by fibrillar beta-amyloid is attenuated by oligomeric beta-amyloid: implications for Alzheimer's disease. *Mol Neurodegener* 6: 45 Doi 10.1186/1750-1326-6-45
- 150 Pardridge WM (2022) A Historical Review of Brain Drug Delivery. *Pharmaceutics* 14: Doi 10.3390/pharmaceutics14061283
- 151 Paresce DM, Chung H, Maxfield FR (1997) Slow degradation of aggregates of the Alzheimer's disease amyloid beta-protein by microglial cells. *J Biol Chem* 272: 29390-29397 Doi 10.1074/jbc.272.46.29390
- 152 Paresce DM, Ghosh RN, Maxfield FR (1996) Microglial cells internalize aggregates of the Alzheimer's disease amyloid beta-protein via a scavenger receptor. *Neuron* 17: 553-565 Doi 10.1016/s0896-6273(00)80187-7

- 153 Parhizkar S, Arzberger T, Brendel M, Kleinberger G, Deussing M, Focke C, Nuscher B, Xiong M, Ghasemigharagoz A, Katzmarski Net al (2019) Loss of TREM2 function increases amyloid seeding but reduces plaque-associated ApoE. *Nat Neurosci* 22: 191-204 Doi 10.1038/s41593-018-0296-9
- 154 Pierantoni GM, Rinaldo C, Esposito F, Mottolese M, Soddu S, Fusco A (2006) High Mobility Group A1 (HMGA1) proteins interact with p53 and inhibit its apoptotic activity. *Cell Death Differ* 13: 1554-1563 Doi 10.1038/sj.cdd.4401839
- 155 Ping L, Duong DM, Yin L, Gearing M, Lah JJ, Levey AI, Seyfried NT (2018) Global quantitative analysis of the human brain proteome in Alzheimer's and Parkinson's Disease. *Sci Data* 5: 180036 Doi 10.1038/sdata.2018.36
- 156 Pitas RE, Boyles JK, Lee SH, Foss D, Mahley RW (1987) Astrocytes synthesize apolipoprotein E and metabolize apolipoprotein E-containing lipoproteins. *Biochim Biophys Acta* 917: 148-161 Doi 10.1016/0005-2760(87)90295-5
- 157 Polazzi E, Monti B (2010) Microglia and neuroprotection: from in vitro studies to therapeutic applications. *Prog Neurobiol* 92: 293-315 Doi 10.1016/j.pneurobio.2010.06.009
- 158 Polvikoski T, Sulkava R, Haltia M, Kainulainen K, Vuorio A, Verkkoniemi A, Niinisto L, Halonen P, Kontula K (1995) Apolipoprotein E, dementia, and cortical deposition of beta-amyloid protein. *N Engl J Med* 333: 1242-1247 Doi 10.1056/NEJM199511093331902
- 159 Prokop S, Miller KR, Labra SR, Pitkin RM, Hoxha K, Narasimhan S, Changolkar L, Rosenbloom A, Lee VM, Trojanowski JQ (2019) Impact of TREM2 risk variants on brain region-specific immune activation and plaque microenvironment in Alzheimer's disease patient brain samples. *Acta Neuropathol* 138: 613-630 Doi 10.1007/s00401-019-02048-2
- 160 Rangaraju S, Dammer EB, Raza SA, Rathakrishnan P, Xiao H, Gao T, Duong DM, Pennington MW, Lah JJ, Seyfried NT et al (2018) Identification and therapeutic modulation of a pro-inflammatory subset of disease-associated-microglia in Alzheimer's disease. *Mol Neurodegener* 13: 24 Doi 10.1186/s13024-018-0254-8
- 161 Reiman EM, Arboleda-Velasquez JF, Quiroz YT, Huentelman MJ, Beach TG, Caselli RJ, Chen Y, Su Y, Myers AJ, Hardy J et al (2020) Exceptionally low likelihood of Alzheimer's dementia in APOE2 homozygotes from a 5,000-person neuropathological study. *Nat Commun* 11: 667 Doi 10.1038/s41467-019-14279-8
- 162 Richard BC, Kurdakova A, Baches S, Bayer TA, Weggen S, Wirths O (2015) Gene Dosage Dependent Aggravation of the Neurological Phenotype in the 5XFAD Mouse Model of Alzheimer's Disease. *J Alzheimers Dis* 45: 1223-1236 Doi 10.3233/JAD-143120
- 163 Robinson MD, McCarthy DJ, Smyth GK (2010) edgeR: a Bioconductor package for differential expression analysis of digital gene expression data. *Bioinformatics* 26: 139-140 Doi 10.1093/bioinformatics/btp616
- 164 Rodriguez GA, Tai LM, LaDu MJ, Rebeck GW (2014) Human APOE4 increases microglia reactivity at Abeta plaques in a mouse model of Abeta deposition. *J Neuroinflammation* 11: 111 Doi 10.1186/1742-2094-11-111
- 165 Safaiyan S, Besson-Girard S, Kaya T, Cantuti-Castelvetri L, Liu L, Ji H, Schifferer M, Gouna G, Usifo F, Kannaiyan Net al (2021) White matter aging drives microglial diversity. *Neuron* 109: 1100-1117 e1110 Doi 10.1016/j.neuron.2021.01.027
- 166 Sahasrabudhe V, Ghosh HS (2022) Cx3Cr1-Cre induction leads to microglial activation and IFN-1 signaling caused by DNA damage in early postnatal brain. *Cell Rep* 38: 110252 Doi 10.1016/j.celrep.2021.110252
- 167 Saito T, Matsunaga A, Fukunaga M, Nagahama K, Hara S, Muso E (2020) Apolipoprotein E-related glomerular disorders. *Kidney Int* 97: 279-288 Doi 10.1016/j.kint.2019.10.031

- 168 Sando R, 3rd, Baumgaertel K, Pieraut S, Torabi-Rander N, Wandless TJ, Mayford M, Maximov A (2013) Inducible control of gene expression with destabilized Cre. *Nat Methods* 10: 1085-1088 Doi 10.1038/nmeth.2640
- 169 Santos SD, Xavier M, Leite DM, Moreira DA, Custodio B, Torrado M, Castro R, Leiro V, Rodrigues J, Tomas H et al (2018) PAMAM dendrimers: blood-brain barrier transport and neuronal uptake after focal brain ischemia. *J Control Release* 291: 65-79 Doi 10.1016/j.jconrel.2018.10.006
- 170 Saraiva C, Praca C, Ferreira R, Santos T, Ferreira L, Bernardino L (2016) Nanoparticle-mediated brain drug delivery: Overcoming blood-brain barrier to treat neurodegenerative diseases. *J Control Release* 235: 34-47 Doi 10.1016/j.jconrel.2016.05.044
- 171 Saunders AM, Strittmatter WJ, Schmechel D, George-Hyslop PH, Pericak-Vance MA, Joo SH, Rosi BL, Gusella JF, Crapper-MaLachlan DR, Alberts MJ et al (1993) Association of apolipoprotein E allele epsilon 4 with late-onset familial and sporadic Alzheimer's disease. *Neurology* 43: 1467-1472 Doi 10.1212/wnl.43.8.1467
- 172 Sayed FA, Telpoukhovskaia M, Kodama L, Li Y, Zhou Y, Le D, Hauduc A, Ludwig C, Gao F, Clelland C et al (2018) Differential effects of partial and complete loss of TREM2 on microglial injury response and tauopathy. *Proc Natl Acad Sci U S A* 115: 10172-10177 Doi 10.1073/pnas.1811411115
- 173 Schmechel DE, Saunders AM, Strittmatter WJ, Crain BJ, Hulette CM, Joo SH, Pericak-Vance MA, Goldgaber D, Roses AD (1993) Increased amyloid beta-peptide deposition in cerebral cortex as a consequence of apolipoprotein E genotype in late-onset Alzheimer disease. *Proc Natl Acad Sci U S A* 90: 9649-9653 Doi 10.1073/pnas.90.20.9649
- 174 Schoch KM, Ezerskiy LA, Morhaus MM, Bannon RN, Sauerbeck AD, Shabsovich M, Jafar-Nejad P, Rigo F, Miller TM (2021) Acute Trem2 reduction triggers increased microglial phagocytosis, slowing amyloid deposition in mice. *Proc Natl Acad Sci U S A* 118: Doi 10.1073/pnas.2100356118
- 175 Schroeder S, Joly-Amado A, Soliman A, Sengupta U, Kaye R, Gordon MN, Morgan D (2017) Oligomeric tau-targeted immunotherapy in Tg4510 mice. *Alzheimers Res Ther* 9: 46 Doi 10.1186/s13195-017-0274-6
- 176 Serrano-Pozo A, Qian J, Monsell SE, Betensky RA, Hyman BT (2015) APOEepsilon2 is associated with milder clinical and pathological Alzheimer disease. *Ann Neurol* 77: 917-929 Doi 10.1002/ana.24369
- 177 Sharma A, Sharma R, Zhang Z, Liaw K, Kambhampati SP, Porterfield JE, Lin KC, DeRidder LB, Kannan S, Kannan RM (2020) Dense hydroxyl polyethylene glycol dendrimer targets activated glia in multiple CNS disorders. *Sci Adv* 6: eaay8514 Doi 10.1126/sciadv.aay8514
- 178 Sharma R, Sharma A, Kambhampati SP, Reddy RR, Zhang Z, Clelland JL, Kannan S, Kannan RM (2018) Scalable synthesis and validation of PAMAM dendrimer-N-acetyl cysteine conjugate for potential translation. *Bioeng Transl Med* 3: 87-101 Doi 10.1002/btm2.10094
- 179 Shi Y, Manis M, Long J, Wang K, Sullivan PM, Remolina Serrano J, Hoyle R, Holtzman DM (2019) Microglia drive APOE-dependent neurodegeneration in a tauopathy mouse model. *J Exp Med* 216: 2546-2561 Doi 10.1084/jem.20190980
- 180 Shi Y, Yamada K, Liddel SA, Smith ST, Zhao L, Luo W, Tsai RM, Spina S, Grinberg LT, Rojas JC et al (2017) ApoE4 markedly exacerbates tau-mediated neurodegeneration in a mouse model of tauopathy. *Nature* 549: 523-527 Doi 10.1038/nature24016
- 181 Sims JR, Zimmer JA, Evans CD, Lu M, Ardayfio P, Sparks J, Wessels AM, Shcherbinin S, Wang H, Monkul Nery E et al (2023) Donanemab in Early Symptomatic Alzheimer Disease: The TRAILBLAZER-ALZ 2 Randomized Clinical Trial. *JAMA* 330: 512-527 Doi 10.1001/jama.2023.13239



- 182 Sirkis DW, Bonham LW, Yokoyama JS (2021) The Role of Microglia in Inherited White-Matter Disorders and Connections to Frontotemporal Dementia. *Appl Clin Genet* 14: 195-207 Doi 10.2147/TACG.S245029
- 183 Song WM, Joshita S, Zhou Y, Ulland TK, Gilfillan S, Colonna M (2018) Humanized TREM2 mice reveal microglia-intrinsic and -extrinsic effects of R47H polymorphism. *J Exp Med* 215: 745-760 Doi 10.1084/jem.20171529
- 184 Spangenberg E, Severson PL, Hohsfield LA, Crapser J, Zhang J, Burton EA, Zhang Y, Spevak W, Lin J, Phan NY et al (2019) Sustained microglial depletion with CSF1R inhibitor impairs parenchymal plaque development in an Alzheimer's disease model. *Nat Commun* 10: 3758 Doi 10.1038/s41467-019-11674-z
- 185 Spangenberg EE, Lee RJ, Najafi AR, Rice RA, Elmore MR, Blurton-Jones M, West BL, Green KN (2016) Eliminating microglia in Alzheimer's mice prevents neuronal loss without modulating amyloid-beta pathology. *Brain* 139: 1265-1281 Doi 10.1093/brain/aww016
- 186 Spiller KJ, Restrepo CR, Khan T, Dominique MA, Fang TC, Canter RG, Roberts CJ, Miller KR, Ransohoff RM, Trojanowski JQ et al (2018) Microglia-mediated recovery from ALS-relevant motor neuron degeneration in a mouse model of TDP-43 proteinopathy. *Nat Neurosci* 21: 329-340 Doi 10.1038/s41593-018-0083-7
- 187 Srinageshwar B, Peruzzaro S, Andrews M, Johnson K, Hietpas A, Clark B, McGuire C, Petersen E, Kippe J, Stewart A et al (2017) PAMAM Dendrimers Cross the Blood-Brain Barrier When Administered through the Carotid Artery in C57BL/6J Mice. *Int J Mol Sci* 18: Doi 10.3390/ijms18030628
- 188 Steinberg S, Stefansson H, Jonsson T, Johannsdottir H, Ingason A, Helgason H, Sulem P, Magnusson OT, Gudjonsson SA, Unnsteinsdottir U et al (2015) Loss-of-function variants in ABCA7 confer risk of Alzheimer's disease. *Nat Genet* 47: 445-447 Doi 10.1038/ng.3246
- 189 Takahashi K, Rochford CD, Neumann H (2005) Clearance of apoptotic neurons without inflammation by microglial triggering receptor expressed on myeloid cells-2. *J Exp Med* 201: 647-657 Doi 10.1084/jem.20041611
- 190 Tallon C, Sharma A, Zhang Z, Thomas AG, Ng J, Zhu X, Donoghue A, Schulte M, Joe TR, Kambhampati SP et al (2022) Dendrimer-2PMPA Delays Muscle Function Loss and Denervation in a Murine Model of Amyotrophic Lateral Sclerosis. *Neurotherapeutics* 19: 274-288 Doi 10.1007/s13311-021-01159-7
- 191 Tiraboschi P, Hansen LA, Masliah E, Alford M, Thal LJ, Corey-Bloom J (2004) Impact of APOE genotype on neuropathologic and neurochemical markers of Alzheimer disease. *Neurology* 62: 1977-1983 Doi 10.1212/01.wnl.0000128091.92139.0f
- 192 Tran KM, Kawauchi S, Kramar EA, Rezaie N, Liang HY, Sakr JS, Gomez-Arboledas A, Arreola MA, Cunha CD, Phan J et al (2023) A Trem2(R47H) mouse model without cryptic splicing drives age- and disease-dependent tissue damage and synaptic loss in response to plaques. *Mol Neurodegener* 18: 12 Doi 10.1186/s13024-023-00598-4
- 193 Uchihara T, Duyckaerts C, He Y, Kobayashi K, Seilhean D, Amouyel P, Hauw JJ (1995) ApoE immunoreactivity and microglial cells in Alzheimer's disease brain. *Neurosci Lett* 195: 5-8 Doi 10.1016/0304-3940(95)11763-m
- 194 Ulrich JD, Ulland TK, Mahan TE, Nystrom S, Nilsson KP, Song WM, Zhou Y, Reinartz M, Choi S, Jiang H et al (2018) ApoE facilitates the microglial response to amyloid plaque pathology. *J Exp Med* 215: 1047-1058 Doi 10.1084/jem.20171265
- 195 van Dyck CH, Swanson CJ, Aisen P, Bateman RJ, Chen C, Gee M, Kanekiyo M, Li D, Reyderman L, Cohen S et al (2023) Lecanemab in Early Alzheimer's Disease. *N Engl J Med* 388: 9-21 Doi 10.1056/NEJMoa2212948

- 196 van Lengerich B, Zhan L, Xia D, Chan D, Joy D, Park JI, Tatarakis D, Calvert M, Hummel S, Lianoglou Set al (2023) A TREM2-activating antibody with a blood-brain barrier transport vehicle enhances microglial metabolism in Alzheimer's disease models. *Nat Neurosci* 26: 416-429 Doi 10.1038/s41593-022-01240-0
- 197 Wang C, Xiong M, Gratuze M, Bao X, Shi Y, Andhey PS, Manis M, Schroeder C, Yin Z, Madore Cet al (2021) Selective removal of astrocytic APOE4 strongly protects against tau-mediated neurodegeneration and decreases synaptic phagocytosis by microglia. *Neuron*: Doi 10.1016/j.neuron.2021.03.024
- 198 Wang S, Mustafa M, Yuede CM, Salazar SV, Kong P, Long H, Ward M, Siddiqui O, Paul R, Gilfillan Set al (2020) Anti-human TREM2 induces microglia proliferation and reduces pathology in an Alzheimer's disease model. *J Exp Med* 217: Doi 10.1084/jem.20200785
- 199 Wang S, Sudan R, Peng V, Zhou Y, Du S, Yuede CM, Lei T, Hou J, Cai Z, Cella Met al (2022) TREM2 drives microglia response to amyloid-beta via SYK-dependent and -independent pathways. *Cell* 185: 4153-4169 e4119 Doi 10.1016/j.cell.2022.09.033
- 200 Wang Y, Cella M, Mallinson K, Ulrich JD, Young KL, Robinette ML, Gilfillan S, Krishnan GM, Sudhakar S, Zinselmeyer BH et al (2015) TREM2 lipid sensing sustains the microglial response in an Alzheimer's disease model. *Cell* 160: 1061-1071 Doi 10.1016/j.cell.2015.01.049
- 201 Wang Y, Ulland TK, Ulrich JD, Song W, Tzaferis JA, Hole JT, Yuan P, Mahan TE, Shi Y, Gilfillan Set al (2016) TREM2-mediated early microglial response limits diffusion and toxicity of amyloid plaques. *J Exp Med* 213: 667-675 Doi 10.1084/jem.20151948
- 202 Webster SD, Yang AJ, Margol L, Garzon-Rodriguez W, Glabe CG, Tenner AJ (2000) Complement component C1q modulates the phagocytosis of Abeta by microglia. *Exp Neurol* 161: 127-138 Doi 10.1006/exnr.1999.7260
- 203 Wegiel J, Wang KC, Imaki H, Rubenstein R, Wronska A, Osuchowski M, Lipinski WJ, Walker LC, LeVine H (2001) The role of microglial cells and astrocytes in fibrillar plaque evolution in transgenic APP(SW) mice. *Neurobiol Aging* 22: 49-61 Doi 10.1016/s0197-4580(00)00181-0
- 204 Wickham H (2009) ggplot2: Elegant Graphics for Data Analysis. *Use R*: 1-212 Doi 10.1007/978-0-387-98141-3
- 205 Wolinsky JB, Grinstaff MW (2008) Therapeutic and diagnostic applications of dendrimers for cancer treatment. *Adv Drug Deliv Rev* 60: 1037-1055 Doi 10.1016/j.addr.2008.02.012
- 206 Xing J, Titus AR, Humphrey MB (2015) The TREM2-DAP12 signaling pathway in Nasu-Hakola disease: a molecular genetics perspective. *Res Rep Biochem* 5: 89-100 Doi 10.2147/RRBC.S58057
- 207 Yasuno F, Kosaka J, Ota M, Higuchi M, Ito H, Fujimura Y, Nozaki S, Takahashi S, Mizukami K, Asada Tet al (2012) Increased binding of peripheral benzodiazepine receptor in mild cognitive impairment-dementia converters measured by positron emission tomography with [(1)(1)C]DAA1106. *Psychiatry Res* 203: 67-74 Doi 10.1016/j.psychresns.2011.08.013
- 208 Yeh FL, Wang Y, Tom I, Gonzalez LC, Sheng M (2016) TREM2 Binds to Apolipoproteins, Including APOE and CLU/APOJ, and Thereby Facilitates Uptake of Amyloid-Beta by Microglia. *Neuron* 91: 328-340 Doi 10.1016/j.neuron.2016.06.015
- 209 Yona S, Kim KW, Wolf Y, Mildner A, Varol D, Breker M, Strauss-Ayali D, Viukov S, Guillems M, Misharin A et al (2013) Fate mapping reveals origins and dynamics of monocytes and tissue macrophages under homeostasis. *Immunity* 38: 79-91 Doi 10.1016/j.immuni.2012.12.001
- 210 Yong SM, Lim ML, Low CM, Wong BS (2014) Reduced neuronal signaling in the ageing apolipoprotein-E4 targeted replacement female mice. *Sci Rep* 4: 6580 Doi 10.1038/srep06580
- 211 Yu L, Boyle PA, Nag S, Leurgans S, Buchman AS, Wilson RS, Arvanitakis Z, Farfel JM, De Jager PL, Bennett DA et al (2015) APOE and cerebral amyloid angiopathy in community-dwelling older persons. *Neurobiol Aging* 36: 2946-2953 Doi 10.1016/j.neurobiolaging.2015.08.008

- 212 Yuan P, Condello C, Keene CD, Wang Y, Bird TD, Paul SM, Luo W, Colonna M, Baddeley D, Grutzendler J (2016) TREM2 Haplodeficiency in Mice and Humans Impairs the Microglia Barrier Function Leading to Decreased Amyloid Compaction and Severe Axonal Dystrophy. *Neuron* 92: 252-264 Doi 10.1016/j.neuron.2016.09.016
- 213 Zhang B, Horvath S (2005) A general framework for weighted gene co-expression network analysis. *Stat Appl Genet Mol Biol* 4: Article17 Doi 10.2202/1544-6115.1128
- 214 Zhang X, Tang L, Yang J, Meng L, Chen J, Zhou L, Wang J, Xiong M, Zhang Z (2023) Soluble TREM2 ameliorates tau phosphorylation and cognitive deficits through activating transgelin-2 in Alzheimer's disease. *Nat Commun* 14: 6670 Doi 10.1038/s41467-023-42505-x
- 215 Zhang Y, Chen K, Sloan SA, Bennett ML, Scholze AR, O'Keeffe S, Phatnani HP, Guarnieri P, Caneda C, Ruderisch Net al (2014) An RNA-sequencing transcriptome and splicing database of glia, neurons, and vascular cells of the cerebral cortex. *J Neurosci* 34: 11929-11947 Doi 10.1523/JNEUROSCI.1860-14.2014
- 216 Zhang Y, Sloan SA, Clarke LE, Caneda C, Plaza CA, Blumenthal PD, Vogel H, Steinberg GK, Edwards MS, Li Get al (2016) Purification and Characterization of Progenitor and Mature Human Astrocytes Reveals Transcriptional and Functional Differences with Mouse. *Neuron* 89: 37-53 Doi 10.1016/j.neuron.2015.11.013
- 217 Zhong L, Sheng X, Wang W, Li Y, Zhuo R, Wang K, Zhang L, Hu DD, Hong Y, Chen Let al (2023) TREM2 receptor protects against complement-mediated synaptic loss by binding to complement C1q during neurodegeneration. *Immunity* 56: 1794-1808 e1798 Doi 10.1016/j.immuni.2023.06.016
- 218 Zhong L, Xu Y, Zhuo R, Wang T, Wang K, Huang R, Wang D, Gao Y, Zhu Y, Sheng Xet al (2019) Soluble TREM2 ameliorates pathological phenotypes by modulating microglial functions in an Alzheimer's disease model. *Nat Commun* 10: 1365 Doi 10.1038/s41467-019-09118-9
- 219 Zhu Y, Liu C, Pang Z (2019) Dendrimer-Based Drug Delivery Systems for Brain Targeting. *Biomolecules* 9: Doi 10.3390/biom9120790